BILINGUAL PUBLISHING CO.
Pioneer of Global Academics Since 1984

Journal of Architectural Environment & Structural Engineering Research

Volume 4 • Issue 2 • April 2021 ISSN 2630-5232 (Online)

Volume 4 Issue 2 • April 2021 • ISSN 2630-5232 (Online)

Journal of Architectural Environment & Structural Engineering Research

BILINGUAL PUBLISHING CO.

Pioneer of Global Academics Since 1984

BILINGUAL PUBLISHING CO.
Pioneer of Global Academics Since 1984

Volume 4 | Issue 2 | April 2021 | Page 1-53
Journal of Architectural Environment & Structural Engineering Research

Contents

ARTICLE

BILINGUAL PUBLISHING CO.
Pioneer of Global Academics Since 1984

Journal of Architectural Environment & Structural Engineering Research
https://ojs.bilpublishing.com/index.php/jaeser

ARTICLE

Bond Behavior between Recycled Concrete Containing CDW and Different Types of Steel Bars

Carine N. S. Reis Paulo Lima* Mônica B. Leite

Department of Technology, Post-graduation Program of Civil and Environmental Engineering, State University of Feira de Santana, Bahia, Brazil

ARTICLE INFO

Article history
Received: 15 January 2021
Accepted: 16 March 2021
Published Online: 30 March 2021

Keywords:
Construction and demolition waste (CDW)
Recycled concrete
Steel-concrete bond behavior

ABSTRACT

The operation of reinforced concrete structures is directly associated with the adhesion between the steel bar and the concrete, which allows the internal forces to be transferred to the reinforcement during the process of loading the structural elements. The modification of the concrete composition, with the introduction of recycled aggregate from construction and demolition waste (CDW), affects the steel-concrete interface and can modify the bonding stress, which is also influenced by the type and diameter of the bar used. In this work, the influence of the recycled fine aggregate (RFA) and types of steel bar on the steel-concrete bond was experimentally evaluated using the pullout test. Conventional concrete and recycled concrete, with RFA replacement level of 25%, were produced. Two types of steel rebars (i.e.,plain and deformed) with diameters of 10.0 and 16.0 mm were considered in this paper. The results indicate a reduction in the adhesion stress with the introduction of recycled aggregate, but this trend is influenced by the diameter of the bar used. The use of ribbed bars modifies the stress bon-slip behavior, with an increase in the average bond strength, which is also observed with the reduction of the diameter of the bar.

1. Introduction

The use of construction and demolition waste for the production of concrete and mortar, as a substitute for natural aggregates, is an important alternative for reducing the environmental impact of the civil construction sector. The application of this type of recycled aggregate, replacing the fine and coarse natural aggregate, in the production of reinforced concrete structural elements, has been successfully evaluated by several researchers around the world [1-4] which will allow the expansion of the reinsertion of this waste in the sector productive.

However, due to the differential characteristics of recycled aggregates, in relation to the natural aggregate, its use in larger quantities can result in a significant reduction of the compressive strength and tensile strength [5] and the fracture mode of the concrete [6]. Due to this, the recycled fine aggregates have been banned or have limited substitution content by some reinforced concrete design standards to be used in structural concrete [7].

The reduction in mechanical properties directly affects the steel-concrete bond and the structural behavior of reinforced concrete elements produced with recycled concrete. According to Mukai et al [8], the use of recycled aggregate can affect the behavior of reinforced concrete beams when the recycled aggregate is used to replace

**Corresponding Author:*
Paulo Lima,
Department of Technology, Post-graduation Program of Civil and Environmental Engineering, State University of Feira de Santana, Bahia, Brazil;
E-mail: lima.prl@pq.cnpq.br

 DOI: https://doi.org/10.30564/jaeser.v4i2.2810

the natural aggregate; the authors found a reduction in the shear strength and crack load of the beams, when compared with the conventional concrete beam, which was attributed to the lower adhesion between steel and recycled concrete. Other studies on the effect of recycled aggregate on steel-concrete bond have been developed but have not shown a consensus between the results. While some researchers did not verify any influence of the recycled aggregate on the bond-slip behavior [9, 10], in another study a reduction in the bond stress was verified with the substitution of the natural aggregate by the recycled aggregate [11]. This apparent contradiction is associated with the characteristics of each work, since several parameters affect the steel-concrete bond behavior, such as composition and type of recycled aggregate, type of steel and diameter of the bar and also the mechanical properties of the concrete.

Thus, in order to allow the application of recycled aggregate in reinforced concrete safely, it is necessary to assess how the parameters associated with the bonding stress, such as bar diameter and bar texture, affect the stress-slip behavior in concrete with recycled aggregate.

The objective of this work is to verify the effect of the addition of recycled fine aggregate and the characteristics of the steel bar on the bond stress-slip behavior. Pullout test was performed to determine the adhesion between concretes with 25% recycled fine aggregate and steel bars. Four types of steel bars were evaluated, with 10 mm and 16 mm diameters and with plain or deformed surface texture.

2. Materials and Methods

2.1 Materials

Two natural fine aggregates used were: fine river quartz sand (NFA1) and medium (NFA2) river quartz sand. The granitic aggregate, with specific gravity of 2.69 kg/dm^3 and maximum size aggregate of 9.5 mm, was used as natural coarse aggregate (NCA). The aggregate properties are presented in Table 1. As a binder, the Portland cement (C) composed with pozzolan (type CP II Z - 32), with a specific mass of 2.89 kg/dm^3, was used. Drinking water was used in all mixtures.

The recycled fine aggregate (RFA) was obtained from the grinding, in a jaw crusher, of demolition waste composed of mortar, ceramics and concrete, in the proportions of 29%, 27% and 44%, respectively. After grinding, the residue was sieved through a 4.8 mm sieve and characterized, as shown in Table 1.

Table 1. Physical properties and granulometric analysis of aggregates

Properties (test method)		Fine aggregates		
		NFA1	NFA2	RFA
Granulometric analysis	Sieve opening (mm)	%passing		
	4.8	99	100	100
	2.4	99	85	85
	1.2	98	52	72
	0.6	87	37	52
	0.3	33	24	30
	0.15	7	21	16
Maximum size aggregate (mm) (NBR NM 248/03)		1.2	4.8	2.4
Fineness (NBR NM 248/03)		1.77	3.47	2.46
Specific gravity (kg/dm³)		2.61	2.57	2.18
Bulk density (kg/dm³) (NBR 7251/82)		1.60	1.46	1.37
Water absorption rate (%)		0.1 [1]	0.2 [1]	18.8 [2]
Fines content (%) (NBR NM 46/03)		2.1	0.8	10.0

[1] Experimental Method: NBR NM 30/03; [2] Experimental Method: Leite [10]

For this investigation, deformed and smooth steel bars with diameters of 10 mm and 16 mm were used. The yield strength of the bars was determined according to NBR ISO 6892 [12] and a value of 800 MPa was obtained.

As shown in Table 2, two mixes were prepared with natural aggregate (REF) and with fine recycled aggregate (25% CDW) replacing the 25%, in volume, of fine natural aggregate. As can be seen in Table 1, the water absorption of the recycled aggregate is around 18%. Because of this, the addition of recycled material in the mixture tends to absorb part of the water used and reduce the workability of the concrete in the fresh state. As a result, there is a difficulty in launching the concrete. In this way, an additional amount of water, called "compensating water", was inserted into the mixtures, to compensate for the aggregate water absorption rate and not to reduce the workability of the concrete in the fresh state. However, to avoid an increase in the water/cement ratio and a possible reduction in mechanical strength, the amount of free water was corrected, considering a water absorption from the recycled aggregate for a time of 10 minutes. This mixing time was then adopted for all concretes. The proportions of the mixture for all lots are detailed in Table 2. A scientific method of mix design, based on the compressible packaging method, was used to provide mixtures, and is presented in detail in [13].

DOI: https://doi.org/10.30564/jaeser.v4i2.2810

Table 2. Composition of concrete

Mix	%CDW	Mix proportions (kg/m^3)								Slump (mm)
		C	NCA	NFA1	NFA2	RFA	water	compensating water	water total	
REF	0	360	892.8	604.8	259.2	-	212.4	0	212.4	100
25%CDW	25			453.6	194.4	198.0		28.8	241.2	115

2.2 Preparation of Pull-out Test Specimens

Figure 1a shows a schematic drawing with the dimensions of the pull-out specimens and positioning of the steel bars. It can be seen in Figure 1b that the production process was carried out with PVC molds supported on wooden structures and with vertical positioning of the bars. The relationship between the diameter of the steel bar and the diameter of the concrete cylinder was kept equal to 10. A portable needle vibrator was used to consolidate the fresh concrete in the samples (Figure 1c).

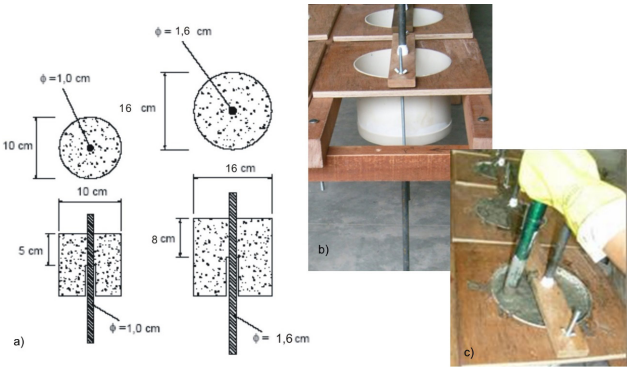

Figure 1. Pull-out specimens production: a) dimensions; b) PVC molds; c) casting and vibraton.

2.3 Test Procedures

The pullout test was carried out according to the RILEM standard [14] and is shown in Figure 2. To assist in the test, a metallic apparatus consisting of two steel plates with central holes, 30 mm thick and connected with four bars threaded was manufactured. The upper plate of the apparatus was connected to the clamp of the test machine and the specimen was positioned inside it. The steel bar of the sample was then attached to the machine's claw at the bottom and subjected to a tensile load. The sliding of the bar was measured by a linear variable differential transformer (LVDT) attached to the upper part of the specimen and the load was measured by a load cell, with a capacity of 300 kN and positioned under the sample, as shown in Figure 2b. An automatic signal acquisition system was used to capture the load and displacement values in real time that allowed obtaining the load-slip curve. A 1000 kN universal test machine with load control was used.

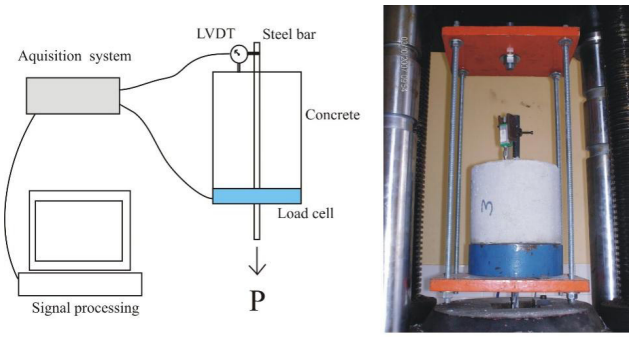

Figure 2. Pullout test setup

To determine the mechanical properties of concretes, axial compression and splitting were carried out in cylindrical samples with 100 mm in diameter and 200 mm in height after 28 days of curing in a humid environment (95% RH). The specimens were tested on a 2000 kN testing machine.

3. Results and Discussion

3.1 Mechanical Properties of Concrete

Table 3 shows the experimental results of mechanical tests.

Table 3. Compressive strength (f_c), splitting strength (f_{td}) and elastic modulus (E_c) of reference and experimental concrete sample

Mixture	%CDW	f_c (MPa)	f_{td} (MPa)	E_c (GPa)
Referência	0	23.65 ± 1.06	2.08 ± 0.04	30.50 ± 0.43
25%CDW	25	22.82 ± 0.58	1.70 ± 0.09	25.58 ± 1.71

It can be seen in Table 3 that the addition of recycled aggregate as substitution to the natural aggregate resulted in a reduction of 3.5%, 18.3% and 16.1% in compressive strength, splitting strength and elastic modulus, respectively.

The reduction in mechanical properties with the introduction of recycled aggregates has been observed by other researchers [15-17] and may be associated with an

 DOI: https://doi.org/10.30564/jaeser.v4i2.2810

increase in the water content of the mixture, the greater fragility of the recycled aggregate grain, when compared to the natural aggregate or due the saturation level of the recycled aggregates may affect the strength of the concretes.

3.2 Bond Stress

The experimental stress bond versus slip curves of pull-out test with 10 mm and the 16 mm diameter bars are presented in Figure 3.

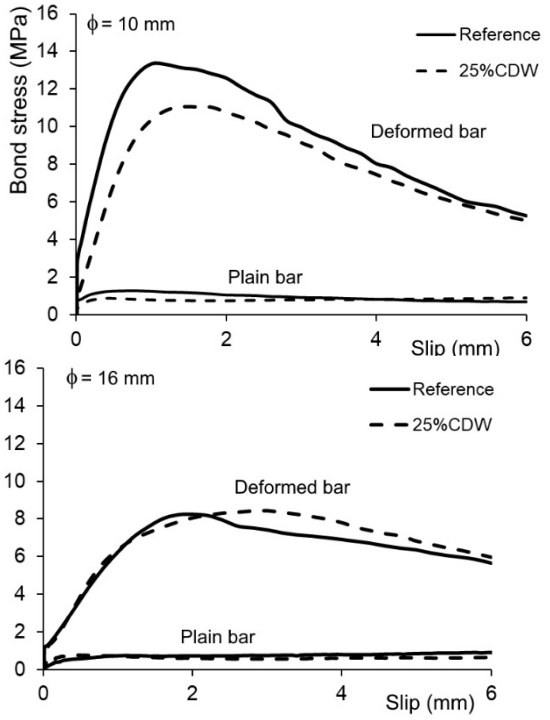

Figure 3. Experimental bond stress-slip curves

The steel-concrete bond is formed by the combination of three components associated with chemical adhesion, mechanical anchoring and friction. When using smooth bars, chemical adhesion is the predominant mechanism, and the adhesion stress is usually weak. In the pullout test with smooth bars, after the rupture of the chemical adhesion, the increase in loading generates the longitudinal cracking of the steel-concrete interface along the bar. Subsequently, a pullout process characterized by an increase in sliding and maintenance of a practically constant load, as schematically shown in Figure 4. This phenomenon was also observed in the experimental results obtained with smooth bars shown in Figure 3.

In the corrugated bars, on the other hand, the ribs provide a mechanical lock that allows the development of greater bond stress after overcoming the chemical adhesion. The mechanical interlock, which is generated by the ribs of the bar and the concrete, provides bearing force against the face of the bar ribs, as shown in Figure 6. The cracking process at the steel-concrete interface is then characterized by an increase in the adherence stress to a maximum stress level, after which the complete rupture of the interface and the reduction of bond stress can be observed in a process called shearing off (Figure 4).

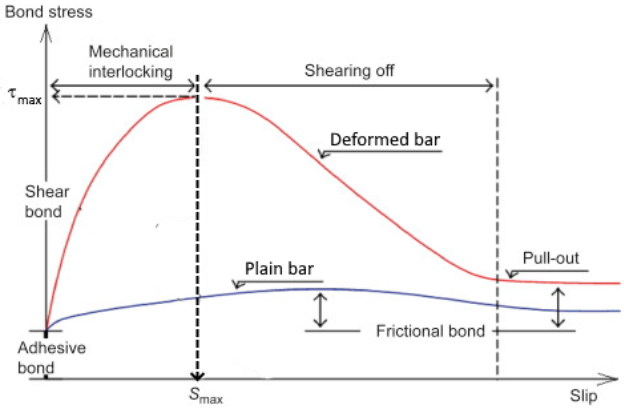

Figure 4. Schematic bond stress-slip relationship [18]

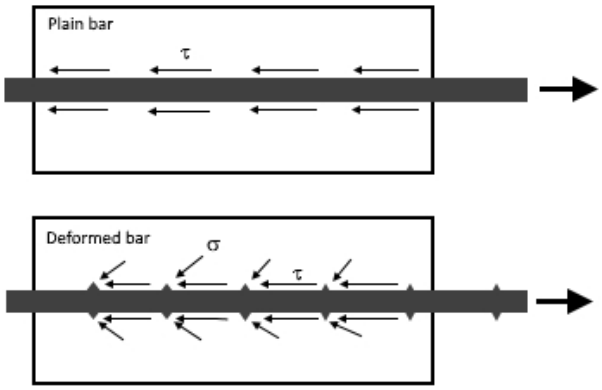

Figure 5. Local bond response on plain and deformed bar (adapted from [19])

Considering the theoretical model shown in Figure 5 [19], the bond stress in the pullout test can be considered constant along the length of the steel bar embedded in the concrete. Thus, the bond stress τ is given by:

$$\tau = \frac{P}{\pi \varphi l_b} \tag{1}$$

where P is the load; l_b is the embedded length of the steel rebar and φ is the diameter of the steel rebar.

The average bond strength τ_m is obtained by media of three bond stresses relatives to slip of 0.01 mm ($\tau_{0.01}$), 0.1 mm ($\tau_{0.1}$) e 1.0 mm ($\tau_{1.0}$):

$$\tau = \frac{\tau_{0.01} + \tau_{0.1} + \tau_{1.0}}{3} \tag{2}$$

From Equation (1) it is possible to obtain the maximum

DOI: https://doi.org/10.30564/jaeser.v4i2.2810

bond strength, τ_{max}, using the maximum load obtained in the test. However, when the maximum load is obtained for a displacement below 1 mm, the value of $\tau_{1.0}$ is adopted as the maximum stress.

Table 4 shows the experimental results of pull-out test.

It can be seen that, when using plain bars, the average bond strength is usually lower, reaching maximum values in the order of 0.98 MPa, as shown in Table 4. For the deformed bars, average bond strength varied from 2.76 MPa to 6.89 MPa, which represents an increase of up to 9 times in the adhesion when compared with the plain bar, due to the mechanical anchoring effect provided by the ribs.

In addition to the surface texture, it is verified in this work that the diameter of the bar affects the development of bond stresses. The results shown in Table 4 indicate that the average bond stress, , decreases with the increase in the bar diameter. For conventional concretes, this reduction is about 62% when the diameter of the bars varies from 10 mm to 16 mm. For recycled concrete, the reduction in the average bonding stress, , with the increase in the bar diameter was 45% for plain bars and 38% for deformed bars. The reduction of the bonding stress with the increase in the diameter of the bars was observed by [20] for conventional reinforced concrete with bars of 12, 16 and 20 mm. According to [16, 17] this phenomenon is associated with the steel-concrete interface; in the 16 mm bars the thickness of the transition zone is greater than in the 10 mm bars, which facilitates the trapping of air and water close to the rib and, consequently, reduces the adhesion of the bar with the concrete. The reduction in mean porous zone thickness can be considered one of the many influencing factors that resulted in increased ultimate bond strength [21]. During the concrete casting process, voids can form under the bars or close to the ribs, generating a bleed water zone [22] that affects the steel-concrete adhesion and even the durability of the bar.

Regarding the use of recycled aggregate, there is a tendency to reduce the average bonding stress, which is mainly influenced by the reduction in the tensile strength of recycled concrete, when compared to conventional concrete, as shown in Table 3. This behavior was identified by Choi and Kang [9] and which verified that the bond strength decreased with the increasing recycled aggregate ratio. However, the bar diameter differently affects the adhesion ratio between steel and recycled concrete. While for deformed bars with 10 mm there is a reduction of about 35% of the average bond stress with the introduction of recycled aggregate, in the test with deformed bars of 16 mm, the introduction of recycled aggregate resulted in an increase of 16% in this bond strength, demonstrating that there is an interaction between these two parameters. For plain bars, the adhesion between the bar and recycled concrete decreased by 39% and 11%, for bars of 10 mm and 16 mm, respectively. The combined effects of recycled aggregate addition, type and diameter of steel the bond strength have shown no clear tendency in the current study. Xiao and Falkner [9] also verified the interaction between the use of recycled aggregate and the type of steel bar; the authors found that the bond strength between the recycled aggregate concrete and the plain rebar decreases while the bond strength between the recycled aggregate concrete and the deformed rebar is similar.

4. Conclusions

Based on the experimental results obtained with

Table 4. Results of the pullout test

Mistura	%CDW	ϕ (mm)	Bar type	$P_{máx}$ (KN)	$\tau_{0.01}$ (MPa)	$\tau_{0.1}$ (MPa)	$\tau_{1.0}$ (MPa)	τ_{max} (MPa)	τ_{m} (MPa)
T0P10	0	10	Plain	2.06 ± 0.20	0.72	0.92	1.27	1.31	0.98
T25P10	25			1.37 ± 0.10	0.26	0.62	0.81	0.91	0.60
T0D10	0	10	Deformed	21.48 ± 1.08	2.81	4.54	13.33	13.68	6.89
T25D10	25			18.73 ± 1.37	0.97	2.03	10.36	11.90	4.45
T0P16	0	16	Plain	3.04 ± 0.10	0.09	0.32	0.69	0.76	0.37
T25P16	25			3.14 ± 0.01	0.11	0.20	0.68	0.79	0.33
T0D16	0	16	Deformed	33.83 ± .41	1.06	1.36	5.85	8.42	2.76
T25D16	25			33.24 ± 3.14	1.08	1.45	7.10	8.27	3.21

 DOI: https://doi.org/10.30564/jaeser.v4i2.2810

pullout tests on concretes containing recycled fine aggregate, it was possible to obtain the following conclusions:

• The use of recycled fine aggregate to replace the natural aggregate reduces the mechanical properties of concrete, affecting the splitting tensile strength more significantly, affecting the splitting strength more significantly than the compressive strength or the elastic modulus, when compared with conventional concrete.

• The general shape of the load versus slip curve between recycled aggregate concrete and steel rebars is similar to the one for normal concrete and steel rebars.

• The stress-slip behavior is not affected by the introduction of the recycled aggregate, being similar to the behavior of the test with conventional concrete and according to the results already observed in the literature. The use of deformed bars, on the other hand, changes the stress-slip behavior, when compared to the result obtained for the plain bar, due to the mechanical component of bond stress resulting from the effect of locking the ribs.

• For the deformed bars, average bond strength varied from 2.76 MPa to 6.89 MPa, which represents an increase of up to 9 times in the adhesion when compared with the plain bar, due to the mechanical anchoring effect provided by the ribs.

• The reduction of the bonding stress with the increase in the diameter of the bars.

• The average bond strength between the recycled aggregate concrete and the plain rebar decreases for the RCA replacement percentage of 25% while the bond strength between the recycled aggregate concrete and the deformed rebar is dependent of diameter of bar. For deformed bars with a diameter of 10 mm there is a reduction in bond strength with the introduction of recycled aggregate while for deformed bars with a diameter of 16 mm there is an increase in adhesion.

Acknowledgements

The authors would like to thank the CAPES which sponsored the first author.

References

[1] Li, X. Recycling and reuse of waste concrete in china. Part II. Structural behaviour of recycled aggregate concrete and engineering applications. Resources, Conservation and Recycling, 2009, 53 (3):107-112.

[2] Etxeberria, M., Mari, A. and Vázquez E. Recycled aggregate concrete as structural material. Materials and Structures, 2007, 40: 529-541.

[3] Fonteboa, B.G. and Abella, F.M. Shear strength of recycled concrete beams. Construction and Building Materials, 2007, 21 (4): 887-893.

[4] Larrañaga, M. E., Experimental study on microstructure and strutural behaviour of recycled aggregate concrete. Doctoral thesis. Universitat Politécnica de Catalunya. Barcelona, 2004. 223p.

[5] Carneiro, J. A., Lima, P. R. L., Leite, M. B., & Toledo Filho, R. D. Compressive stress–strain behavior of steel fiber reinforced-recycled aggregate concrete. Cement and concrete composites, 2014, 46: 65-72.

[6] Lima, P.R.L., Souza, T.S. Avaliação numérica e experimental do modo I de fratura de concreto reciclado. Revista Portuguesa de Engenharia de Estruturas, 2012, Serie II(12): 5-16.

[7] Evangelista L and Brito J. Concrete with fine recycled aggregates: a review. European Journal of Environmental and Civil Engineering, 2012, 18(2): 129-172.

[8] Mukai, T. and Kikuchi, M., ´Properties of reinforced concrete beams consisting recycled aggregate. Reuse of demolition waste´ In Proceedings of the second international Rilem symposium on demolition and reuse of concrete and masonry, Tokyo, Japan, 1988, pp.670-679.

[9] Xiao, J. and Falkner, H., Bond behavior between recycled aggregate concrete and steel rebars. Construction and Building Materials, 2007, 21: 395-401.

[10] Ajdukiewicz, A. and Kliszczewicz, A. Infuence of recycled aggregates on mechanical properties of HS/HPC, Cement and Concrete Composites, 2002, 24 (2): 269-279.

[11] Choi, H.B. and Kang, K.I., Bond behaviour of deformed bars embedded in RAC, Magazine of Concrete Research, 2008, 60 (6): 399-410.

[12] ASSOCIAÇÃO BRASILEIRA DE NORMAS TÉCNICAS. NBR ISO 6892. Materiais metálicos-ensaio de tração à temperatura ambiente. 2002.

[13] Reis, C.N.S. INFLUÊNCIA DA UTILIZAÇÃO DE AGREGADO MIÚDO DE RCD NA ADERÊNCIA AÇO-CONCRETO RECICLADO. Dissertação (Mestrado em Engenharia), Feira de Santana, 2009.

[14] RILEM/FIP/CEB, Essai portant sur l'adhérence des armatures du béton. 1. Essai par flexion (7-II-28D). 2. Essai par tration (7-II-128), Recomamdations Provisoires. Matériaux et Constructions, 1973, 6(32): 96-105.

[15] L. Evangelista a, J. de Brito. Mechanical behaviour of concrete made with fine recycled concrete aggregates. Cement & Concrete Composites, 2007, 29: 397-401.

[16] Poon CS, Shui ZH, Lam L, Fok H, Kou SC. Influence of moisture states of natural and recycled ag-

DOI: https://doi.org/10.30564/jaeser.v4i2.2810

gregates on the slump and compressive strength of concrete. Cement and Concrete Research, 2004, 34: 31-6.

[17] Barra de Oliveira M, Vasquez E. The influence of retained moisture in aggregates from recycling on the properties of new hardened concrete. Waste Management, 1996, 16:113-7.

[18] Hong, S., & Park, S. K. Uniaxial bond stress-slip relationship of reinforcing bars in concrete. Advances in Materials Science and Engineering, 2012.

[19] COMITE EURO-INTERNACIONAL DU BETON. Bond action bond behaviour of reinforcement, Paris, Bulletin d'Information151. 1982.

[20] Bastwadkar, K. K., & Kulkarni, K. S. Effect of Embedded Length and Bar Diameter of Reinforcement on Bond Strength Behavior of High Strength Concrete Subjected to Elevated Temperatures. Civil and Environmental Research, 2016, 8(1): 50-56.

[21] S. Goudar, B. Das, and S. Arya, "Microstructural Study of Steel-Concrete Interface and Its Influence on Bond Strength of Reinforced Concrete. Advances in Civil Engineering Materials, 2019, 8(1): 171-189.

[22] Angst, U. M., Geiker, M. R., Michel, A., Gehlen, C., Wong, H., Isgor, O. B., ... & Buenfeld, N. The steel–concrete interface. Materials and Structures, 2017, 50(2), 143.

 DOI: https://doi.org/10.30564/jaeser.v4i2.2810

BILINGUAL PUBLISHING CO.
Pioneer of Global Academics Since 1984

Journal of Architectural Environment & Structural Engineering Research
https://ojs.bilpublishing.com/index.php/jaeser

ARTICLE

Effect of Aging on Solar Reflectance of White Cool Roof Coatings: Natural Weathering and the Influence on Building Energy Needs for Different Climate Conditions in Brazil

Kelen Almeida Dornelles*

University of Sao Paulo (USP), Institute of Architecture and Urbanism, Avenida Trabalhador São-Carlense, 400, Centro – São Carlos, Brazil

ARTICLE INFO

Article history
Received: 16 January 2021
Accepted: 16 March 2021
Published Online: 30 March 2021

Keywords:
Roof solar reflectance
Aging
Natural weathering
Cleaning process
Thermal comfort
Energy savings
Tropical climate

ABSTRACT

The use of cool materials on the building envelope is one of the most cost-effective ways to increase indoor thermal comfort conditions in hot climates and decrease the cooling energy needs. Despite the benefit of reducing cooling loads, researches have demonstrated that aging of roof coatings changes the initial solar reflectance (SR), which influences the long term building thermal and energy performance. Thus, this work presents preliminary natural weathering tests performed on samples of nine white coatings exposed to natural weathering for one year in the city of Sao Carlos, Brazil. Solar reflectances were measured with a spectrophotometer before and after exposure, every 3 months, for identifying the effect of aging along the time. The findings showed changes of 13% to 23% on SR after one year of natural weathering, with higher decrease on SR for rougher surfaces. The cleaning process restored from 90% to 100% of the original SR, which means maintenance can be an effective solution to restore the initial SR. Simulations indicated that roofs with higher solar reflectance increase indoor thermal comfort conditions and decrease the cooling energy need for buildings in hot climates, but the aging of white coatings increased the cooling energy needs along the time.

1. Introduction

The continuous population growth and urban sprawl directly influence the negative effects of global warming and climate change, with the increase of buildings and paved surfaces, and the reduction of vegetation in urban areas. In this case, the predominance of impermeable surfaces contributes with the rise on solar energy absorption by different materials, with direct impact on surface and ambient temperatures, given rise to the microclimate phenomena called urban heat islands (UHI) [1-4].

The UHI is mainly characterized by urban areas with higher temperature when compared to their surrounding rural environment. This phenomenon can be more intense in cities with hot climate conditions, located mainly in latitudes from 15° North to 15° South, where the solar radiation is an important issue regarding building heat gains [5]. In Brazil, for example, solar radiation is one of the most important contributors with the thermal load

**Corresponding Author:*
Kelen Almeida Dornelles,
University of Sao Paulo (USP), Institute of Architecture and Urbanism, Avenida Trabalhador São-Carlense, 400, Centro – São Carlos, Brazil;
Email: kelend@usp.br

DOI: https://doi.org/10.30564/jaeser.v4i2.2812

of buildings. According to the Brazilian standard NBR 15220-3 [6], the country is mainly characterized by tropical and hot conditions, with solar radiation levels sufficiently high and no active heating required for buildings even during the winter season. In contrast, the summer overheating usually adversely influences indoor comfort conditions in the built environment and increases energy need for cooling systems [7].

It is already known that the building sector is responsible for more than 40% of the global energy consumption [8]. Considering the energy needs mainly related to HVAC systems, this effect is increased primarily in countries with predominance of hot climate conditions. The Brazilian Energy Balance for 2019 [9] demonstrated that buildings account for 52% of the electric energy use, with 26.1% for the residential sector and 25.9% for non-residential buildings, mainly related to HVAC systems. More specifically, the cooling energy need has increased considerably in the last decades, as the use of cooling systems has been more intense to control the overheating in the built environment, associated primarily to climate change and urban development [10]. Furthermore, Ascione [11] demonstrated a worldwide increase of cooling degree days through a large literature review concerning building envelope, HVAC systems and renewables.

Over the years, different solutions were suggested to control the negative effects of global warming and urban heat islands on buildings thermal-energy performance, including building design strategies [12-14]. One of this solution is the use of cool coatings on the building envelope in order to decrease cooling energy needs in buildings and improve indoor thermal comfort in summer conditions. Cool materials are characterized by high solar reflectance and thermal emittance, which can maintain a lower surface temperature, reducing the solar heat gains by the building envelope [15,16]. However, building envelopes in the urban environment are subject to weather and the deposition of particulate matter present in the air, with direct effects on the solar reflectance of these surfaces [17]. Results from several researches indicated that natural weathering of roof surfaces decreased the original solar reflectance over time [18-23]. By this way, durability has become an important issue for new materials considering the potential of preserving high SR over time, since the higher initial investment must be paid back by cooling energy savings [24].

According to Bretz and Akbari [25], the high initial solar reflectance of surfaces likely to decrease mainly due to material degradation and surface materials accumulation as dirt and microbial growth. In this case, the surface accumulations may not be permanent, depending on their water solubility. According to the authors, microbial growth is more common in humid areas. Degradation, however, induces chemical changes in the material with permanent alteration of the solar reflectance. Previous researches have indicated that degradation of roof coatings is mainly related to insolation (particularly UV radiation), temperature variation of the roof (daily time-averaged), moisture (humidity, rain, and dew), and natural and anthropogenic pollutants [19,20,23]. Furthermore, the solar reflectance degradation of coatings occurred primarily within the first year of application, and even within the first two months of exposure [18-20]. However, an accurate maintenance procedure can reduce albedo changes by natural aging, as presented by Levinson *et al.* [26].

The effect of natural weathering on solar reflectance has been continuously analyzed [27-31]. Alchapar and Correa [27] assessed the influence of natural weathering on the thermal behavior of 19 roof tiles and roof paint. They concluded that all materials tend to reduce their reflectance capacity after three years of weathering exposure, and identified that morphological characteristics of color, composition, and finish (for new materials) and color, finish, and shape (for aged materials) impact the thermal performance. Ferrari *et al.* [28] investigated the effect of natural aging on the solar reflectance for clay roof tiles exposed to natural weathering in Arizona for three years. The results indicated that Arizona weathering condition affects the solar reflectance up to 0.05. On the other hand, De Masi *et al.* [29] found that the solar reflectance of a white cool roof coating decreased from 0.67 to 0.48 after 1 year of outdoor natural weathering in Benevento, Italy, under Mediterranean climatic conditions. Dornelles *et al.* [30] analyzed the effect of natural aging for 20 coatings after 18 months of exposure in tropical climate conditions, in Brazil. The results confirmed a reduction on the solar reflectance mainly related to dust and soot deposition for most of the samples. Two coatings with dark colors (SR<0.15) presented an increase on the SR, probably associated to degradation from UV radiation.

In addition, some studies also assessed the influence of natural aging of coatings on buildings thermal-energy performance. Mastrapostoli *et al.* [31] found a decrease of 72% on cooling energy demand with the application of a new cool roof coating when compared to the aged cool roof, through simulations with Energyplus. Aoyama *et al.* [32] conducted a study to evaluate the potential of increasing the durability of a high-reflectance coating due to its self-cleaning capability when exposed to natural aging tests at Kobe University. After one year of exposure, the results indicated differences of 0.09 on SR from the self-cleaning (0.70) and conventional (0.79)

 DOI: https://doi.org/10.30564/jaeser.v4i2.2812

roofs, and the energy saving of the self-cleaning coating and the cool roof was great during the year. Paolini *et al.* [33] investigated the performance of wall finishes with high solar reflectance and thermal emittance after four years of aging in Milan, Italy. The authors find a reduction on the solar reflectance of 0.20 for white coats and 11% increase in cooling energy need for a typical residential building with aged white walls without exterior insulation. In a previous study of natural aging in Roma and Milan, Italy, Paolini *et al* [17] identified a reduction of 0.14 on the initial SR of white roof membranes in Rome and 0.22 for samples aged in Milano after two years of exposure. For a typical commercial building highly insulated in Milan, an aged white roof may reach a surface temperature 16°C higher than a new white roof. The study confirmed that the decrease on SR after natural aging influences the energy needs of buildings and the surface temperature of the roofing membrane.

Based on the above, this work presents preliminary natural aging tests for samples of cool white coatings exposed to natural weathering for one year in São Carlos, SP, Brazil. Spectral and solar reflectances were measured with a spectrophotometer before and after exposure, every 3 months, for identifying the effect of aging along the time. A cleaning process was also conducted to identify the ability of the coatings to restore the initial solar reflectance after the period of natural weathering. Computer simulations were performed to assess the cooling and energy need for a residential building located in different climate conditions in Brazil, considering new and aged solar reflectances of samples analyzed in this research.

2. Methodology

Specimens were prepared for the characterization of the material properties (solar reflectance and thermal emittance) in laboratory, according to specific standards. Natural weathering exposure procedure was conducted for 12 months to identify the effects of aging and cleaning on the solar reflectances of 9 cool white roof coatings. As a case study, computer simulation for a single-story residential building located in 4 different climate conditions in Brazil estimated the thermal performance and energy need to restore indoor comfort conditions, considering different roof's reflectance. Procedures and instruments are following described.

2.1 Selected Materials

In this work, nine coatings available in the market were selected: three standard white acrylic coatings (STD) and six white coatings formulated with ceramic microspheres (CER), according to information provided in Table 1. Samples were prepared with ceramic specimens with smooth surface (80 x 80 mm) to minimize the roughness effect on the solar reflectance results.

Table 1. Characteristics of analyzed coatings

Sample	Coating description	Type	Color
S1-STD	Acrylic, elastomeric coating	Standard	White
S2-CER	Acrylic, elastomeric coating with ceramic microspheres	Ceramic microspheres	White
S3-CER	Acrylic, elastomeric coating with ceramic microspheres	Ceramic microspheres	White
S4-CER	Acrylic, elastomeric coating with ceramic microspheres	Ceramic microspheres	White
S5-CER	Acrylic, elastomeric coating with ceramic microspheres	Ceramic microspheres	White
S6-CER	Acrylic, elastomeric coating with ceramic microspheres	Ceramic microspheres	White
S7-CER	Acrylic, elastomeric coating with ceramic microspheres	Ceramic microspheres	White
S8-STD	Styrene acrylic coating	Standard	White
S9-STD	Styrene acrylic coating	Standard	White

2.2 Laboratory Measurements

2.2.1 Spectral Reflectance Measurements

In this work, spectral reflectance laboratory measurements for optical analyses were conducted according to the ASTM E903-20 standard [34]. The equipment is a double-beam spectrophotometer (Varian CARY 5G), fitted with an integrating sphere of 150 mm diameter. The spectral reflectance was measured from 300 to 2500 nm, at wavelength intervals of 1 nm. The solar reflectance was calculated by weighted averaging, based on a standard solar spectrum provided by ASTM G173-20 [35] as the weighting function.

2.2.2 Thermal Emittance Measurements

Thermal emittance measurements were performed with the emissometer model AE1 from Devices and Services, according to the standard ASTM C1371-15 [36]. This equipment measures the total thermal emittance when compared to standard materials with low and high emittance (0.06 and 0.87, respectively), calibrated before each measurement. The thermal emittance was conducted for the nine white coatings for initial conditions, before exposure to natural weathering.

2.3 Natural Weathering Procedure

The samples with 9 acrylic cool coatings were exposed to natural weathering conditions for 12 months in the city of São Carlos, SP, Brazil (22°S, 48°W, 860 m). The

DOI: https://doi.org/10.30564/jaeser.v4i2.2812

specimens were positioned on a low sloped roof surface (8°) to avoid standing water and to maximize the effect of soiling in a short testing period (Figure 1).

Figure 1. Low sloped roof with exposed specimens and detail of investigated samples

A weather station continuously monitored air temperature, relative humidity, global solar radiation, and precipitation) on site. The main assessment criteria for durability were the variation on solar reflectance and appearance along the time. The solar reflectance is related to the thermal performance of materials and the appearance is associated to the aesthetic condition. Soiling was supposed to have the major effects on solar reflectance loss, and this result must be differentiated from the contribution from other weathering agents like insolation, air temperature, and relative humidity. In this research, the natural aging considering both weathering and soiling actions was quantified through the reflectance loss over time for specimens exposed to natural weathering conditions. Solar and spectral reflectance for the cool coating samples were measured in laboratory before the exposure (new specimens), and every three months for aged specimens.

Finally, reflectances of each soiled specimen was remeasured followed by a cleaning process of washing with dishwashing detergent, water, and natural air drying, until the appearance of the coating stabilized. This procedure was intended to simulate an artificial cleaning mechanism.

2.4 Building Energy Simulation

The numerical analysis was carried out to assess the impact of cool white coatings on the indoor thermal comfort conditions and building energy needs of residential buildings located in 4 different climate conditions in Brazil. Computer simulations were conducted with EnergyPlus simulation software, based on solar reflectance data (new and aged) obtained for nine different white coatings considered in this work. Table 2 presents the latitude, longitude, and altitude of selected cities, with different climate conditions according to the Brazilian National Standard NBR 15220 [6].

Table 2. Latitude, longitude, and altitude of selected cities with different climates in Brazil.

Climate Zone	City / State	Latitude (°)	Longitude (°)	Altitude (m)	Climate Classification
1	Curitiba, PR	-25.52	-49.18	934	Subtropical
4	Brasília, DF	-15.78	-47.92	1171	Tropical (dry winter)
7	Petrolina, PE	-9.35	-40.55	376	Hot Semi-Arid
8	Belém, PA	-1.38	-48.48	10	Humid tropical

Meteorological data were based on the weather database of the US Department of Energy for Energyplus Software [37], typically used also for dynamic thermal-energy simulation of buildings. The building considered as a base case for simulation is a single story with a flat roof (Figure 2). This building is a real example of residential buildings currently built in Brazil in the last decade, mainly for low-cost houses. Its height is assumed to be 2.7 m, with walls and ceiling made of 10 cm of concrete. The solar reflectance of walls was assumed 0.5 and window area of 1.44 m² each one with clear 3 mm glass. The roof is covered with a 6 mm fibrocement tile, with solar reflectance according to the laboratory measurements of the selected white coatings. Bathroom has one window with 0.36 m² of clear 3 mm glass.

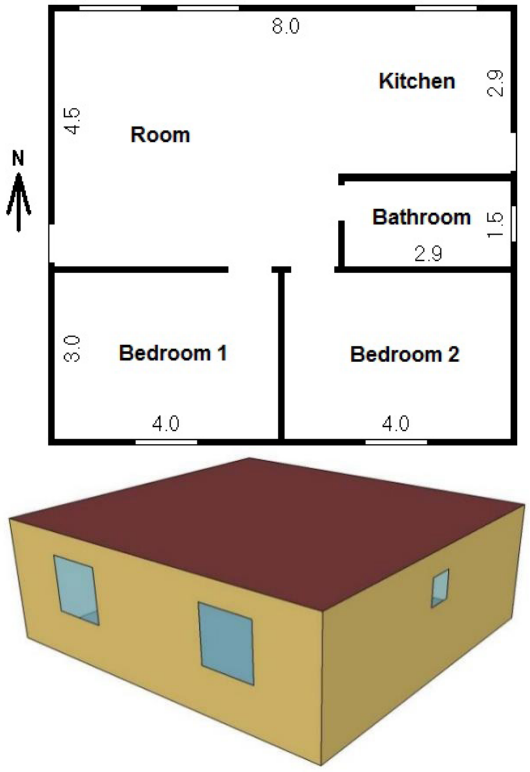

Figure 2. Case study – reference building

Infiltration and ventilation rates were set as 1/hour, according to the Brazilian standard NBR 15575 [38]. Regarding internal gains, simulations considered thermal

loads from the rooms' occupancy (people, lighting, and equipment), according to a typical Brazilian family [7] for which this kind of buildings are designed for (low-cost houses): 2 adults (100 W/person) and 2 children (60 W/person) in sedentary activities; lighting (18 h-24 h, 100 W) and TV (15 h-24 h, 50 W); kitchen equipment (lighting: 2 h/day, 100 W/hour; refrigerator: 24 h/day, 90 W/h; stove: 8 h/day, 60 W).

This building configuration may not necessarily be representative of houses in different tropical and hot climates. However, the purpose of this work was to assess the influence of roof reflectance on indoor thermal comfort conditions and energy use for different climate conditions in Brazil. In addition to the solar reflectance obtained in this study for the nine different samples (new and aged white coatings), it was included in the simulation procedure one fibrocement tile widely used for roofing in developing tropical countries. The new and aged solar reflectance for the fibrocement tile was obtained from earlier study [39].

In order to assess indoor thermal comfort conditions, comfortable temperature intervals were considered according to Equation 1, from ASHRAE 55-2017 [40] for natural ventilated buildings. The main advantage of this standard is its adaptative nature, which means that this standard recognizes that occupants used to living in warm climates prefer higher temperatures than those in cold climates, and vice versa.

$$Tc = 17.9 + 0.31 * To \quad (1)$$

Where:

Tc: temperature for comfort conditions (ºC);

To: Arithmetic average of the mean daily minimum and mean daily maximum outdoor (dry bulb) temperatures per month (ºC). Equation 1 is valid for 10.0 ºC ≤ *To* ≤ 33.5 ºC.

ASHRAE [40] indicates comfortable temperature range with *upper limit* calculated from Equation 2 and *lower limit* from Equation 3.

$$\text{Upper limit} = Tc + \text{tolerance} \quad (2)$$

$$\text{Lower limit} = Tc - \text{tolerance} \quad (3)$$

Where:

Tc: temperature for comfort conditions (ºC);

Tolerance: in this work it was considered a tolerance of 2.4 °C, which satisfies 90% of the occupants according to ASHRAE 55 [40]. For 80% of the occupants, standard ASHRAE 55-2017 indicates a tolerance of 3.4 °C.

Table 3 presents the temperature intervals (upper and lower limits) for indoor thermal comfort conditions, in order to obtain the degrees-hour of discomfort for summer (December) and Winter (June) design days, for each selected climate zone in Brazil.

Table 3. Comfortable limits for indoor air temperatures analyzed in building simulations.

Zone	City	To (°C)		Tn (°C)		Lower limit (°C)		Upper limit (°C)	
		Jun	Dec	Jun	Dec	Jun	Dec	Jun	Dec
1	Curitiba	14.82	19.78	22.49	24.03	20.09	21.63	24.89	26.43
4	Brasília	18.44	21.26	23.62	24.49	21.22	22.09	26.02	26.89
7	Petrolina	24.32	27.08	25.44	26.30	23.04	23.90	27.84	28.70
8	Belém	26.24	26.29	26.03	26.05	23.63	23.65	28.43	28.45

The indoor thermal discomfort was quantified in degrees-hour (Kh) of heat or cold conditions. Each degree-hour (1 K/h) relates to the discomfort due to dry-bulb temperature once this is under the lower limit (cold) or when it is above the upper limit (heat). Daily, monthly, or annual discomfort levels are the sum of these during the corresponding period.

For the building energy performance, Szokolay [41] presents a simplified method to estimate the cooling or heating energy required to restore indoor thermal comfort, according to Equation 4:

$$E = DH * q \quad (4)$$

where *E* is the energy for cooling or heating the building (Wh/day), *DH* is the daily degrees-hour of discomfort (Kh/day), and *q* is the heat flux by conduction (*qc*) and convection (*qv*), according to Equations 5. *qc* and *qv* are calculated according to Equations 6 and 7:

$$q = qc + qv \quad (5)$$

$$qc = \sum_{i=1}^{n} (A \times U)_i \quad (6)$$

$$qv = 0.33 * V * N \quad (7)$$

qc is the heat flux by conduction (W/K), *A* is the total area of the envelope (walls, roof, windows, floor - m²); *U* is the thermal transmittance (W/m²K), *n* is the number of external parts of the building envelope. *qv* is the heat flux by convection (W/K), *N* is the ventilation rate (volumes/h) and *V* is the room volume (m³).

3. Results and Discussion

3.1 Laboratory Measurements for New and Aged Samples

Spectral reflectances measured in laboratory for

DOI: https://doi.org/10.30564/jaeser.v4i2.2812

new and aged samples are presented in Figure 3. Solar reflectance and thermal emittance are presented in Table 4, for the 9 coatings considered in this research. The thermal emittance was measured only for conditions before natural weathering (new). The measurements show that all the cool white coating samples have high thermal emittance, ranging from 0.89 to 0.91, which confirm the non-metallic material characteristics.

Results showed that the standard white coating S1-STD presented higher solar reflectance (0.91) when compared to cool white coatings with ceramic microspheres, or to standard white coatings S8 and S9 (Table 4). Actually, all coatings presented high rsolar (higher than 0.74) when new, before natural exposure, once conventional white based colors are characterized by the high near-infrared reflectance due to the intrinsic properties of the titanium dioxide (Figure 3).

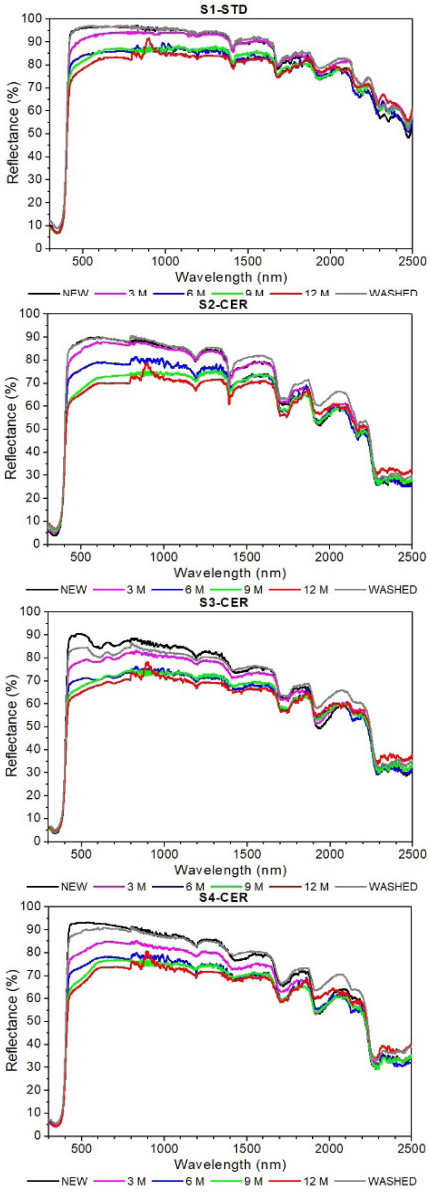

Figure 3. Spectral reflectance for new and aged coatings (3, 6, 9, 12 months) and after a cleaning process.

Figure 4 indicates solar reflectance ranges over time for weather conditions of São Carlos, SP, Brazil. During the first six months of natural weathering, a significant decrease on solar reflectance was observed, mainly related to the specimens weathering. Reflectance modifications are

 DOI: https://doi.org/10.30564/jaeser.v4i2.2812

Table 4. Thermal emittance (ε) and solar reflectance (ρ_{solar}) of the selected samples.

Sample	Thermal Emittance (ε)	Solar Reflectance (ρ_{solar})							
		New	3 months	6 months	9 months	12 months	Washed	$\Delta\rho_{new-12m}$ (-)	$\Delta\rho_{new-12m}$ (%)
S1-STD	0.90	0.91	0.89	0.82	0.82	0.79	0.92	0.12	13
S2-CER	0.91	0.82	0.80	0.73	0.68	0.66	0.83	0.16	19
S3-CER	0.90	0.81	0.75	0.68	0.68	0.66	0.78	0.15	19
S4-CER	0.90	0.85	0.77	0.72	0.70	0.69	0.84	0.16	19
S5-CER	0.91	0.81	0.75	0.68	0.68	0.67	0.80	0.14	17
S6-CER	0.90	0.85	0.81	0.73	0.67	0.69	0.87	0.16	19
S7-CER	0.89	0.78	0.70	0.63	0.62	0.61	0.75	0.18	23
S8-STD	0.91	0.74	0.62	0.62	0.61	0.61	0.74	0.12	17
S9-STD	0.90	0.76	0.71	0.65	0.67	0.62	0.73	0.14	19

mostly due to dust accumulation during the dry period in São Carlos (months 3 to 6), with dust removal as a result of precipitation after the winter (months 6 to 9). The cleaning process restored the solar reflectance for all specimens to a range very similar to the initial solar reflectances (Table 4).

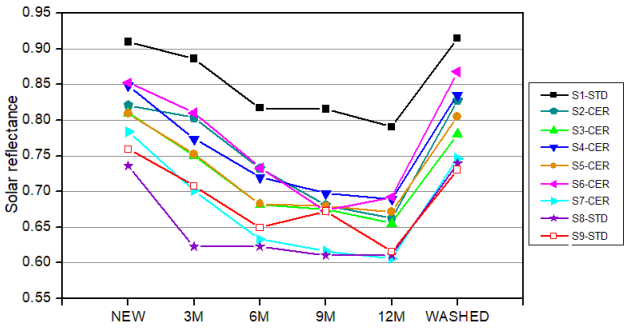

Figure 4. Solar reflectance vs. time and for washed condition after 1 year of natural weathering exposure.

Sample S1 (standard) presented higher solar reflectance reduction after month 6 (from 0.91 to 0.82), with a small reduction from month 6 to 12 of exposure. The SR for sample S1 presented a total reduction of 13% for one year of natural weathering exposure, the lower reduction from all the coatings analyzed in this work. The reduction of solar reflectance during the first 6 months was similar for samples S3 and S4 (with ceramic microspheres), but with a total decrease of 19% after one year. For samples S5, S6, and S7, the reduction was also significant during the first 6 months, with higher difference during the total period of 12 months for sample S7 (23%, rsolar from 0.78 to 0.61).

Sample S2-CER had a significant decrease in the SR after 9 months of exposure (from 0.82 to 0.68), keeping it in this range after 12 months (0.66), with a final reduction of 19%. Sample S8 had a very significant decrease in solar reflectance since the first 3 months (0.74 to 0.62) and kept this range of SR for the next 9 months, with a final solar reflectance of 0.61. On the other hand, sample S9 presented a gradual reduction during all the period of exposure, from 0.76 to 0.62 (total decrease of 19%).

After one year of natural weathering, the coatings' solar reflectance decreased 13% to 23% (respectively for specimens S1 and S7). In addition to weather conditions, soiling (dust and soot deposition, biological growth, etc.) has a large effect on white coatings. Combined actions of weathering and soiling on the specimens can be mainly observed on the spectral reflectance curves in the visible range (380-780 nm) from the solar spectrum (Figure 3). This decrease validates the influence of soiling on the surface appearance [10,24,26,27]. The average decrease about 19% for the samples analyzed in this work are very similar with results obtained by Bretz and Akbari [25]. The authors found 20% solar reflectance reduction for 26 different roofs during the first year of natural weathering.

On the other hand, the surface roughness of specimens with coatings with ceramic microspheres is higher than in smooth standard acrylic coatings. For this reason, the soiling accumulation on the surface is increased according to the surface roughness, which decreases the specimen's solar reflectance. As rougher is the roof surface, higher is the dust deposition, and then the decrease in the long-term solar reflectance [42]. This condition was mainly observed for sample S7, the rougher from all the samples analyzed in this work, as can be noticed in Figure 4, which compares the appearance of the sample for two different conditions: new and after 12 months of natural weathering exposure.

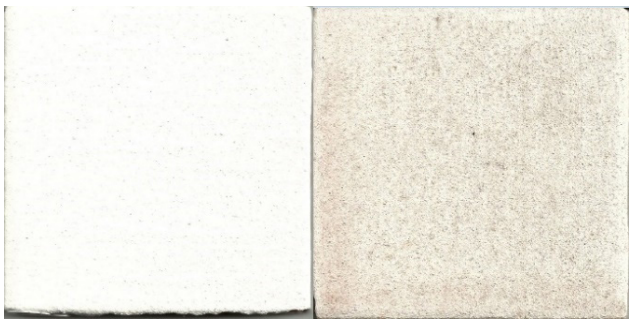

Figure 4. Sample S7-MEC, new and after 12 months of natural weathering exposure

DOI: https://doi.org/10.30564/jaeser.v4i2.2812

The cleaning process restored from 90% to 100% of the original solar reflectance, which means the cleaning process is a very efficient approach to keep the good thermal performance of white roofs, mainly in hot climates. Similar results were achieved by Bretz and Akbari in earlier study [25] and Levinson *et al.* [26].

3.2 Building Simulation Results

3.2.1 Indoor Thermal Comfort for Summer and Winter Conditions

Table 5 presents the degrees-hour/day (Kh/day) of heat discomfort for the simulated building with 9 different solar reflectances (new), and after 12 months of exposure (aged). The results showed that as higher is the roof solar reflectance, the lower is the heat discomfort for buildings located in cities with hot climate (ZB4 and ZB8).

Furthermore, the degrees-hour/day of cold discomfort are presented in Table 6. In this case, the results indicate that as higher is the solar reflectance of a roof surface, the higher is the heating need for colder climates (ZB1 and ZB4), considering the Brazilian scenario. Furthermore, no heating energy was needed for hot climates of ZB7 and ZB8.

The results confirmed that using cool white coatings for cooling roof surfaces are efficient to decrease the indoor heat discomfort for buildings located in tropical/ hot climates. According to the findings, a building with fibrocement roofing (FIBCIM) with solar reflectance of 0.48 presents 70.6 Kh/day of heat discomfort for Belem (ZB8). If this roof was covered with cool white coatings (solar reflectance higher than 0.8), the heat discomfort could be more than 50% reduced in this building, offering indoor thermal comfort conditions for users. And this condition would directly influence the cooling energy needs in buildings, as mentioned in the next analyses.

3.2.2 Building Energy Needs

Based on the degrees-hour of heat (Table 5) and cold discomfort (Table 6), the following cooling and heating energy needs were obtained from Equation 4, as presented in Figure 5 and Figure 6. The results indicated that aging

Table 5. Degrees-hour/day of heat discomfort

Sample	Solar Reflectance		Degrees-hour of discomfort (Kh/day) - Heat							
	rsolar		ZB1		ZB4		ZB7		ZB8	
	New	Aged (12M)	New	Aged	New	Aged	New	Aged	New	Aged
S1-STD	0.91	0.79	0	0	0	0.9	35.4	50.0	27.5	40.1
S2-CER	0.82	0.66	0	0.3	0	3.4	45.6	64.2	36.2	51.8
S3-CER	0.81	0.66	0	0.3	0.2	3.4	46.8	64.2	37.3	51.8
S4-CER	0.85	0.69	0	0	0	1.6	42.5	58.1	33.5	46.5
S5-CER	0.81	0.67	0	0.2	0.3	3.3	47.0	64.0	37.4	50.7
S6-CER	0.85	0.69	0	0	0	1.6	41.9	58.1	33.1	46.5
S7-CER	0.78	0.61	0	1.4	0.8	5.4	49.8	70.0	39.8	57.0
S8-STD	0.74	0.61	0	1.4	1.9	5.4	55.3	70.0	44.5	57.0
S9-STD	0.76	0.62	0	1.1	1.3	4.8	52.7	68.4	42.3	55.5
FIBCIM	0.48	0.39	5.9	9.9	11.2	16.1	84.5	94.7	70.6	79.9

Table 6. Degrees-hour/day of discomfort by cold

Sample	Solar Reflectance		Degrees-hour of discomfort (Kh/day) - Cold							
	rsolar		ZB1		ZB4		ZB7		ZB8	
	New	Aged (12M)	New	Aged	New	Aged	New	Aged	New	Aged
S1-STD	0.91	0.79	104.9	97.7	7.1	4.3	0	0	0	0
S2-CER	0.82	0.66	99.8	55.0	5.1	1.4	0	0	0	0
S3-CER	0.81	0.66	99.2	55.0	4.8	1.4	0	0	0	0
S4-CER	0.85	0.69	101.3	57.1	5.7	2.5	0	0	0	0
S5-CER	0.81	0.67	99.1	56.0	4.8	2.1	0	0	0	0
S6-CER	0.85	0.69	101.6	57.1	5.8	2.5	0	0	0	0
S7-CER	0.78	0.61	97.7	53.3	4.3	1.0	0	0	0	0
S8-STD	0.74	0.61	95.0	53.3	3.4	1.0	0	0	0	0
S9-STD	0.76	0.62	96.3	53.8	3.9	1.1	0	0	0	0
FIBCIM	0.48	0.39	49.15	46.3	0.24	0	0	0	0	0

 DOI: https://doi.org/10.30564/jaeser.v4i2.2812

of white coatings after 1 year of natural weathering increased the cooling energy needs, and this difference is very significant for white coatings with higher initial SR, when compared to the fibrocement tile.

The highest cooling energy need was for the fibrocement roof, when compared to the white coatings, mainly for hot climates (ZB7 and ZB8). The effect of using cool materials (white coatings) can contribute significantly for the reduction of cooling energy needs, as confirmed for some earlier studies [4,43,44].

The simulations showed that, for the climate of Petrolina (ZB7), with very hot and dry conditions, and for the city of Belem (ZB8) with hot and humid climate, the building system considered for simulation demonstrated weak thermal performance, despite the use of white roofs, with high solar reflectance. On the other hand, the use of white roofs decreased the cooling energy needs in these climates, when compared to the fibrocement tile with SR of 0.48 or 0.39.

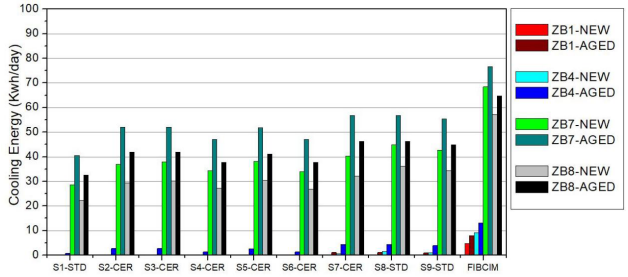

Figure 5. Cooling energy needs estimated for new and aged coatings in different climate conditions

Considering the city of Curitiba (ZB1), subtropical climate with cold winter, the heating energy needs is high for all the solar reflectances considered in the simulation, once the building characteristics are not appropriate for the climate conditions of this zone. However, the difference between energy needs is significant when compared to new and aged roofs, after one year of natural weathering exposure (Figure 6). These results confirm the importance of the maintenance during the lifecycle of roofs, in order to restore the solar reflectance of coatings near to initial condition.

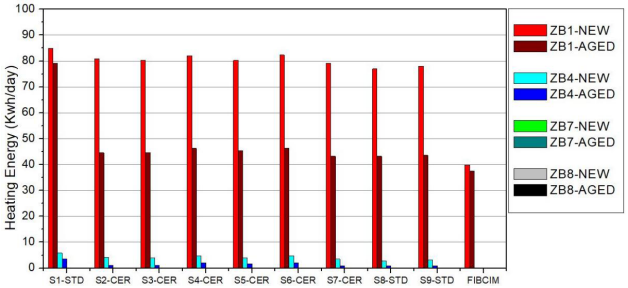

Figure 6. Heating energy needs estimated for new and aged coatings in different climate conditions

Figure 7 presents the correlations between the roof solar reflectance and the energy needs for cooling and heating, according to the outdoor climate conditions. The results showed that, as higher is the solar reflectance of roofs, for the base case analyzed in this work, lower is the cooling energy needs, mainly in hot climate conditions (ZB7 and ZB8). Considering subtropical climates with cold winter in Brazil (ZB1), the heating energy need is higher, but these results are directly related also to the building constructive system simulated. Furthermore, the heating energy need is negligible for tropical and hot climates in Brazil.

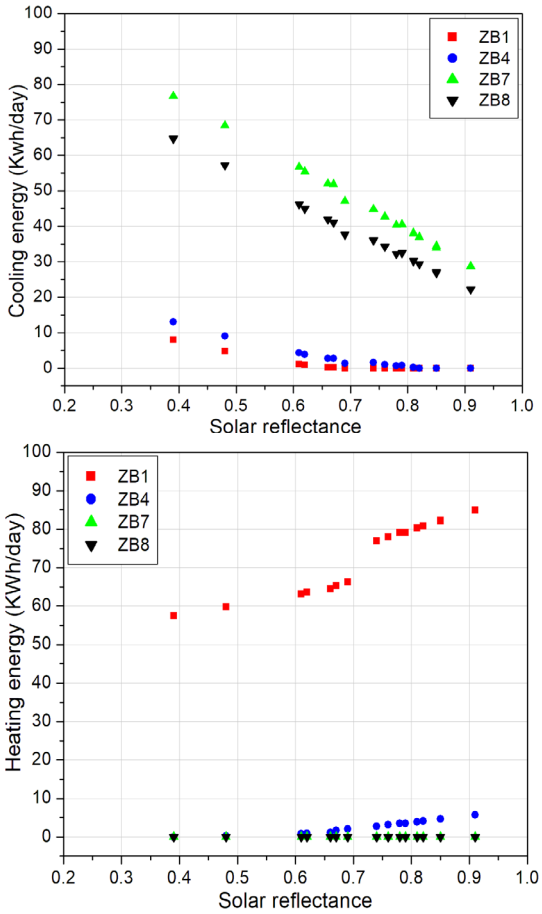

Figure 7. Correlation between roof solar reflectances and the cooling and heating energy needs for different climate conditions in Brazil

4. Conclusions

Cool roofs are effective in maintaining indoor thermal comfort conditions and decreasing the cooling energy needs of buildings, mainly in hot climates. However, solar reflectance may be strongly affected by weathering and soiling after a long period of natural exposure. In this work, nine commercially available white coatings with

DOI: https://doi.org/10.30564/jaeser.v4i2.2812

high solar reflectance were analyzed. Specimens were exposed to natural weathering conditions in a middle-size city in Brazil (São Carlos, SP) for one year. Solar and spectral reflectances were measured in laboratory before exposure (new) and after 3, 6, 9 and 12 months (aged samples). The results indicated that changes on the solar reflectance of cool white specimens were mainly affected by weathering and soiling, even within the first 6 months. After one year of natural weathering, the coatings' solar reflectance decreased 13% to 23%. The average decrease in solar reflectance about 19% for the samples analyzed in this work are very similar with results from earlier studies.

Considering the roughness of the samples, the results indicated that the soiling accumulation on the specimens are higher for rough surfaces, and as rougher is the coating surface, higher is the dust deposition. In consequence, there is a significant decrease in the long-term solar reflectance, mainly observed for sample S7 in this study. A cleaning process was also conducted to identify the capability of the coatings to restore the initial solar reflectance after the period of natural weathering. The cleaning process restored from 90% to 100% of the original solar reflectance, which means the maintenance is a very efficient approach to keep the good thermal performance of white cool roofs, mainly in hot climates.

Computer simulations were conducted to assess the cooling and heating energy needs for a residential building located in different climate conditions in Brazil, considering new and aged solar reflectances of samples analyzed in this research. The results indicate that as higher is the solar reflectance of roof surfaces, the lower is the heat discomfort and the cooling energy need for buildings located in hot climate cities (ZB7 and ZB8). On the other hand, as higher is the solar reflectance, the heating energy need increases for buildings located in subtropical climates with cold winters, considering the Brazilian scenario. The results also indicated that the aging of white coatings increased cooling energy needs, and this difference is very significant for white coatings with higher initial SR, when compared to the fibrocement tile with initial SR of 0.48.

In conclusion, the proposed analysis showed how the use of cool coatings on roofs could be a passive solution for buildings in tropical and hot climates, which contribute to increase indoor thermal comfort conditions and decrease cooling energy needs. In particular, the weathering and soiling of roof surfaces may be considered in these analyses once the effect on the solar reflectance over time cannot be neglected. In this case, maintenance through cleaning processes can be an effective solution to restore the initial solar reflectance. The effect of aging on the thermal performance of materials from the building envelope is significant and cannot be ignored in the design of green buildings. The results emphasized the importance of developing a new generation of cool coatings, relatively easy to clean and also able to maintain the initial solar reflectance for a long period.

The findings presented in this work apply to a particular building configuration under to specific climate conditions. Future research is needed to account for the aging of the coatings after 3 years of natural weathering exposure, as recommended by the Cool Roofing Rating Council [45] and earlier studies [20,24]. Different building systems may also be analyzed to identify the influence on the cooling and heating energy needs according to the aging of roofs solar reflectance.

Acknowledgements

This work was funded by The State of São Paulo Research Foundation (FAPESP, Nº 08/58700-0), and the National Council for Scientific and Technological Development (CNPq, N° 402720/2016-4).

References

[1] Kleerekoper, L.; Van Esch, M.; Salcedo, T.B. How to make a city climate-proof, addressing the urban heat island effect [J]. Resour. Conserv. Recycl., 2012, 64: 30-38. (http://dx.doi.org/10.1016/j.resconrec.2011.06.004).

[2] Muscio, A. The solar reflectance index as a tool to forecast the heat released to the urban environment: potentiality and assessment issues [J] Climate, 2018, 6,12. (http://dx.doi.org/10.3390/cli6010012).

[3] Wang, C.; Wang, Z.; Kaloush, K. E. Critical review and gap analysis of impacts from pavements on urban heat island [R]. National Center of Excellence for Smart Innovations, Arizona State University. 2020. Final Report. (https://ncesmart.asu.edu/gap-analysis-of-impacts-from-pavements-on-uhi/).

[4] Synnefa, A.; Santamouris, M.; Akbari, H. Estimating the effect of using cool coatings on energy loads and thermal comfort in residential buildings in various climatic conditions [J]. Energy and Buildings, 2007, 39: 1167-1174. (https://doi.org/10.1016/j.enbuild.2007.01.004).

[5] Jayasinghe, M. T. R.; Attalage, R. A.; Jayawardena, A. I. Roof orientation, roofing materials and roof surface colour: their influence on indoor thermal comfort in warm humid climates [J]. Energy for Sustainable Development, 2003, 7, n.1: 16-27 (https://doi.org/10.1016/S0973-0826(08)60345-2).

[6] Brazilian Standard. NBR 15220-3: Thermal performance in buildings - Brazilian bioclimatic zones and building guidelines for low-cost houses [S]. Rio de Janeiro: ABNT, 2005. (In Portuguese).

 DOI: https://doi.org/10.30564/jaeser.v4i2.2812

[7] Ramos, G. *et al*. Adaptive behaviour and air conditioning use in Brazilian residential buildings [J]. Building Research & Information, 2020. DOI:org/10.1080/09613218.2020.1804314.

[8] United Nation Environment Programme. Building and climate change: status, challenges and opportunities [R]. 2007. (http://hdl.handle.net/20.500.11822/7783).

[9] Empresa de Pesquisa Energética. Brazilian Energy Balance 2020: Year 2019 [R]. Rio de Janeiro: EPE, 2020. (https://www.epe.gov.br/sites-pt/publicacoes-dados-abertos/publicacoes/PublicacoesArquivos/publicacao-479/topico-528/BEN2020_sp.pdf).

[10] Jacob, D.; Kotova, L.; Teichmann, C.; Sobolowski, S.; Vautard, R.; Donnelly, C.; Koutroulis, A.; Grillakis, M.; Tsanis, I.; Damm, A.; Sakalli, A.; van Vliet, M. Climate impacts in Europe under +1.5◦C global warming [J]. Earth's Future, 2018, 6: 264-285. DOI: 10.1002/2017EF000710

[11] Ascione, F. Energy conservation and renewable technologies for buildings to face the impact of the climate change and minimize the use of cooling [J], Solar Energy, 2017, 154, 15: 34-100. DOI:10.1016/j.solener.2017.01.022.

[12] Santamouris, M.; Synnefa, A.; Karlessi, T. Using advanced cool materials in the urban built environment to mitigate heat islands and improve thermal comfort conditions [J]. Solar Energy, 2011, 85: 3085-3102. (http://dx.doi.org/10.1016/j.solener.2010.12.023).

[13] Zinzi, M.; Agnoli, S. Cool and green roofs. An energy and comfort comparison between passive cooling and mitigation urban heat island techniques for residential buildings in the Mediterranean region [J]. Energy and Buildings, 2012, 55: 66-76. (http://dx.doi.org/10.1016/j.enbuild.2011.09.024).

[14] Piselli, C.; Castaldo, V. L.; Pisello, A. L. How to enhance thermal energy storage effect of PCM in roofs with varying solar reflectance: Experimental and numerical assessment of a new roof system for passive cooling in different climate conditions [J]. Solar Energy, 2019, 192:106-119. (https://doi.org/10.1016/j.solener.2018.06.047).

[15] Santamouris, M.; Synnefa, A; Kolokotsa, D; Dimitriou, V. Passive cooling of the built environment – use of innovative reflective materials to fight heat islands and decrease cooling needs [J] International Journal of Low-Carbon Technologies, 2008, 3, 2: 71-82. (https://doi.org/10.1093/ijlct/3.2.71).

[16] Gentle, A. R.; Aguilar, J. L. C.; Smith, G. B. Optimized cool roofs: Integrating albedo and thermal emittance with R-value [J]. Sol. Energy Mater. Sol. Cells, 2011, 95, 12: 3207-3215. (https://doi.org/10.1016/j.solmat.2011.07.018).

[17] Paolini, R.; Zinzi, M.; Poli, T., Carnielo, E., Mainini, A. G. Effect of ageing on solar spectral reflectance of roofing membranes: Natural exposure in Roma and Milano and the impact on the energy needs of commercial buildings [J]. Energy and Buildings, 2014, 84:333-343. (http://dx.doi.org/10.1016/j.enbuild.2014.08.008).

[18] Revel, G. M.; Martarelli, M.; Bengoche, M. A.; Gozalbo, A.; Orts, M. J.; Gaki, A.; Gregou, M.; Taxiarchou, M.; Bianchin, A.; Emiliani, M. Nanobased coatings with improved NIR reflecting properties for building envelope materials: development and natural aging effect measurement [J]. Cement Concrete Composites, 2013, 36: 128-135. (https://doi.org/10.1016/j.cemconcomp.2012.10.002).

[19] Tsoka, S.; Theodosiou, T.; Tsikaloudaki, K.; Flourentzou, F. Modeling performance of cool pavements and the effect of their aging on outdoor surface and air temperatures [J]. Sustainable Cities and Society, 2018, 42: 276-288. DOI:10.1016/j.scs.2018.07.016.

[20] Sleiman, M.; Ban-Weiss, G.; Gilbert, H. E.; Francois, D.; Berdahl, P.; Kirchstetter, T. W.; Destaillats, H.; Levinson, R. Soiling of building envelope surfaces and its effect on solar reflectance - Part I: Analysis of roofing product databases [J]. Solar Energy Materials and Solar Cells, 2011, 95, 12: 3385-3399. DOI:10.1016/j.solmat.2011.08.002.

[21] Sleiman, M.; Kirchstetter, T. W.; Berdahl, P.; Gilbert, H. E.; Quelen, S.; Marlot, L.; Preble, C. V.; Chen, S.; Montalbano, A.; Rosseler, O. Soiling of building envelope surfaces and its effect on solar reflectance-Part II: Development of an accelerated aging method for roofing materials [J]. Solar Energy Materials and Solar Cells, 2014, 122: 271–281. DOI:10.1016/j.solmat.2013.11.028.

[22] Sleiman, M.; Chen, S.; Gilbert, H. E.; Kirchstetter, T. W.; Berdahl, P.; Bibian, E.; Bruckman, L. S.; Cremona, D.; French, R. H.; Gordon, D. A. Soiling of building envelope surfaces and its effect on solar reflectance–Part III: Interlaboratory study of an accelerated aging method for roofing materials [J]. Solar Energy Materials and Solar Cells, 2015, 143: 581-590. DOI:10.1016/j.solmat.2011.08.002.

[23] Ferrari, C.; Santunione, G.; Libbra, A.; Muscio, A.; Sgarbi, E. How accelerated biological aging can affect solar reflective polymeric based building materials [J]. Journal of Physics: Conference Series, 2017, 923. DOI:10.1088/1742-6596/923/1/012046.

[24] Akbari, H.; Berhe, A. A.; Levinson, R.; Graveline,

DOI: https://doi.org/10.30564/jaeser.v4i2.2812

S.; Foley, K. Aging and weathering of cool roofing membranes [R]. Report LBNL-58055. Berkeley: Lawrence Berkeley National Laboratory, 2005.

[25] Bretz, S.; Akbari, H. Long-term performance of high-albedo roof coatings [J]. Energy and Buildings, 1997, 25, 2: 159-167. (https://doi.org/10.1016/S0378-7788(96)01005-5).

[26] Levinson, R.; Berdahl, P.; Berhe, A.; Akbari. H. Effect of soiling and cleaning on reflectance and solar heat gain of a light-colored roofing membrane [J]. Atmospheric Environment, 2005, 39: 7807-7824. DOI:10.1016/j.atmosenv.2005.08.037.

[27] Alchapar, N.; Correa, E. Aging of roof coatings solar reflectance stability according to their morphological characteristics [J]. Construction and Building Materials, 2016, 102: 297-305. DOI:10.1016/j.conbuildmat.2015.11.005.

[28] Ferrari, C.; Touchaei, G. A.; Sleiman, M.; Libbra, A.; Muscio, A.; Siligardi, C.; Akbari, H. Effect of aging processes on solar reflectivity of clay roof tiles [J]. Advances in Building Energy Research, 2014, 8, 1: 28-40. DOI:10.1080/17512549.2014.890535.

[29] De Masi, R. F.; Ruggiero, S.; Vanoli; G. P. Acrylic white paint of industrial sector for cool roofing application: Experimental investigation of summer behavior and aging problem under Mediterranean climate [J]. Solar Energy, 2018, 169: 468–487. DOI:10.1016/j.solener.2018.05.021.

[30] Dornelles, K. A.; Caram, R. M.; Sichieri, E. Natural Weathering of Cool Coatings and its Effect on Solar Reflectance of Roof Surfaces [J]. Energy Procedia, 2015, 78: 1587-1592. (https://doi.org/10.1016/j.egypro.2015.11.216).

[31] Mastrapostoli, E.; Santamouris, M.; Kolokotsa, D.; Vassilis, P.; Venieri, D.; Gompakis, K. On the ageing of cool roofs: Measure of the optical degradation, chemical and biological analysis and assessment of the energy impact [J]. Energy and Buildings, 2016, 114: 191-199. DOI:doi.org/10.1016/j.enbuild.2015.05.030.

[32] Aoyama, T.; Sonoda, T.; Nakanishi, Y.; Tanabe, J.; Take-bayashi, H. Study on aging of solar reflectance of the self-cleaning high reflectance coating [J]. Energy and Buildings, 2017, 157: 92-100. DOI:10.1016/j.enbuild.2017.02.021.

[33] Paolini, R.; Zani, A.; Poli, T.; Antretter, F.; Zinzi, M. Natural aging of cool walls: Impact on solar reflectance, sensitivity to thermal shocks and building energy needs [J]. Energy and Buildings 153 (2017) 287–296. (http://dx.doi.org/10.1016/j.enbuild.2017.08.017).

[34] ASTM. ASTM E903-96: standard test method for solar absorptance, reflectance, and transmittance of materials using integrating spheres [S]. ASTM International, 1996.

[35] ASTM. ASTM G173-03: standard tables for reference solar spectral irradiances – direct normal and hemispherical on 37° tilted surface [S]. ASTM International, 2003.

[36] ASTM. ASTM C1371-15. Standard Test Method for Determination of Emittance of Materials Near Room Temperature Using Portable Emissometers [S]. ASTM International, 2015.

[37] U.S. Department of Energy's (DOE) Building Technologies Office (BTO). EnergyPlus – Weather Data [R]. (https://energyplus.net/weather).

[38] Brazilian Standard. NBR 15575: Residential buildings: performance [S]. Rio de Janeiro: ABNT, 2013. (In Portuguese).

[39] Coelho, T. C. C.; Gomes, C. E. M.; Dornelles, K. A. Thermal performance and solar absorptance of asbestos free fibercement roof tiles under different natural aging processes [J]. Ambiente Construído, 2017, 17, 1: 147-161. (dx.doi.org/10.1590/s1678-86212017000100129)

[40] ASHRAE 55: thermal environmental conditions for human occupancy [S]. ASHRAE. Atlanta, 2017.

[41] Szokolay, S. V. Introdução à ciência arquitetônica: a base do projeto sustentável [M]. 2019. Perspectiva, São Paulo. (in Portuguese).

[42] Seker, D. Z.; Tavil, A. Ü. Evaluation of exterior building surface roughness degrees by photogrammetric methods [J]. Building and Environment, 1996, 31, 4.

[43] Pisello, A. L.; Rossi, F.; Santamouris, M.; Synnefa, A.; Wong, N.; Zinzi, M. Local climate change and urban heat island mitigation techniques - the state of the art [J]. Journal of Civil Engineering and Management, 2016, 22: 1-16. DOI:10.3846/13923730.2015.1111934.

[44] Rosado, P.; Levinson, R. Potential benefits of cool walls on residential and commercial buildings across California and The United States: Conserving energy, saving money, and reducing emission of greenhouse gases and air pollutants [J]. Energy and Buildings, 2019, 199: 588-607. DOI:10.1016/j.enbuild.2019.02.028.

[45] Cool Roof Rating Council Portland, 2021. (https://coolroofs.org/).

 DOI: https://doi.org/10.30564/jaeser.v4i2.2812

BILINGUAL PUBLISHING CO.
Pioneer of Global Academics Since 1984

Journal of Architectural Environment & Structural Engineering Research
https://ojs.bilpublishing.com/index.php/jaeser

ARTICLE

Maintenance Management Research of a Large-span Continuous Rigid Frame Bridge Based on Reliability Assessment by Using Strain Monitored Data

Yinghua Li[1*] Kesheng Peng[2] Junyong He[3] Qiangjun Shuai[4] Gang Zou[5]

1. Shixing County Bureau of transportation, Shixing County, Shaoguan City, Guangdong Province, 512500, China
2. HARDA (XIAMEN) PLASTIC CO.,LTD, No.37, Huili Zone, TongAn Industrial Area, Xiamen, China
3. Guangdong College of Industry and Commerce, No. 1O98, Guangzhou North Road, Tianhe District, Guangzhou, China
4. 48-13B, Baohe road 81, Long Gang District, Shenzhen, Guangdong, China;
5. 54-28D, Yi Jin Yuan, Long Cheng Street, Long Gang District, Shenzhen, Guangdong, China

ARTICLE INFO

Article history
Received: 23 April 2021
Accepted: 20 May 2021
Published Online: 27 May 2021

Keywords:
Structural health monitoring
Punctiform time-varying reliability
Critical load effects distribution function
Maintenance reliability threshold
Continuous rigid frame bridge
"Three Sigma" principle

ABSTRACT

When the bridge components needing maintenance are the world problem at present, and the health monitoring system is considered to be a very helpful tool for solving this problem. In this paper, a large number of strain data acquired from the structural health monitoring system (SHMS) installed on a continuous rigid frame bridge are adopted to do reliability assessment. Firstly, a calculation method of punctiform time-dependent reliability is proposed based on the basic reliability theory, and introduced how to calculate reliability of the bridge by using the stress data transformed from the strain data. Secondly, combined with "Three Sigma" principle and the basic pressure safety reserve requirement, the critical load effects distribution function of the bridge is defined, and then the maintenance reliability threshold for controlling the unfavorable load state which appears in the early operation stage of this type bridge is suggested, and then the combination of bridge maintenance management and health monitoring system is realized. Finally, the transformed stress distribution certifies that the load effects of concrete bridges practically have a normal distribution; as for the concrete continuous rigid frame bridge with C50 strength grade concrete, the retrofit reliability threshold should be valued at 6.13. The methodology suggested in this article can help bridge engineers do effective maintenance of bridges, which can effectively extend the service life of the bridge and bring better economic and social benefits.

1. Introduction

In the world, people have recognized the importance of the SHMS for monitoring large-span bridges during in construction and service. At present, the health monitoring system becomes an indispensable part of long-span bridges, of which the role is to supply safety evaluation of bridge construction and operation [1-8]. In recent years, the technology of the SHMS has got a significant improvement, mainly in sensing technology,

**Corresponding Author:*
Yinghua Li,
Shixing County Bureau of transportation, Shixing County, Shaoguan City, Guangdong Province, 512500, China;
Email: lyh304236@163.com

DOI: https://doi.org/10.30564/jaeser.v4i2.3128

sensing systems, innovative strategies for monitored data analysis etc. Ni Y.Q. [9] designed and implemented a sophisticated long-term SHMS consisting of more than 700 sensors with 16 types on the Canton Tower from construction to service. Kim M. H. et al [10] introduced a typical hull monitoring system (HMS) for ship structures, which adopts Long-based strain gauges (LBSG), motion sensors and pressure sensors. Habel W. R. and Rodrigues C. et al [11-12] presented an innovative monitoring method of the SHMS for concrete structures mainly based on the increasingly used Fibre-optic sensor technology. Although many scholars in the world have put forward many data analyzing methods and many structures are installed with SHMS, however, the real function of the health monitoring system has not been realized so far [13-17].

Due to many influence factors of the data collected from the SHMS, such as: environmental factors, large size of the data itself, instability of material properties and the structure shape, the structure load and the material resistance changing with time during the bridge construction and operation stages etc., it makes evaluate the bridge safety in bridge construction or operation stage by the data collected from the SHMS or other methods very difficult. At present, many international experts and scholars have done effective work in the area of using the information acquired from the SHMS for rational maintenance planning of gradually deteriorating structures. For developing advanced bridge management systems, taking RC bridges as an example. Thoft-Christensen [18] proposed to apply reliability theory in bridge management systems, but the paper is strongly based on the reports produced within the EU project. The international workshop [19-20] on structural reliability in bridge engineering has demonstrated the advantages of using reliability based methods in the key field of civil infrastructure systems, but the application of reliability techniques in bridge engineering has lagged behind application in other types of structural systems and there are some limitations of the reliability concepts using in bridge applications. In order to estimate the reliability distributions for bridges, Frangopol and Das [21], and Thoft-Christensen [22] defined the bridges' reliability states and proposed a procedure to estimate the reliability distribution for bridge maintenance, but they just suggested the maintenance reliability threshold of the steel- concrete composite bridge taking the value 4.6 mainly based on theory and experience. In order to shed some light on the past, present, and future of life-cycle management of highway bridges, Frangopol D. M. [23] systematically concluded the birth and growth of bridge management systems, and suggested that the limitations of current bridge management systems could be overcome by using the reliability-based approach. In the process of summary of the recent technology developments in the field of SHM and their application to large-scale bridge projects, Kim J. M. et al [24] suggested an idea of calculating the bridge reliability by using the basis reliability theory and the stress monitored data, but they lack long-term monitoring data and so they don't establish the linkage between structural health monitoring technology and the bridge inspection, maintenance and management exercises. In order to forecast the lifetime performance of a reinforced concrete bridge by the probabilistic framework, Akgul F. and Frangopol D. M. [25] explored general methods for the analysis of the bridge performance in the life cycle and applied their research achievements in more than a dozen concrete bridges located in American Crow Leader states, but there is lack of site-specific or lab test data to revise the deterioration models. For predicting the likelihood and extent of cracking for RC surfaces exposed to chloride ion attack, Stewart M. G. and Mullard J. A. [26] proposed a space and time related reliability analysis method to forecast the probability of crack and damage degree of concrete bridges under environmental erosion, but they achievements need to be used in conjunction with a life-cycle cost analysis to optimize maintenance strategies, inspection intervals and durability design specifications for RC structures. In the case that most of SHM applications focusing on damage detection, Mustafa G. and Catbas F. N. [27] paid attention to investigate the statistical pattern recognition for SHMS by using time series modeling of theory and experimental verification, but the tests are just conducted by using two different structures in laboratory conditions and didn't do a sensitivity analysis to examine the effects of different parameters of the methodology. For cost-effective monitoring planning of a structure system, Kim S. and Frangopol D. M. [28] provided an approach with a time-dependent normalized reliability importance factor (NRIF) of structural components, however, further studies are needed to develop a general framework for cost-effective life time optimal monitoring of structural systems taking into account the uncertainty. How to determine the best maintenance strategies under budget constraints, Orcesia A. D. and Frangopol D. M. [29] researched the optimal maintenance strategies based on monitoring information and shown the benefits of SHMS, however, the lifetime reliability of structures is characterized by survivor functions and the SHM data is only used to update the probability density function of time to failure through a Bayesian process.

 DOI: https://doi.org/10.30564/jaeser.v4i2.3128

In order to do construction safety assessment and long-term prediction of prestressed concrete bridges, Helder S. et al [30] built revised Finite Element Models and set up a long-term monitoring system, and discussed the differences between the measurements and the results obtained with the numerical model, namely the trends due to shrinkage and creep and the variations due to the temperature, but they didn't do in-depth analysis of the long-term monitoring data for bridge construction assessment. How to build reasonable resistance prediction model and load effect prediction model to predict reliability of aging bridges, Liu Y. F. et al [31] adopted the Bayesian dynamic models (BDMs) to predict the structural load effects based on the monitored data, and calculated the structural reliability indexes with First Order Second Moment method (FOSM), however, the monitored load effect data is little and the monitoring duration is in short time, and so the predicted results could not be consistent with the actual condition. How to use different methods to obtain a fast and accurate evaluation result with the SHM, Dong and Yuan [32] presented a multi-agent fusion and coordination system to deal with the damage identification by the strain distribution and structure joint failure, however, the validation study of multi-agent system should be considered in the future.

As can be seen from the above literature, the limitations of current bridge management systems can be overcome by using the reliability-based approach, but there is still lack of long-term health monitoring data to validate the above idea. In addition, there is little monitoring data from SHMS for the assessment of bridge safety at the time, and the bridge maintenance strategy by the use of SHMS during construction or operation is mainly based on expert experience and theoretical analysis. Therefore, in this paper, combined with large amount of strain monitoring data of a bridge SHMS, we presented a methodology of calculating reliability, of which the main purpose is to make the association between SHM technology and bridge inspection, maintenance and management exercises. This method is useful for bridge engineers to do bridge maintenance. The background bridge will be used as a case study for this work.

2. Illustration of the Bridge SHMS and Initial Data Processing

2.1 SHMS of the Background Bridge

The background bridge is located in Zhaoqing city of The Pearl River Delta in Guangdong province. The superstructure of the bridge main beam is a continuous box-beam system with a total of eight main piers and 7 main spans. The first span is 145.4 m long and the sixth span is 87 m long, and the 4 center spans are all 144 m long. The cross section of box girder is a single-box and single-chamber. The width of box girder top plate is 12.5 and the width of the base plate is 6.8 m. The transverse slope of the bridge deck is 2.0% and the longitudinal slope of the bridge deck is 0.15%. The heights, thickness of base plate and thickness of web plate vary from 8 m to 2.8 m (change according to 1.6 order power parabola), 1 m to 0.32 m and 0.9 m to 0.45 m respectively in cross sections from the supporting base to the mid-span. The main beam is fully prestressed concrete structure with the arrangement of vertical, horizontal and longitudinal prestress, and the prestressing tendons are $15\Phi^j 15.24\,\text{mm}$ steel strand (strength: $R_y^b = 1860\,\text{MPa}$), $2\Phi^j 12.7\,\text{mm}$ steel strand (strength: $R_y^b = 1395\,\text{MPa}$) and high strength rebar respectively.

The measuring points of the SHMS in girder locate near piers, in mid-span and in 1/4 span. The section locations are illustrated in Figure 1. The embedded locations of strain variety sensor (The sensor is shown in Figure 1) in each section are illustrated in Figure 3 with given numbers. The manufacture of the sensors is CHANGSHA KINGMACH HIGHTECHNICS CO., LTD [33]. With the given name of cross section and number, a sensor in the SHMS can be located in the girder uniquely, such as a sensor is named 3-4MID-1, which means it locates in the top plate center of the mid-span cross-section between pier 3# and pier 4#. The measuring time interval of each sensor is 1 hour. The sampling parameters of JMZX-215 type strain gauge are listed in Table 1. So far, monitoring of the bridge is still continuing and data for the past few years has been acquired.

Table 1. Sampling parameters of JMZX-215 type strain gauge

Type	Range	Sensitivity	Length	Remarks
Intelligent digital vibrating strain gauge	±1500$\mu\varepsilon$	1$\mu\varepsilon$	157 mm	Strain gauge embedded in concrete

Figure 1. Gauge installed inside the bridge prestressed concrete beam before casting

DOI: https://doi.org/10.30564/jaeser.v4i2.3128

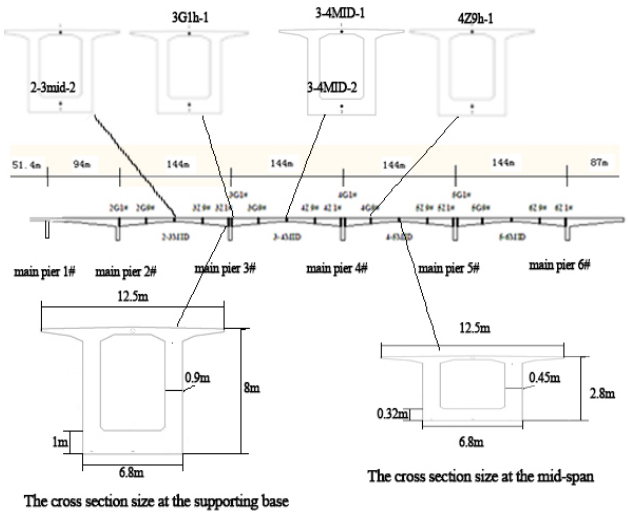

Figure 2. Cross section size and locations with sensors in the bridge of SHMS

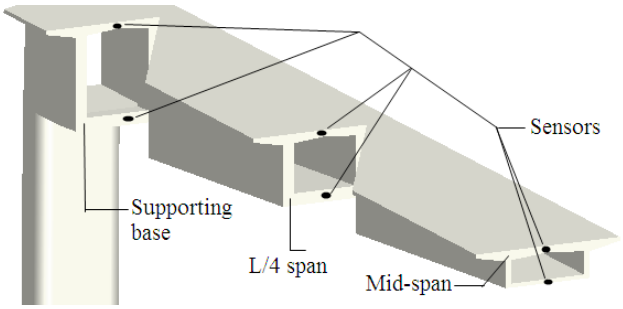

Figure 3. Typical positions of the sensors with the half-span bridge

2.2 Monitoring Data

At present, the bridge has been monitored for more than 4 years. In the paper, the data from the sensors named 3G1H-1, 3-4MID-1, 4Z9H-1 and 3-4MID-2 are used as examples, of which the monitoring time range is from March 2006 to April 2010. In fact, there are tens of thousands of data collected from the health monitoring system. The monitored data should be pre-processed firstly to delete some singular values which may be induced by strong thunders and other unexpected factors. The principle of deleting the singular values is: firstly, find out the difference between the values of each sampling point and its previous sampling point; then, if the value of the difference is greater than 200 micro-strains (engineering experience value [34]), the signal value of this sampling point is regarded as singular value and will be removed. Figure 4 shows the outline of the original data after the singular values are deleted. Some gaps appear in Figure 4, which signifies that some data are not collected due to data acquisition system fault.

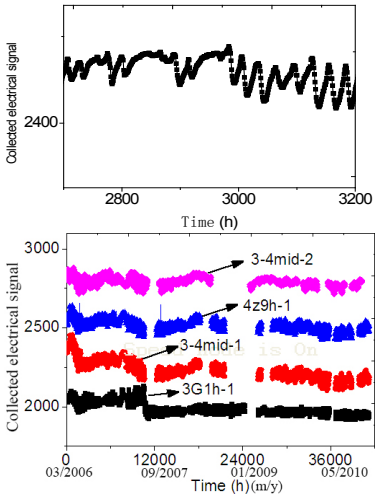

Figure 4. The data profile of the sensor

2.3 Data Pre-treatment

2.3.1 The Step of Pre-treatment

Because the monitored strain data can't be used for reliability calculation directly, and they should be implemented some processing for transforming into stress data, and then used to calculate the reliability index. The data processing method is as follows:

(1) Read the sensor initial setting value after the cast concrete is solidified. As the sensors were embedded before the concrete casting, the concrete hydration heat will produce initial strain in sensors. So, this value should be subtracted from the monitored strain value, of which the goal is to get setting values of the each sensor after the concrete is solidified.

(2) Subtract the shrinkage and creep strain values from the monitored strain value. As for those lacking of monitored data, they can use the finite element technology and build the finite element model of the bridge calibrated by field measured data to get the shrinkage and creep values. In this paper, we acquire the shrinkage and creep values corresponding to each sensor position from the long-term monitored strain data and then subtract this value from the measured strain values. The shrinkage and creep strain data extraction method is instructed in section 3.4 in detail. Of course, the extracted shrinkage and creep values are just approximate value.

(3) Subtract the thermal expansion strain value from the monitored strain value. As for the variation of environmental temperature, the monitored strain data include thermal strain. As we mentioned on the above paper, the sensor adopted in this paper can simultaneously monitor temperature. So, we can easily remove the thermal strain from the monitored strain, the elimination formula is as follows:

 DOI: https://doi.org/10.30564/jaeser.v4i2.3128

$$\varepsilon_r = \varepsilon - (T - T_0)(F - F_0) \quad (1)$$

In the above formula: F_0=10$\mu\varepsilon$/°C, which is the coefficient of linear expansion of the sensor steel wire as for concrete bridges; T_0 is the initial temperature; F is the coefficient of linear expansion of structure; ε is the measured strain; T is the measured temperature.

After processing, the stress data can be converted from the processed strain data by the following formula:

$$\sigma = E \cdot \varepsilon \quad (2)$$

In the formula: E is the concrete elastic modulus, and the value is: $E = 3.45 \times 10^4 MPa$ (28 days of age). This paper focuses on the performance of the bridge during early service, and the time lasts not long. During this time section, the change of modulus E tends to be stable, and so this paper neglect the effects caused by the concrete elastic modulus E.

In case of a limited number of measurements of SHMS, Bayesian methodology [31] can be used to update the structural resistance and load effects. Nevertheless, continuous monitoring over a long-term period can increase the reliability of the assessment and prediction of structural performance. In general, the damage development speed of bridges is very slow. Considering this reason and the data sample size etc., this paper determines each statistical time section of the monitoring data is 6 months, and so the data sample size of each statistical time section will reach 4000, and are enough for statistics. The derived load effects include the influence of environmental temperature, the bridge beam curve shape, the traffic loads (contain heavy loads) and resistance changing with time during the bridge operation etc. Due to many influence factors, the derived load effects are very hard to relate to absolute stresses.

According to the climate characteristics of the bridge which locates in Chinese Pearl River Delta area, then, the time statistics section has two kinds: one is called summer section, from May to October; another is called winter section, from November to April of the next year. In this paper, the statistical time starting point is 2006 May and the end point is 2010 April, and each statistical time section is named in a series A, B, C, D, E, F, G, H.

2.3.2 Extraction of creep and shrinkage deformations from the monitoring data

The shrinkage and creep data extraction method is to extract data from the same time in a day during different periods, and assumes that the temperature field is the same at the moment, detailed steps are:

(1) Select the data monitored between the time 2:00 ~ 4:00, because the traffic flow is small at this time section and the elastic strain caused by vehicle load can be ignored.

(2) We assume that the temperature of the top and base plate of the box girder cross section is the same at the selected time section. Only in this way, the influence of the non-uniform temperature stress along the bridge longitudinal and vertical direction can be eliminated.

In addition, another data extraction principle is as follows: firstly, give the time series $(t_1, t_2, \cdots t_n)$; then, due to the creep and shrinkage of concrete growth rate gradually slows down, so, when determine the time series $(t_1, t_2, \cdots t_n)$, we should make the time series firstly dense and then sparse, and make the time interval increase gradually. Give the first calculation age t_1 and the second calculation age t_2. The other time point can be calculated in the following way [35]:

$$\frac{t_i - t_1}{t_{i-1} - t_1} = 10^{1/10} \quad (3)$$

Based on the above means, we can get the shrinkage and creep values corresponding to each sensor. Here, we show the shape of the extracted shrinkage and creep values of the sensors named 2G9h-1, 3Z9h-1and 3Z9h-2 in Figure 5. Then, based on the acquired shrinkage and creep values and Interpolation method, we can get shrinkage and creep values at any time. Figure 5 is just to illustrate the extracted results of creep and shrinkage strain values. From Figure 5, we can see that the extracted shrinkage and creep values change greatly and then become basically stable after a year or so. So, we subtract 1year shrinkage and creep strain values from the monitoring data, of which the main purpose is to delete the effect of concrete shrinkage and creep. Of course, these extracted values are just approximate values. As for the sensor 2-3M ID-2 adopted in Section 4.1, the concrete shrinkage and creep strain value about 1 year take 52.3 ($\mu\varepsilon$), and we deduct this value from the monitoring data of the sensor 2-3M ID-2.

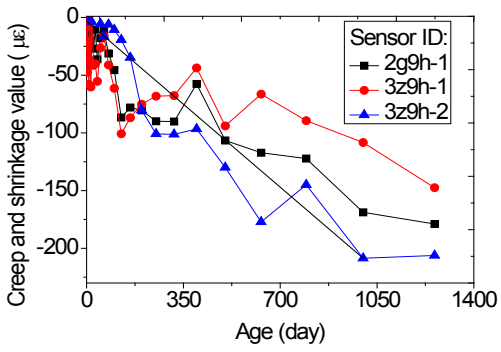

Figure 5. The measured trend of shrinkage and creep strains

DOI: https://doi.org/10.30564/jaeser.v4i2.3128

3. Main Idea of Reliability Calculation Based on Strain Monitoring Data

3.1 Calculation Procedure

According to the method adopted by Ko and Ni [24] (Ko, 2005), the failure probability P_f of the structural components can be calculated by using the member resistance R and the load effects S [36]. However, the derived result is accurate only if the random variables statistics are independent and obey the normal distribution, and then we can only get approximate results. If the probability density functions $f_R(r)$ of the resistance R and the probability density functions $f_S(S)$ of the load effects S both obey normal distribution respectively, the calculation formula of the reliability index β can be written as:

$$\beta = -\Phi^{-1}(P_f) = (\mu_R - \mu_S) / (\sigma_R^2 + \sigma_S^2)^{1/2} \tag{4}$$

In the formula: Φ^{-1} is the inverse function of the standard normal distribution; μ_R and μ_S are the mean of the resistance and load effects respectively; σ_R and σ_S are the standard deviation of the resistance and load effects respectively.

3.2 Structure Resistance Probability Density Function

For prestressed concrete bridges, as the applied stresses and stress capacities both are dependent on concrete material properties, and the correlation between the applied stresses and stress capacities is basically independent, so, the concrete strength probability distribution function is taken as the probability density function of the resistance R, which generally obeys Gaussian distribution and can be obtained by in situ material tests. As for the concrete tensile properties, An equation is applied to describe the concrete tensile strength distribution function:

$$f_{Rt}(r) = \frac{1}{\sqrt{2\pi}\sigma_t} e^{-\frac{(r-\mu_t)^2}{2\sigma_t^2}} \tag{5}$$

In the above: $f_{Rt}(r)$ are the Gaussian distribution function of the tensile strength of concrete; μ_t is the mean of the tensile strength of concrete; σ_t^2 is the variance of the tensile strength of concrete.

The concrete compressive strength distribution function alsoobeys Gaussian distribution. The mean compressive strength μ_c of concrete material is obtained by in situ test in this article. With regard to the variance σ_c^2 of the compressive strength of concrete, according to the highway reinforced concrete and prestressed concrete design specification [37], the variation coefficient can take δ_f=0.11, and then the variance σ_c^2 of the concrete compression strength used in the bridge can be obtained. In this paper, the initial compressive strength mean and standard deviation of the concrete used in the bridge can be acquired, seen in Table 2. Because of lacking concrete field test tensile strength data, so, we estimate tensile strength parameters theoretically. According to the specification [37], the relationship between the concrete mean axial tensile strength and the mean standard cube compressive strength is:

$$\mu_f = 0.88 \times 0.395 \mu_{f150}^{0.55} \tag{6}$$

Therefore, the concrete member axial tensile strength μ_{ft} can be obtained by the above formula. Also, according to the variation coefficient δ_f suggested in the specification [37], which can take the value 0.11, then, the variance $\sigma_t^2$of the concrete axial tensile strength can be acquired. Therefore, the concrete initial tensile strength mean and standard deviation used in the bridge can be derived, which is shown in Table 2.

Table 2. The concrete compressive and tensile strength mean and standard deviation values (28 days curing)

Parameters	Mean (units: MPa)	Standard deviation (units: MPa)
compressive	55.12	6.063
tensile	3.2783	0.361

In fact, due to the durability and fatigue and other factors, concrete strength changes over time. As for bridge structures, live load effects are also quite significant. In addition to the factor of durability, the material fatigue can also cause concrete strength decay, and its effect should not be ignored in practical engineering. Zhang J. L. et al [38] tested the concrete strength of more than 10 old bridges located in the Central South and the South China regions by means of hammer, core samples drilled and ultrasonic wave methods, and 703 useful data were obtained, and suggested the time-varying model of concrete compressive strength for concrete bridges given by:

$$\begin{cases} \mu_{fcu}(t) = \mu_{fcu0} \cdot \eta(t) = \mu_{fcu0} \cdot [1.378 e^{-0.0187(\ln(t)-1.7282)^2}] \\ \sigma_{fcu}(t) = \sigma_{fcu0} \cdot \zeta(t) = \sigma_{fcu0} \cdot [0.0347t + 0.9772] \end{cases} \tag{7}$$

In the above: μ_{fcu0} and σ_{fcu0} are the concrete mean and standard deviation of cube compressive strength respectively (28 days curing); $\mu_{fcu}(t)$ and $\sigma_{fcu}(t)$ are the concrete cubes mean and standard deviation functions of the compressive strength respectively after t years service. The symbols $\eta(t)$ and $\zeta(t)$ are the mean and standard deviation

 DOI: https://doi.org/10.30564/jaeser.v4i2.3128

variation functions of the concrete compressive strength respectively. In fact, Equation (7) is revised by means of the bridge structure in situ measured data, which is under the dual roles of durability and fatigue and close to the actual bridge structure conditions. As the bridge adopted in this article lacks actual traffic statistical data and it also located in South China's Pearl River Delta region, Equation (7) is so adopted here to deduce the changing law of concrete tensile strength, combined with Equation (6) and Equation (7), this paper suggests:

$$\begin{cases} \mu_t(t) = \mu_{t0} \cdot \eta(t)^{0.55} = \mu_{t0}[1.378e^{-0.0187(\ln(t)-1.7282)^2}]^{0.55} \\ \sigma_t(t) = \sigma_{t0} \cdot \zeta(t)^{0.55} = \sigma_{t0}[0.0347t + 0.9772] \end{cases} \quad (8)$$

In the above: μ_{t0} and σ_{t0} are the concrete cube mean and standard deviation of tensile strength with 28 days curing respectively; $\mu_t(t)$ and $\sigma_t(t)$ are the time-varying equations of the mean and standard deviation respectively after the concrete cube services t years.

3.3 Probability Density Function of Structural Load Effects

Jo K. M. and Ni Y. Q. [24] assumed that the probability density function of load effects of the bridge members also obey normal distribution. So, the load effects probability density function can be expressed as:

$$f_s(s) = \frac{1}{\sqrt{2\pi}\sigma_s} \exp\left(-\frac{(s-\mu_s)^2}{2\sigma_s^2}\right) \quad (9)$$

In the above: $f_s(s)$ is the Gaussian distribution function of load effects of the bridge concrete members ; μ_s is the component load effects mean; σ_s^2 is the component load effects variance.

As the resistance and load effects of the bridge components are both obey normal distribution, therefore, the reliability index can be calculated according to Equation (4). Because the resistance R of the concrete has two probability density functions, therefore, according to Equation (4), there are two reliability indexes responding to the load effect probability density function $f_s(s)$. In view of this, the calculation methodology in this paper is: if there is $|\mu_s - \mu_c| < |\mu_s - \mu_t|$, we calculate the reliability index β_c by Equation (4), of which the meaning is that the load stress distribution is gradually close to concrete compressive with time; if not, we calculate the reliability index β_t, of which the meaning is that the load stress distribution is gradually close to tensile strength distribution with time. The calculation diagram is shown below:

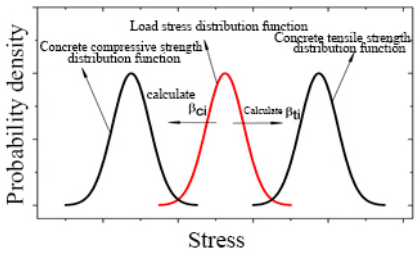

Figure 6. The reliability index calculation diagram

4. Calculation of the Reliability Index

4.1 Resistance and Load Effects Distributions

We take the monitored data collected from the sensor named 2-3MID-2 embedded in the mid-span section base plate between the bridge 2# and 3# pier for example, and we process the data according to the process method suggested in Section 3.3. The transformed strain data are presented in Figure 7.

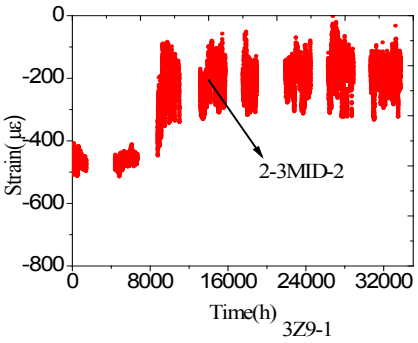

Figure 7. The strain data transformed from the monitoring data

We convert the above processed data into stress data according to Equation (2), and then do statistical analysis of the stress data, seen from Figure 7. We find that the stress data are basically normally distributed, and so we deal with the statistical data by Gaussian distribution fitting, seen in Figure 8. A vertical line in some pictures in Figure 8 with the value -3 MPa means that the stress distribution is close to the concrete tensile strength distribution.

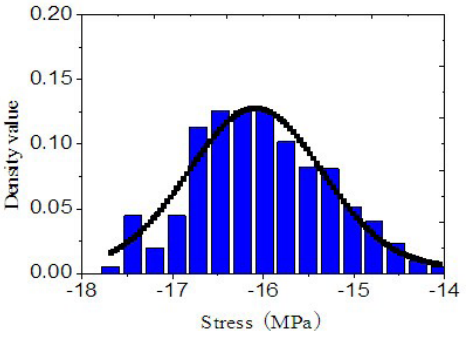

(A) 2006.05 ~ 2006.10

DOI: https://doi.org/10.30564/jaeser.v4i2.3128

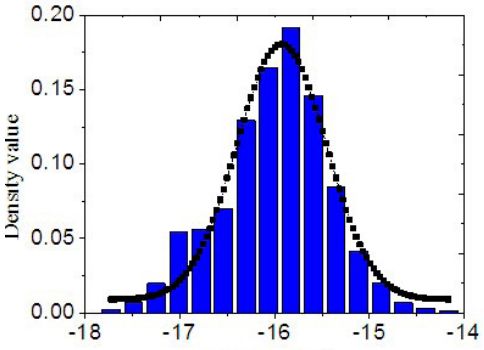

(B) 2006.11 ~ 2007.04

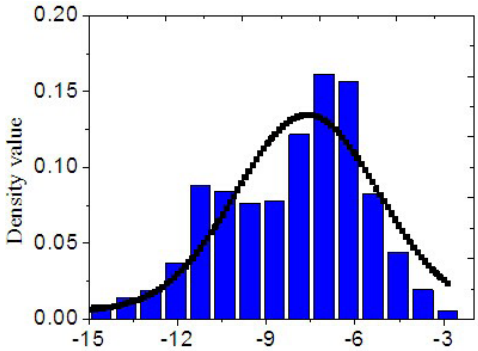

(C) 2007.05 ~ 2007.10

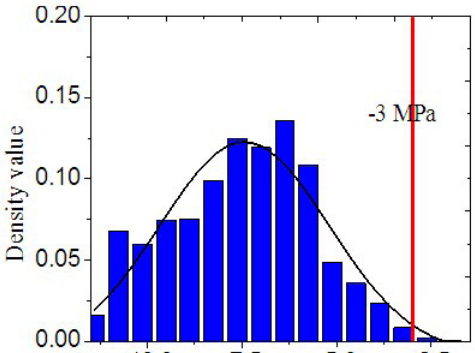

(D) 2007.11 ~ 2008.04

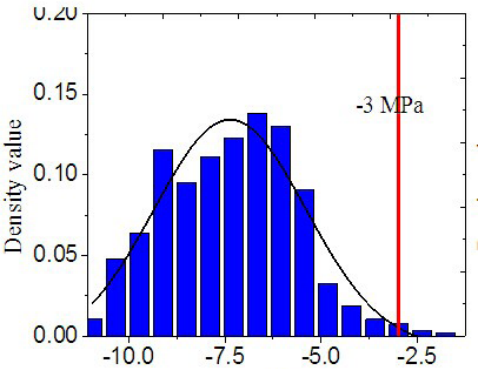

(E) 2008.05 ~ 2008.10

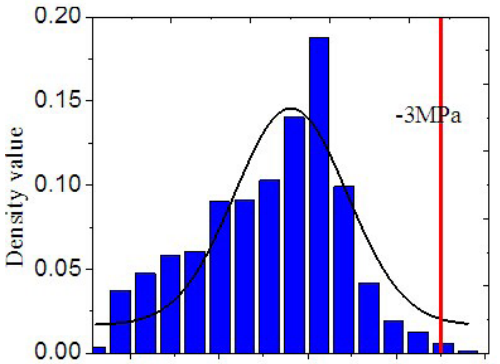

(F) 2008.11 ~ 2009.04

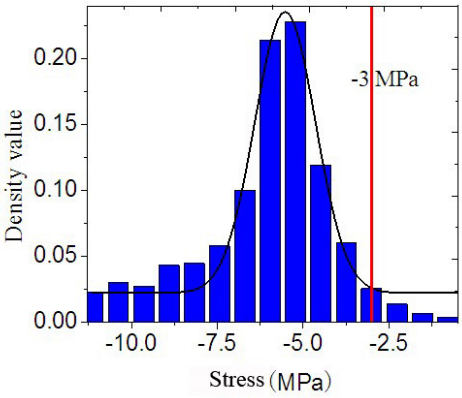

(G) 2009.05 ~ 2009.10

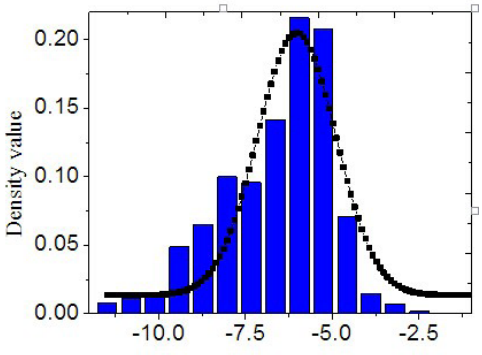

(H) 2009.11 ~ 2010.04

Figure 8. Gaussian distribution fitting of the stress distribution statistics

Through the above statistics analysis of the converted data, the load effect mean and standard deviation of probability distribution can be obtained for each time section, of which the standard deviation is shown in Table 3. We can see that the results of statistics analysis in Table 3 are variable, and the main reason may be that it is caused by the climate change, data loss etc.

 DOI: https://doi.org/10.30564/jaeser.v4i2.3128

Table 3. The load effect mean and standard deviation of probability distribution of each time section (units: MPa)

Time series	A	B	C	D	E	F	G	H	Mean
Mean values	-16.09	-15.93	-7.62	-7.44	-7.37	-6.38	-5.52	-6.01	
Standard deviation	0.733	0.944	2.403	2.24	1.97	1.27	0.886	1.13	1.447

As can be seen in Figure 7, the load effect distribution $f_s(s)$ is gradually close to the tensile strength distribution $f_{Rt}(r)$ and then basically keep stable. Therefore, this paper only calculates β_t of the position in the mid-span base plate. Based on the methodology in the above, we can calculate the punctiform time-dependent reliability index around the sensor embedded position in the bottom plate of the mid-span cross-section, which is illustrated in Figure 9, and it shows that the reliability index β_t reduced significantly after the bridge was in service about a year's time or so. Fortunately, it remains stable a year later. As for this phenomenon, the main reason may be that the concrete creep and shrinkage strain values change rapidly in the first few years and lead to the mid-span sinking of the concrete bridge, which can be reflected in section 3.3.2, and the design of the bridge doesn't consider this factor precise enough.

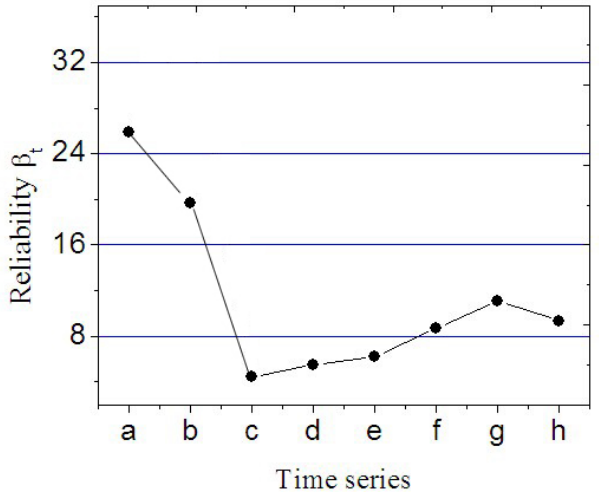

Figure 9. The reliability β_t change over time which is calculated by $f_{Rt}(r)$

As the reliability index calculated by the above proposed methodology only reflects the state around the sensors, so, we name it punctiform time-varying reliability.

4.2 Brief Introduction of "Three Sigma" Principle and Maintenance Reliability Threshold

Since the last twentieth century, the human productivity continuously develops, and the product and quality are continuously improved. In twenty-first century, the quality becomes the theme of the new century. There is firstly "Three Sigma" principle in quality management in the past, and now "Six Sigma principle" is suggested. At present, the procedure guarantee capability and management level of the majority enterprises (including construction enterprises) in the world is in the range about "Three Sigma" to "Four Sigma" [39].

"Three Sigma" principle itself is generated from normal distribution of the statistics. The normal distribution is determined by two important parameters: the mean and standard deviation. In total quality management, there is:

$$P(\mu - 3\sigma < x < \mu + 3\sigma) = \Phi(3) - \Phi(-3) = 0.9973 \qquad (10)$$

The above formula shows that the probability of the quality characteristic values falling without the confidence interval (μ-3σ, μ-3σ) is only 0.27%.

4.3 Determination of Maintenance Reliability Threshold

Bridge construction project is inherently a planned or under construction building products, and obsess the same quality connotation with other products, namely a set of natural characteristics to meet the need, which includes: safety, adaptability, reliability, economy and environmental suitability etc, of which the main influence factors are: the human factors, technical factors, management factors, environmental factors and social factors etc. Therefore, the idea of total quality management can also be applied on the bridge from design, construction, operation, to maintenance.

Frangopol [21] put forward 5 kinds of bridge reliability status, and assume that the bridge life can be seen as a reliable state process from the intact state ($\beta \geq 9.0$) to the unacceptable state ($\beta < 4.6$). However, Frangopol just suggested the maintenance reliability threshold 4.6 (corresponding to the failure probability 1e-6) of the steel-concrete composite bridge mainly according to theory and experiences. Ko J. M. and Ni Y. Q. [24] just suggested an idea of calculating the bridge reliability based on the basis reliability theory and the stress monitored data, and not propose how to decide the maintenance reliability threshold with the monitored data. As for this problem, combined with the monitoring data, this paper puts forward a method to determine the maintenance reliability threshold of the prestressed concrete bridge during early operation stage.

As can be seen in Figure 8, the stress state of the mid-span base plate is gradually changed from compression to tension, and then the pressure safety reserve becomes small. Seen from Figure 8 (d) - (g), there is compressive

DOI: https://doi.org/10.30564/jaeser.v4i2.3128

stress between 2 ~ 3 MPa of the unfavorable load state which is unfavorable on the bridge, which means that the pressure safety reserves is too low and is inconsistent to the general engineering experience value requests that the pressure safety reserve is at least 2 ~ 3 MPa under the most unfavorable load conditions.

According to the above description, at present, the procedure guarantee ability and management level of most enterprises in the world are about in the range from "Three Sigma" to "Four Sigma". Therefore, this paper adopts "Three Sigma" standard management level to determine the maintenance reliability threshold of the bridge. According to the request that the pressure safety reserve is at least 2 ~ 3 MPa under the most unfavorable load condition, this paper takes the value -2 MPa. Then, the bridge maintenance reliability threshold is calculated as follows:

Firstly, according to "Three Sigma" standard and the minimum -2 MPa of pressure safety reserve requirement, this article defines a critical load effects distribution function for calculating the maintenance reliability threshold, and the calculation diagram is shown in Figure 10, in which we only consider the probability of the abnormal load effects fall in the right confidence interval [$-2MPa$, $+\infty$], and the reason is: taking into account the compressive properties of the concrete, the probability of the abnormal load effects not complying with the design requirements of falling in the left confidence interval [$+\infty$, μ-3σ] is too small and can be basically neglected. Among them, the standard deviation σ_{th} of the defined critical load distribution function is obtained by the monitoring data, and this paper takes the mean σ_{th}=1.447 from Table 3 in Section 4.1. So, based on Figure 10 and σ_{th}=1.447, we can get the mean value of the defined critical load effects distribution function, which is μ_{th}=-5.86MPa.

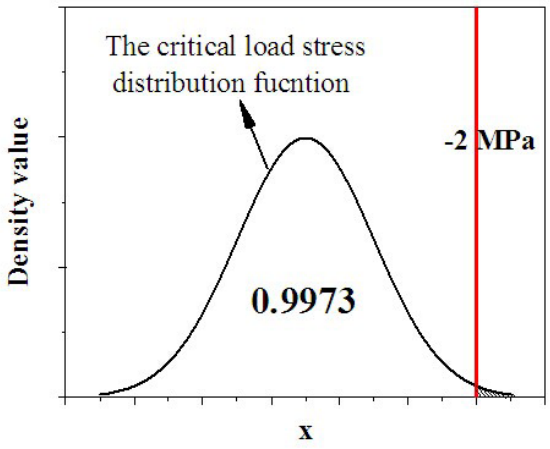

Figure 10. Diagram of the determination of the critical load effect distribution function

Secondly, based on the mean μ_{th} and standard deviation σ_{th} of the defined critical load effects distribution function, using the mean and the standard deviation of the tensile strength shown in Table 2, combined with Equation (4), we have calculated and found the corresponding critical reliability value β_{tth}=6.13, and this value is taken as the maintenance reliability threshold of the background bridge.

Actually, the maintenance reliability threshold is calculated by the concrete tensile strength in the bridge early operation. Therefore, the maintenance reliability threshold suggested in this paper is mainly aimed at the regulation of the early appeared unfavorable internal force state because of the early concrete shrinkage and creep, prestress loss etc.

However, the critical reliability value β_{tth}=6.13 should be revised, of which the main reason is that the traffic loads of each bridge is different and so leads to the calculated values of the Equation (7) and Equation (8) not precise enough.

5. Conclusions

As for the difficulties to make the bridge maintenance strategy, based on the monitored data collected from the SHMS of the background bridge, this paper put forward a calculation methodology of punctiform time-varying reliability and maintenance reliability threshold of this type bridge, and the main conclusions are as follows:

- A method is suggested for the strain monitoring data processing of SHMS (elimination of creep, shrinkage and thermal effects) to get stress data.
- The statistical analysis of the transformed stress data shows that the load effects of concrete bridges basically obey Gaussian distribution, and should be further proved based on hypothesis tests in the next research work plan.
- Based on "Three Sigma" management principle and the transformed stress data, the critical load effects distribution function of this kind bridge is suggested in this manuscript. Then, we suggest that the maintenance reliability threshold of the bridge should be valued 6.13, and finally the combination of bridge maintenance management and health monitoring system is realized.
- The next research project should focus on the bridge maintenance reliability threshold study taking into account the bridge material strength degradation.
- Some important parameter values should be revised by field test data. The methodology suggested in this paper can provide a reference for bridge engineers doing rational bridge maintenance in bridge operation.

Acknowledgements

During the research, the classmates Peng etc. provide

 DOI: https://doi.org/10.30564/jaeser.v4i2.3128

useful help for the study. So, the corresponding author thanks very much for this.

References

[1] Muria V. D. et al., 1991. "dynamic structural properties of cable stayed tampico bridge". J. Struct. Eng., 11 (117).

[2] Cheung M. S., Tadros G. S., 1997. "Field monitoring and research on performance of the confederation bridge". J. CIV. Eng., 6 (24), 951-962.

[3] Curran P., Tilly G., 1999. "Design and Monitoring of the Flintshire Bridge". STRUCT. ENG. INT., 3 (9), 225-228.

[4] Cheung M. S., Naumoski N., 2002. "The first smart long-span bridge in Canada—health monitoring of the Confederation Bridge". Proceedings of the 1st international workshop on structural health monitoring of innovative civil engineering structures, Winnipeg, ISIS Canada Corporation.

[5] Wong K. Y., 2004. "Instrumentation and health monitoring of cable-supported bridges". STRUCT. CONTROL HLTH., 11 (2), 91-124.

[6] Chan T.H.T. et al., 2006. "Fiber Bragg grating sensors for structural health monitoring of Tsing Ma bridge: Background and experimental observation". Eng. Struct., 28 (5), 648-659.

[7] Simon D. N. et al., 2011. "Messina Bridge-Structural Health Monitoring System".

[8] Li H. N. et al., 2014. "Reviews on innovations and applications in structural health monitoring for infrastructures". Struct. Monit. and Maint., 001-045.

[9] Ni Y.Q., 2014. "Sensing solutions for assessing and monitoring super-tall towers". Sensor Technologies for Civil Infrastructures, Woodhead Publishing Series in Electronic and Optical Materials, Volume 2, 246-274.

[10] Kim M.H., Lee J.M., 2014. "Sensing solutions for assessing and monitoring offshore structures". Sensor Technologies for Civil Infrastructures, Woodhead Publishing Series in Electronic and Optical Materials, (2), 50-564.

[11] Habel W.R., 2010. "Structural health monitoring systems for reinforced concrete structures". Non-Destructive Evaluation of Reinforced Concrete Structures: Non-Destructive Testing Methods,Woodhead Publishing Series in Civil and Structural Engineering, (2), 63-94.

[12] Rodriguesa C. et al., 2010. "Development of a long-term monitoring system based on FBG sensors applied to concrete bridges". Engineering Structures, 8(32), 1993-2002.

[13] Abbiati G. et al., 2015. "Time-dependent estimators for on-line monitoring of full-scale structures under ambient excitation". Mechanical Systems and Signal Processing, (60–61), 166-181.

[14] Behmanesha I. et al., 2015. "Hierarchical Bayesian model updating for structural identification". Mechanical Systems and Signal Processing, (64-65), 360-376.

[15] Santos I. L. d. et al., 2014. "A localized algorithm for Structural Health Monitoring using wireless sensor networks". Information Fusion, Special Issue: Resource Constrained Networks, (15), 114-129.

[16] Engel A. et al., 2014. "Hardware-accelerated Wireless Sensor Network for Distributed Structural Health Monitoring". Procedia Technology, 2nd International Conference on System-Integrated Intelligence: Challenges for Product and Production Engineering, (15), 737-746.

[17] Ditommaso R., Ponzo F.C., 2015. "Automatic evaluation of the fundamental frequency variations and related damping factor of reinforced concrete framed structures using the Short Time Impulse Response Function (STIRF)". Engineering Structures, (82), 104-112.

[18] Thoft-Christensen P., 1995. "Advanced bridge management systems". Struct. Engrg. Rev. Oxford, England, 7(3), 151-163.

[19] Frangopol D. M., Hearn G. et al., 1996a. "Structural reliability in bridge engineering". McGraw-Hill, New York.

[20] Frangopol D. M. et al., 1998b. "Structural reliability in bridge engineering". J. Bridge Eng., ASCE, 3(4), 151-154.

[21] Frangopol D. M., Das P. C., 1999. "Management of bridge stocks based on future reliability and maintenance costs". Current and future trends in bridge design, construction, and maintenance. Thomas Telford, London, 45-58.

[22] Thoft-Christensen P., 1999. "Estimation of bridge reliability distributions". Current and future trends in bridge design, construction, and maintenance. Thomas Telford, London, 15-25.

[23] Frangopol D. M. et al., 2001. "RELIABILITY-BASED LIFE-CYCLE MANAGEMENT OF HIGHWAY BRIDGES". J. COMPUT. CIVIL ENG., 15(1), 27-34.

[24] Ko J. M., Ni Y. Q., 2005. "Technology developments in structural health monitoring of large-scale bridges". ENG. STRUCT., 27, 1715-1725.

[25] Akgul F., Frangopol D. M., 2005. "Lifetime Performance Analysis of Existing Reinforced Concrete Bridges". J. INFRASTRUCT SYST., 11(2), 122-128.

[26] Stewart M. G., Mullard J. A., 2007. "Spatial

  DOI: https://doi.org/10.30564/jaeser.v4i2.3128

Time-Dependent Reliability Analysis of Corrosion Damage and the Timing of First Repair for RC Structures". Eng. Struct., (29), 1457-1464.

[27] Mustafa G., Catbas F. N., 2009. "Statistical pattern recognition for Structural Health Monitoring using time series modeling: Theory and experimental verifications". MECH. SYST. SIGNAL PR., 23 (7), 2192-2204.

[28] Sunyong K., Frangopol D. M., 2010. "Optimal planning of structural performance monitoring based on reliability importance assessment". PROBABILIST ENG. MECH., 25 (1), 86-98.

[29] Orcesia A. D., Frangopol D. M., 2011. "Optimization of bridge maintenance strategies based on structural health monitoring information". STRUCT. SAF., 33 (1), 26-41.

[30] Helder S. et al., 2013. "Construction assessment and long-term prediction of prestressed concrete bridges based on monitoring data". ENG. STRUCT., 52, 26-37.

[31] Liu Y. F. et al., 2014. "Reliability updating and prediction of bridge structures based on proof loads and monitored data". CONSTR. BUILD. MATER., 66(15), 795-804.

[32] Liang D., Yuan S. F., 2015. "Structural health monitoring system based on multi-agent coordination and fusion for large structure". Advances in Engineering Software, (86), 1-12.

[33] Sheng Ouyang, 2009. "CONTROL TECHNOLOGY OF CONSTRUCTING T-RIGID FRAME TURRET BRIDGE OF NO.1 BRIDGE FOR AN EXPRESSWAY". Industrial buildings, Suppl (39), 1079-1065.

[34] Zhang W. et al, 2007. "The strain field method for structural damage identification using Brillouin optical fiber sensing". Smart Mater. Struct, 16, 843-850.

[35] Duan M. D., 1998. "The calculation of creep coefficient and application of< the highway reinforced concrete and prestressed concrete bridge culvert design specifications>". Journal of China Highway, (10), 70-76.

[36] Ministry of Housing and urban-rural development of the people's Republic of china. 2008. "Unified Standard for Reliability design of Engineering Structures (GB50153-2008)". China Building Industry Press, Beijing.

[37] The transportation department specification of the people's Republic of china, 2004. "Code for Design of Highway Reinforced Concrete and Prestressed Concrete Bridges and Culverts (JTG D62-2004)". China Communications Press, Beijing.

[38] Zhang J. L., Liu Y, 2004. "Statistical Models for the Lifetime Resistance of Concrete Bridges". Journal of Changsha University of Science, 1(1), 27-33.

[39] James Evans, William M. Lindsay, 2010. The Management and Control of Quality (7th international edition). South-Western, Division of Thomson Learning.

 DOI: https://doi.org/10.30564/jaeser.v4i2.3128

BILINGUAL PUBLISHING CO.
Pioneer of Global Academics Since 1984

Journal of Architectural Environment & Structural Engineering Research
https://ojs.bilpublishing.com/index.php/jaeser

ARTICLE

The Factor that Affects Biophilia Application at the Workplace

Ebtesam Alawadhi Jamilah Othman* Haza Hanurhaza Md Jani

Department of Landscape Architecture, Kulliyyah of Architecture and Environmental Design, International Islamic University, Malaysia

ARTICLE INFO

Article history
Received: 11 May 2021
Accepted: 9 June 2021
Published Online: 11 June 2021

Keywords:
Biophilia
Human and nature
Awareness
Preference

ABSTRACT

Many theories in sociology and psychology encourage people to maintain and contact with nature. Biophilia, for instance, examines the connection between humans and nature within the built environment. It is considered one of the solutions to human isolation from nature, especially in the workplace. This study examined the factors of employee's awareness and preference that affect biophilia application at the workplace. This study's primary data collection method is a survey questionnaire through which responses from 167 employees at the International Islamic University Malaysia (IIUM) were collected. The findings show that employee's awareness and preference have a significant positive effect on the biophilia application. Further research on this topic is necessary to understand other factors that may affect human's connection with nature at the workplace.

1. Introduction

The term biophilia, highlighted by E.O. Wilson, is defined as "innate tendency to focus on life and lifelike processes", "innately emotional affiliation of human beings to other living organisms" [33], a form of humans' deep intimacy with nature that originates from biological production [20]. Biophilia aims to create places saturated with positivity, emotional experience, and life enjoyment [13]. Biophilia creates an escape from the concrete jungle and a better balance between humans and nature. Modern urban areas often isolate people from nature. The workplace has become a virtual environment due to the significant global shift in industrialisation and the economy [3]. According to Kellert, it is essential to understand the workplace environment and the effect of nature on occupant productivity [4,18]. Employees and employers should have crucial roles in the comprehensive view of the work environment [7].

According to Nieuwenhuis and Haslam, workers who work in a green workplace are happier and more satisfied than those who do not [25]. The Human Space Survey revealed that almost 47% of workplaces worldwide lack natural light, and 58% lack green spaces [7]. Workers are affected by the work environment the most because they spend approximately 90% of their time indoors [27]. As a result, they are exposed to many detrimental effects of the work environment, including mental health and occupational stress [16]. Many workers also complain of job depression and sick building syndrome in the workplace. According to the AIA Malaysia Survey in 2018, 50.2% of workers became stressed or depressed, and the number of days off due to occupational sickness increased to 73.1 days per employee per year [1]. Furthermore, 98% of Malaysian workers are at risk of bed trauma and long-term

**Corresponding Author:*
Jamilah Othman,
Department of Landscape Architecture, Kulliyyah of Architecture and Environmental Design, International Islamic University, Malaysia;
Email: jamilah_61164@iium.edu.my

DOI: https://doi.org/10.30564/jaeser.v4i2.3221

mental health issues [1]. Biophilic designs are known to achieve "inner sustainability", which seek to restore nature's elements for humans to create a higher perception.

There is a widely-held belief that the triumph of sustainable design is linked to conscious user behaviour rather than the building's intelligent structures. Based on the users' sense of confidence, approval, and happiness, it is undoubtedly possible to grasp users' behaviour in the desired direction. The biophilic tendency in architectural engineering and the built environment draws attention to space, which have recently been discussed in greater depth [17]. Biophilic interventions should consider the social nature of people's behaviour, which is explored mainly by environmental psychology [14]. Kellert and Calabrese mention that some factors affect biophilia design in the built environment, such as culture, project size, varying economic, and logistical [19]. In particular, this study focuses on the impact of awareness and preference of employees on the biophilia application.

2. Literature Review

Biophilia Application

Biophilia application is applying principles and processes of biophilia to build environmental design. Cooper and Browning argue that biophilic design can be organised into three categories: nature in the space, natural analogues, and nature of the space [7]. These categories can facilitate the implementation of biophilic. Nature in the space includes plant life, animals, water, sounds, scents, and other natural elements into the built environment, which means the direct physical, and ephemeral presence of nature in space. Natural analogues are found in objects, materials, colours, shapes, sequences, and patterns, focusing on the organic, non-living, and indirect evocations of nature. The nature of the space is the innate human desire to see beyond immediate human surroundings and have visual exit opportunities [6].

Biophilia Theory

Biophilia is against old tendencies such as isolation from nature. In addition, biophilia theory believes that humanity could not ignore the inborn tendencies to natural ecosystems and should instead consider them [21]. Landscape architecture is one of biophilia's interest. It evaluates natural and cultural resources that make biophilia part of sustainability [22]. However, there are contradictions between biophilia and sustainable architecture. Unlike sustainable architecture, biophilia is interested in human emotional and psychological well-being. In a sense, biophilia can be considered the missing piece in current sustainable design [8]. Biophilia has a relationship with the environmental psychology theory, such as restorative environment, prospect-refuge, etc.

Browning and Cooper outline three benefits of biophilia at the workplace [7]: 1) Well-being: reducing stress is crucial in keeping positive well-being. Some countries, including Canada, provide green space to increase the worker's well-being. Natural landscapes have a more positive impact than urban landscapes. 2) Productivity: there is a positive relationship between well-being and productivity. A good mood equates to doing more. 3) Creativity: the surrounding environment influences creativity. A working environment with natural elements such as plants and daylight would increase employees' creativity. Several studies show that biophilia benefits employees in terms of mental health and economics [2].

Factors Affect Biophilia Application

A healthy environment seeks to renew the resources needed to maintain and promote health, well-being, and biophilia by connecting humans with nature. Restorative environment design requires a balance between culture, history, preference, and awareness. Some theories study preference and awareness and focus on human behaviour toward nature. This study focuses on the employee' preference and awareness of the biophilia application, as shown in Table 1.

Table 1. Factors extracted from psychology and sociology theories related to biophilia.

Theories	Construct	Factors
Pro-environment behaviour	Taking the initiative [5,26,31]	Awareness
Environmental awareness Nature awareness Biophilia	Attitude Perception [12,18]	
Attention restoration Directed attention theory Environment preference Biophilia	Attracted Interest Affective reaction [15,32]	Preference

Employee's Awareness on Biophilia Application

The concept of biophilia explains the depth of the relationship between human and nature. Wilson argues that there is an innate tendency within the human being toward nature [33]. In agreement, nature awareness (NA) supports an emotional attachment within the human to nature [11,23]. Furthermore, the theory of nature awareness suggests a cognitive effect on people who live around nature [10]. On the other hand, people living in an urban area tend to experience many environmental problems due to a lack of nature. Environmental awareness theory encourages

 DOI: https://doi.org/10.30564/jaeser.v4i2.3221

sustainability awareness through three variables, i.e., emotional, attitude, and practice [12]. Environmental awareness leads humans to protect natural environments. Nature is necessary for human emotional gratification as well as improved knowledge and cognitive capacities. Kellert suggests that a person's aggressive behaviour against nature may manifest as early as childhood [18]. The theory of Pro-Environmental Behaviour (PEB) demonstrates that the individual has a role in protecting nature and reducing any harm that threatens it. There are five factors related to PEB, i.e., conserving, avoiding harm, transforming, influencing, and taking the initiative [5,26,31].

Employees' Preference on Biophilia Application

Humans have different preferences towards nature. The environmental preference theory explains that humans like the attractiveness of nature and environmental aesthetic [32]. Humans prefer space that include natural elements such as daylight and water [30]. The Prospect-Refuge Theory further supports the idea of different preferences towards nature. Some factors are affecting individual preferences, including social, history, and culture. Nasar asserts that successful design requires understanding the visual environment and the humans affected by it [24]. The human sense can feel attracted or repulsed by aesthetic qualities [15].

3. Methodology

Data were collected from administrative employees at the International Islamic University Malaysia (IIUM) using a survey questionnaire. The total number of employees working indoors was 339. After deducting the outliers and missing data, the total number of respondents gathered was 167. This sample size was adequate to address the research objectives [29]. The gender composition of the sample was typical of the administrative employee population in IIUM Malaysia, with 71% being female. The age bracket groups are as follows: 21-30 (29.3%), 31-40 (31.1%), 41-50 (23.4%), and 51-60 (13.8%). The majority (61%) of the sample live in urban areas.

This study used a 13-item questionnaire that measures the awareness and preference of employees at the workplace. The items were extracted from the attributes of biophilia theories, shown in Table 1, and verified by four experts in landscape architecture. The questionnaire was divided into two sections. The first section was on respondents' demographics information, and the second section covered biophilia application. There are 22 items divided into three parts, all of which uses a 5-point Likert scale format (1 = strongly disagree to 5 = strongly agree).

The collected data were analysed using SPSS version 25, in which descriptive statistics analysis was to determine individual and group mean and percentage.

Table 2. Items measured

Code	Items	Mean	SD	Alpha
	Awareness			.878
AWQ1	Employers should take the initiative to provide plant at the workplace.	3.96	.806	
AWQ2	Staff should take the initiative to provide plant at a workplace	3.89	.779	
AWQ3	Staff should take the initiative to provide water element at a workplace	3.76	.808	
AWQ4	Plants inside the workplace can increase oxygen	4.26	.678	
AWQ5	Plant at the workplace can reduce stress	4.15	.758	
AWQ6	Plant at the workplace can adjust your negative mood	3.98	.795	
AWQ7	Plant at the workplace can clean air	4.21	.657	
	Preference			.872
PRQ1	I prefer having a green plant at my workplace.	4.00	.736	
PRQ2	I prefer having a flowering plant at my workplace	4.01	.728	
PRQ3	I prefer having an aquatic plant on my desk	3.59	.886	
PRQ4	I prefer having a plant in a pot on my desk	3.74	.843	
PRQ5	I prefer having a fountain at my workplace	3.51	.917	
PRQ6	I prefer having a fountain at my workplace	3.52	.962	
	Biophilia application			.895
BAQ1	The plants should be close to the window to have sunlight.	3.96	.763	
BAQ2	The plant should be on the table because it does not need high light.	3.49	.870	
BAQ3	The plant should be hung on walls so that it does not take up space in the workplace.	3.41	.989	
BAQ4	The plant should be in any area of the office. It does not matter.	3.39	.884	
BAQ5	The water elements should be a fountain.	3.49	.904	
BAQ6	The water elements should be an aquarium.	3.49	.863	
BAQ7	The water elements should be a wall fountain so that it does not take up space.	3.38	.846	
BAQ8	The water elements should be a table fountain so that it gives an aesthetic look.	3.50	.863	
BAQ9	The water elements should be a giant aquarium in the reception hall.	3.29	.912	

DOI: https://doi.org/10.30564/jaeser.v4i2.3221

Individual items were combined to determine an overall score for each dimension. During data analysis, summated scales were created to determine the relationship between the variable. According to Sekaran, for the value of Cronbach's alpha, ≥ 0.70 is acceptable [28]. The alpha of the items was between .872 and .901. Hypothetically, the independent variables, namely awareness and preference, influence biophilia application as the dependent variable. The regression analysis demonstrates how a change in independent variables is related to change independent variables. In other words, it indicates employees' awareness and preference for biophilia application.

4. Results

This section presents the results of the multiple regression that addresses the objective of the study. First, the Pearson moment correlations were used to determine the coefficient of relationship between the variables, followed by the tested coefficients and hypotheses.

1) Adequacy of the measure of factors

Table 2 shows the descriptive statistics of the items. The mean score of all items was above the hypothetical mean of 3.0. The minimum value of the reliability index was .87, and it satisfied the cut-score of .70 deemed critical for a reliable measure. Cronbach's alpha indicates that the internal consistency index of the employees' responses to the related items was reasonable.

2) Adequacy of the factors model.

Simultaneous multiple regression was conducted to investigate the best predictors from the variables to achieve the biophilia application. The means, standard deviations, and inter-correlations are shown in Table 3. The average mean of awareness was 31.90 (standard deviation= 31.90), and the standard deviation was 3.71for preference (standard deviation =.766).

Table 3. Biophilia application and predictors variables

Variable	M	SD	Application	Awareness	Preference
Application	35.05	6.60	1.000		
Awareness	31.90	5.18	.595	1.00	
Preference	3.71	.7661	.656	.581	1.00

The beta coefficients are also presented in Table 4. The combination of variables to predict the biophilia application from awareness and preference was statistically significant, F= 88.1, p<.001. The result suggests that awareness and preference significantly predict the biophilia application. The adjusted R^2 value is 49, indicating that the model explains 49% of the variance in biophilia application.

Table 4. Simultaneous multiple regression analysis for awareness and preference

Variable	B	SEB		T	P
Constant	6.922	2.260		3.663	.0003
Awareness	.411	.683	.322	4.92	.000
Preference	4.042	.564	.469	7.17	.000

R = .49 F= 88.1 P<.001.

5. Discussion

This study examined the factors that affect biophilia application at the workplace. Specifically, it tested the influence of employee's awareness and preference on workplace biophilia application. Fatoki asserts that environmental knowledge has no significant effect on the employees' pro-environmental behaviour [9]. However, the findings suggest that the first factor of employee's awareness can affect biophilia elements (plants and water) at their workplace. They appeared to know about the initiative. The question "*Staff should take the initiative to provide plant or water at a workplace*" emphasised the importance of having plants or water elements at their workplace. The findings indicate that there is a positive effect of awareness on biophilia application. The findings also show that the second factor, which is the employee's preferences to have plant and water at their workplace, also affect biophilia application. As revealed by the descriptive statistics analysis, the respondents had different choices when it came to plants, such as green and flowering, or the water elements, such as fountain and aquarium. Similarly, Wilke and Stavridou (2013) found that employees prefer waterscapes. There is a positive perception among the respondents on the visual and auditory waterscape that are laden with rich greenery and surrounded by vast open water bodies.

6. Conclusions

Many theories focus on human behaviour to nature. Biophilia is different from other theories because of its focus on human emotion. This theory views that humans have an innate emotional affiliation with nature. The concept of biophilia also appears to have a positive effect in the workplace. Biophilia at the workplace can be achieved in various ways by using two main elements, i.e., water and plants. This study focuses on the factors related to the employee's behaviour toward nature and demonstrates the connection between nature and nature protection. In this regard, this study examined two factors that affect the application of biophilia at the workplace, namely awareness and preference. Further studies should be conducted to identify other determinants of biophilia at the workplace.

 DOI: https://doi.org/10.30564/jaeser.v4i2.3221

References

[1] AIA HWP. (2019). Healthiest Workplace by AIA Vitality | AIA Insurance. https://healthiestworkplace.aia.com/malaysia/eng/home/.

[2] Alawadhi, E., Othman, J., & Md Jani, H. H. (2020). Reviewing the impacts of biophilic elements at workplace. PalArch's Journal of Archeology of Egypt/Egyptology, 17(9), 7410-7420. https://www.researchgate.net/publication/348836357.

[3] Al Horr, Y., Arif, M., Kaushik, A., Mazroei, A., Katafygiotou, M., & Elsarrag, E. (2016). Occupant productivity and office indoor environment quality: A review of the literature. Building and Environment, 105, 369-389.

[4] Alker, J., Malanca, M., Pottage, C., & O'Brien, R. (2014). Health, well-being & productivity in offices: The next chapter for green building. World Green Building Council. https://www.worldgbc.org/sites/default/.

[5] Bamberg, S., & Rees, J. (2015). Environmental Attitudes and Behaviour: Measurement. International Encyclopedia of the Social & Behavioral Sciences (Second Edition), 699-705. https://doi.org/10.1016/B978-0-08-097086-8.91066-3.

[6] Browning, W., Ryan, C., & Clancy, J. (2014). 14 Patterns of Biophilic Design: Improving Health & Well-Being in the Built Environment. Terrapin Bright Green, LLC, 1-60.

[7] Cooper, C., & Browning, B. (2015). Human Space: The Global Impact of Biophilic Design in the Workplace. Human Spaces Report. http://www.humanspaces.com/.

[8] Dillon, B. R. (2008). Rebuilding Biophilia. (Unpublished Master Thesis). University of Cincinnati.

[9] Fatoki, O. (2019). Employees'pro-Environmental Behaviour in Small and Medium Enterprises: The Role of Enjoyment, Connectedness to Nature and Environmental Knowledge. Academy of Entrepreneurship Journal, 25(4), 1-15.

[10] Freese, M., & Fultz, A. (2012). Nature Awareness and Science Achievement in Middle School: A Correlational Study. (Unpublished Master Degree). Johnson University.

[11] Geng, X., Sy, C. A., Kwiecien, T. D., Ji, X., Peng, C., Rastogi, R., ... & Ding, Y. (2015). Reduced cerebral monocarboxylate transporters and lactate levels by ethanol and normobaric oxygen therapy in severe transient and permanent ischemic stroke. Brain Research, 1603, 65-75.

[12] Hassan, A. A., Noordin, T. A., & Sulaiman, S. (2010). The status on the level of environmental awareness in the concept of sustainable development amongst secondary school students. Procedia Social and Behavioural Sciences, 2(2), 1276-1280.

[13] Heerwagen, J. (2009). Biophilia, Health, and Well-being. In: L. Campbell and A. Wiesen (Eds.), Restorative Commons: Creating Health and Well-being through Urban Landscapes (pp. 39-57). Newtown Square: USDA Forest Service.

[14] Hidalgo, A. K. (2014). Biophilic design, restorative environments and well-being. Proceedings of the Colors of Care: The 9th International Conference on Design & Emotion (pp. 535-544).

[15] Holahan, C. (1984). Cognition and Environment: Functioning in an Uncertain World. Psyccritiques, 29(1).

[16] Hui, F. K. P., & Aye, L. (2018). Occupational stress and workplace design. Buildings, 8 (10), 133.

[17] Kayhan, K. S. (2017). Examination of Biophilia Phenomenon in the context of sustainable architecture. International Sustainable Buildings Symposium (pp. 80-101). Springer, Cham.

[18] Kellert, S. R. (1993). The Biological Basis for Human Values of Nature. In: S.R. Kellert and E.O. Wilson (Eds.), The Biophilia Hypothesis, 42-69. New Washington: Island Press.

[19] Kellert, S., & Calabrese, E. (2015). The Practice of Biophilic Design. London: Terrapin Bright LLC.

[20] Kellert, S. R., Heerwagen, J., & Mador, M. (2011). Biophilic Design: the Theory, Science and Practice of Bringing Buildings to Life. New York: John Wiley & Sons.

[21] Krčmářová, J. (2009). E.O. Wilson's concept of biophilia and the environmental movement in the USA. Klaudyán: Internet J Histor Geogr Environ History, 6(1/2), 4-17.

[22] Kurnia, D. (2017). Concept of Sustainability and Biophilic Design in Landscape Architecture. Вестник Росздравнадзора, 4, 9-15.

[23] Mayer, F. S., & Frantz, C. M. (2004). The Connectedness to Nature Scale: A Measure of Individuals' Feeling in Community with Nature. Journal of environmental psychology, 24(4), 503-515.

[24] Nasar, J. L. (1984). Visual Preferences in Urban Street Scenes: a Cross-cultural Comparison between Japan and the United States. Journal of cross-cultural psychology, 15(1), 79-93.

[25] Nieuwenhuis, M., Knight, C., Postmes, T., & Haslam, S. A. (2014). The Relative Benefits of Green versus Lean Office Space: Three Field Experiments. Journal of Experimental Psychology: Applied, 20(3), 199.

[26] Ones, D. S., & Dilchert, S. (2012). Environmental sustainability at Work: A Call to Action. Industri-

DOI: https://doi.org/10.30564/jaeser.v4i2.3221

al and Organisational Psychology, 5(4), 444-466. https://doi.org/10.1111/j.1754-9434.2012.01478.x.

[27] RCF Group. (2018). The Workspace NudgeTM for Well-Being. https://www.thercfgroup.com/files/resources/Workspace_Nudge/.

[28] Sekaran, U. (2003). Research Methods of Business: A Skill Building Approach. New York: John Wiley and Sons, Inc.

[29] Taherdoost, H. (2017). Determining sample size; How to calculate survey sample size. International Journal of Economics and Management Systems, 2(2), 237-239. http://www.iaras.org/iaras/journals/ijems.

[30] Ulrich, R. S. (1993). Biophilia, Biophobia, and Natural Landscapes. In: S.R. Kellert and E.O. Wilson (Eds.), The Biophilia Hypothesis, 42-69. New Washington: Island Press.

[31] Wiernik, B. M., Dilchert, S., & Ones, D. S. (2016). Age and Employee Green Behaviours: A Meta-Analysis. Frontiers in psychology, 7, 194.

[32] Wilkie, S., & Stavridou, A. (2013). Influence of Environmental Preference and Environment Type Congruence on Judgments of Restoration Potential. Urban Forestry & Urban Greening, 12(2), 163-170. http://www.tlu.ee/~arro/Happy%20Space%20EKA.

[33] Wilson, E. O. (1984). Biophilia, the Human Bond with Other Species. Cambridge: Harvard University Press, pg.157.

 DOI: https://doi.org/10.30564/jaeser.v4i2.3221

BILINGUAL PUBLISHING CO.
Pioneer of Global Academics Since 1984

Journal of Architectural Environment & Structural Engineering Research
https://ojs.bilpublishing.com/index.php/jaeser

ARTICLE

Augmented Reality Based on Object Recognition for Piping System Maintenance

Ana Regina Mizrahy Cuperschmid* **Mariana Higashi Sakamoto**

School of Civil Engineering, Architecture and Urban Design, Department of Architecture and Construction, University of Campinas (UNICAMP), Campinas, SP, 13083-889, Brazil

ARTICLE INFO

Article history
Received: 1 June 2021
Accepted: 21 June 2021
Published Online: 25 June 2021

Keywords:
Augmented reality
3D object tracking
Maintenance
Pipe
Facility management

ABSTRACT

Augmented Reality (AR) applications can be used to improve tasks and mitigate errors during facilities operation and maintenance. This article presents an AR system for facility management using a three-dimensional (3D) object tracking method. Through spatial mapping, the object of interest, a pipe trap underneath a sink, is tracked and mixed onto the AR visualization. From that, the maintenance steps are transformed into visible and animated instructions. Although some tracking issues related to the component parts were observed, the designed AR application results demonstrated the potential to improve facility management tasks.

1. Introduction

Augmented Reality (AR) is a technology that allows a composite visualization of the physical environment superimposed with virtual elements [1]. AR is a subdomain of Mixed Reality, defined as the intermediate environment between real and virtual worlds [2]. It is an alternative and complementary technology to traditional means of accessing information since it facilitates the data interpretation by overlapping virtual elements in the real world, considering the time, place and the real context of the design [3].

AR can contribute to the Architecture, Engineering, Construction and Operation (AECO) processes as it can structure additional information that enables better understanding. The complex nature of AECO makes the use of AR ideal on at least three levels: visualization, information retrieval and interaction [4]. This complexity is observed in the maintenance work of Mechanical, Electrical and Plumbing (MEP) systems. The difficulties that MEP operators face, range from the need for expertise in the area for interpreting MEP technical drawings loaded with symbology to the lack of updated information for as-built maintenance [5].

Hence, AR can offer maintenance procedure visualization in more natural and interactive way because it can present, in real time, superimposed models and information on the physical world. The maintenance of plumbing systems supported by AR technology has great

**Corresponding Author:*
Ana Regina Mizrahy Cuperschmid,
School of Civil Engineering, Architecture and Urban Design, Department of Architecture and Construction, University of Campinas (UNICAMP), Campinas, SP, 13083-889, Brazil;
Email: cuper@unicamp.br

DOI: https://doi.org/10.30564/jaeser.v4i2.3305

potential, because end users do not have the expertise and easy access to the maintenance data of systems like specialists. This study assumes that AR has the potential for aiding the maintenance of plumbing systems, as it presents a more intuitive and accessible communication for the non-specialist user.

The issue that leads this research is whether and how AR could be used as a tool to assist the maintenance of plumbing systems. The proposal is to convert the maintenance steps into visible and explicit visualization through an AR experience. To contextualize the research and allow the exploration, the maintenance process of a pipe trap underneath a sink is used. Among the main problems about this equipment are: odor entry into the environment, clogging, preventing the flow of sanitary sewage, and leakage, compromising the environment in which it is installed [6].

2. Related Works

In the last five years, numerous studies have been conducted on the use of AR to assist operation and maintenance processes of pipe systems. AR has been applied to, e.g., examine its relation to human spatial cognitive abilities on assembly [7]; assist facility management using the image-based indoor localization [8]; improve work productivity through a piping management system [9]; locate virtual pipes behind a real wall with "X-ray vision" to establish relationships between task performance and spatial factors [10]; develop a framework to extract and visualize 3D models of structures connected with pipes [11]; understand spatial cognition on craft-worker eye-gaze patterns in building a scale-model pipe assembly [12]; provide an application scenario for cooling tower and pipe shutdown protocol [5]. These related cases are summarized in Table 1.

Table 1. Related works

	Description	Reference
Objective	Framework development to test AR impact for inspection or maintenance	[5,8,9,11]
	Compare user performance in assembling or locating tubes with different information formats	[7,10,12]
Evaluation	Quantitative and Statistical Analysis	[7,10,12]
	The application of ETS cognitive tests	[7,9,12]
	Qualitative analysis - Performance evaluation	[5,8,9,11]
Tracking	marker based	[9]
	markless based	[5,7,8]
Display device	HMD	[8,12]
	Tablet	[7,9]
	Smartphones	[5,11]
	Notebook	[10]

These studies can be classified into two groups, according to their macro-goals: (i) system development for task optimization and (ii) human spatial cognition during operation and maintenance tasks.

Within the first macro-proposal there were cases of application development for the maintenance of leaks in a university building in Korea [8] and in Taiwan [5]. Some cases were applied to piping systems of the naval industry for the control of tubes for shipbuilding [9] and for the maintenance of offshore equipment [11].

The cases that fall under the second macro-proposal involve performance studies: in the assembly of tubes aided by AR versus traditional paper based drawings [7]; for positioning tubes on the wall with the aid of AR [10]; and in the assembly of tubes measured using eye-tracking technology [12]. In these cases, the assembling activities, when assisted by AR, presented better performance results - especially for people with little experience in the area or low spatial cognition ability [12].

The technological solution adopted was approached in different ways by the authors. In all cases the integration of AR and Building Information Modeling (BIM) was mentioned, except the case involving the application for a ship factory [9].

Overall, the studies discussed the disadvantages and advantages of four types of AR displays: Head Mounted Display (HMD), tablets, smartphones, and laptops. The HMDs were seen by maintenance professionals as impractical due to the size and inaccessible due to the price, in addition to representing a risk to the operator's safety [7], while the notebook presented the setback of being fixed, which was mentioned to be a disadvantage for the notion of depth in the pipe assembly task [10]. However, smartphones and tablets have the advantage of being more portable and mobile, in addition, its built-in flashlight can illuminate dark indoor or outdoor night environments [5].

An essential part of AR application is the correct connection between virtual information and the real world [13]. One way to connect this information is using markers, recognized in real-time and used as a reference object to precisely superimpose virtual 3D content onto the camera's live view. Markers were used in large quantities to identify tubes, and each tube received a unique identifying sticker that allowed access to information about the shipbuilding process [9]. The disadvantage of this technology is that there is a risk that the marker will be damaged by bad weather and that there is a need for prior installation.

Another way of connecting virtual data is through Simultaneous Localization and Mapping (SLAM)

 DOI: https://doi.org/10.30564/jaeser.v4i2.3305

technology. This technology was used with the HMD Microsoft HoloLens [8], and a smartphone [5] and was applied together with a structured light scanner and an iPad [7]. This markless technology advantage is that it does not interfere with the environment aesthetics [11].

Other similarities found in the related works involve the forms of assessment used in the studies. Most studies performed usability tests by inviting multiple participants. The studies that rated their participants' spatial cognitive abilities adopted ETS tests for 2D and 3D image recognition. Four studies performed a quantitative analysis of their results, statistically analyzing explanatory variables about the performance of the participants. While the other three cases applied a qualitative analysis, interviewing participants about feedback on the proposed solution.

3. Methodology

The proposed procedure, expressly addressed to the pipe trap maintenance aided by AR, consists of four main stages (i) establish the maintenance requirements; (ii) model the components; (iii) develop the AR application; (iv) evaluate the application performance.

3.1 Maintenance Requirements

The user experience level in relation to the piping system maintenance domain can influence the sink trap maintenance procedure. Therefore, users with little experience may present some difficulties, such as (i) recognition of the components, since each sink trap model or brand has its particularities; (ii) small parts, metal rings and sealing rubbers can easily get lost during the procedure or be misplaced in the fittings; (iii) the components assembly and reassembly requires a correct order, otherwise there is a risk of deforming the parts or leaking.

From a practical experimentation with the procedures that users normally make for the installation and maintenance of a cup-shaped trap, especially in the clogging event, it was possible to establish the potential contributions of the proposed system.

The procedure performed was (1) sink trap removal and cleaning; (2 and 3) sealing the two threaded pipe connections with PTFE tape; and (4) reassembling the trap and checking for leaks, Figure 1.

Figure 1. Sink trap maintenance process

Aiming to reduce the difficulties raised in the sink trap installation and maintenance procedure, five main requirements for applying the proposed AR application were defined: (1) list the sink trap components; (2) identify/recognize the main components; (3) warning of rubber seal's position; (4) order of components in the assembly; (5) present the image of the complete sink trap installed.

3.2 Components Modeling

Duratex, a Brazilian manufacturer, under the Deca e Hydra brands, produces valves for discharging the water systems of toilets, faucets for bathrooms and kitchens, among other related products. The Deca brand makes available on its website, a library of its products in different file formats for AutoCAD (DWG), Revit (RFA) and Sketchup (SKP). For this research, it is used for both physical and digital models of the sink trap.

To add details to the digital model, the Revit family RFA format file was used as the basis. The Revit software was chosen because it is a popular BIM software in the AECO industry. From the solid modeling tools, such as extrusion and revolution, the necessary details were added, such as the connection to the waste pipe, Figure 2.

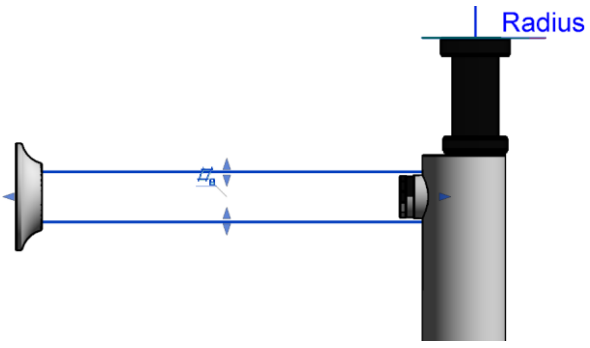

Figure 2. Sink trap modeling using Revit

DOI: https://doi.org/10.30564/jaeser.v4i2.3305

The sealing parts and the inspection cover were also modeled using the combination of elementary solids, in this case a cylinder and a torus and ~~add~~ different colors and textures from images. The addition of fitting elements and sink trap components was necessary to provide visual information about all parts, allowing the development of the maintenance steps.

3.3 Application Development

To develop an application with three-dimensional (3D) object recognition, it was necessary to choose an SDK. Several SDKs offer this possibility, as Vuforia [14], Wikitude [15] and VisionLib [16]. From the VisionLib SDK for Unity [17], it is possible to create AR experiences for platforms compatible with Windows Desktop, iOS and Android, but the most interesting is the possibility of creating web based experiences.

Unity is an ecosystem for developing applications, games, or multi-platform 2D and 3D experiences. This engine was also the most cited, three of the seven related cases used this tool.

According to the VisionLib documentation, the potential of this technology lies in the fact that it improves computer vision through model-based tracking. The advantage of this tracking over SLAM tracking, is the greater accuracy for locating a point in the real world and with a higher level of stability, as it is not affected by changes in lighting or object movement.

It was decided to use VisionLib, because: (i) object-based AR for the piping system maintenance was not yet identified in related cases; (ii) versatility in the creation of Unity's multi-platform interfaces and resources; (iii) it was possible to obtain a valid academic license during the development of this research.

Based on the requirements, an application was developed considering a sink trap exploded view, 3D object animation, and maintenance step visualization. First, it was decided to show an exploded view of the sink trap components, accompanied by an animation. The animation shows the complete set to its exploded view - aiding the visualization of each component in the recommended position.

The instructions (according to the manufacturer) were divided into four steps: (1) screwing the trap in the sink, (2) measuring distance between the tail pipe and the wall, (3) installing and (4) maintenance. In the application, each step was accompanied by a small animation to better illustrate the instruction.

The user interface was developed in Unity. It was composed of a panel containing the sink trap handling information and the tracked object visualization on the screen, accompanied by an animation. User interaction with AR application can happen through buttons, or by moving the camera at different angles or by clicking/touching the screen - on the green cylindrical mesh attached to the model, Figure 3.

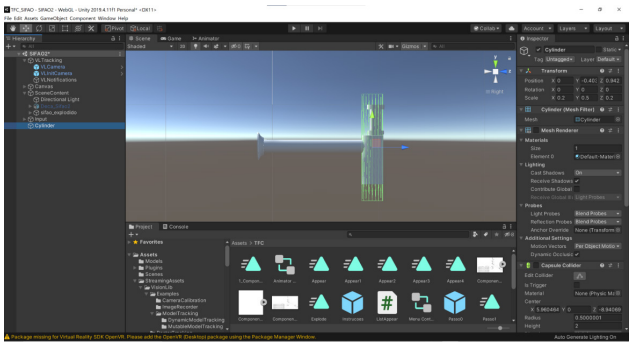

Figure 3. User interface development in Unity

The Unity left-side menu contains all the application objects, including VL Tracking (VisionLib pre-configured features), Canvas (panels containing the instructions textual elements) and SceneContent (composed of the scene objects). The right-side menu shows the selected element properties. The bottom menu presents a library or user objects that can be used in the application.

A C# script was used to customize user interactions with objects in the scene. The Animator Controller was applied to order the animation, Figure 4. Each gray box represents an animation of the sink trap digital model.

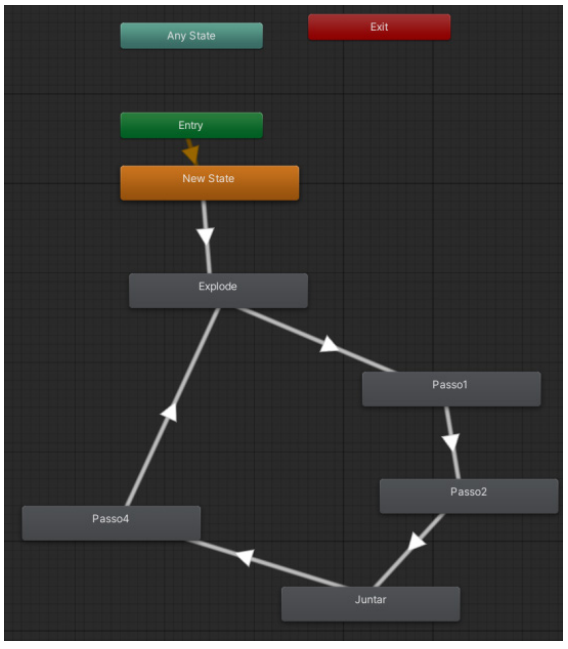

Figure 4. Animator Controller: animation order

Each animation was recorded separately. In a timeline, it was positioned frame by frame the objects on the scene, Figure 5.

 DOI: https://doi.org/10.30564/jaeser.v4i2.3305

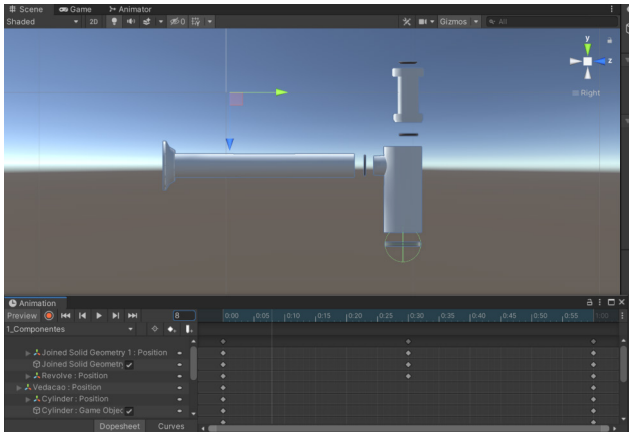

Figure 5. Animation development in Unity

3.4 Evaluation

In this section, the performance of the developed application is evaluated. The developed application tracks the physical sink trap to overlay maintenance information in AR[1], Figure 6.

Figure 6. AR application evaluation

The initial screen (A) presents the application general information and its authorship. When pressing the start button, it is possible to choose which camera connected to the device will feed the AR.

Initially, the 3D model appears on the screen with a red outline and the Model Tracking feature is activated. When the geometry of the real sink trap is partially detected, the digital model outline changes to yellow according to (B). Then, when fully tracking the object, it changes its color to green and the digital model is superimposed on the real object. So, when approaching the camera or moving the real object, the digital model also accompanies the sink trap.

Scene (C) shows a list of the components for replacement and an animation of the exploded model in its three demountable parts (trap, tail pipe and waste pipe) and other parts (sealing rubbers and inspection cover). When the camera approaches the real sink trap, it is possible to view in more detail the sealing rubbers evidenced by the scene (C) with an exploded view, Figure 7.

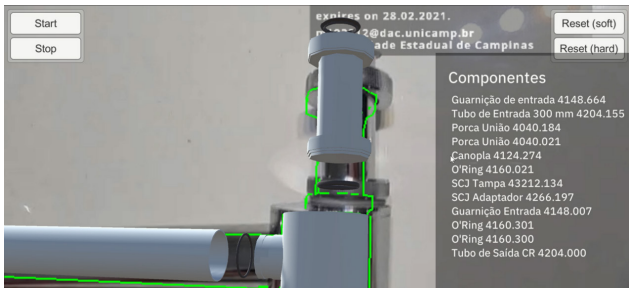

Figure 7. Exploded view superposing the real sink trap

The following four scenes (D, E, F, and G) describe the maintenance instructions provided by the product manufacturer, in summary, respectively: screw the tail pipe into the sink's drain point, measure the distance from the waste pipe to the wall (cut if necessary), connect the trap, and open the inspection cover for maintenance. The four scenes are accompanied by a short animation to illustrate each of these steps. In all moments, the digital model is superimposed on the real sink trap, and it is possible to see the same scene from different angles and distances. The application developed was published for Android devices and Windows platform.

In order to demonstrate the result, the AR application was tested with a washbasin faucet, in which the shape vaguely resembles the sink trap, Figure 8. At first, the developed application recognizes the faucet shape as part of the sink trap, but as soon as the camera changes the angle, it captures the edges incompatibilities between the real object and the digital model[2].

Figure 8. AR application: tracking test

1 Video available at: https://youtu.be/APE49oRgR2g

2 Video available at: https://youtu.be/SVd0CtORVXA

DOI: https://doi.org/10.30564/jaeser.v4i2.3305

4. Discussion

The results obtained are discussed according to its adherence to the initial proposals, and the difficulties and limitations during development are also observed. Among the five requirements, three were fully completed and the others were partially met.

The first requirement (list the sink trap components) has been fully completed. In addition to being possible to list all the components, it was possible to bring extra information for each part, such as its commercial name.

The second requirement (identify/recognize the main components) has been partially completed. The application could successfully recognize the assembled model, relating the digital model to the real model when in AR visualization. However, it was not possible to recognize the three main parts (trap, tail pipe and waste pipe) independently and simultaneously, which would allow the user to detect the sink trap at different stages of its maintenance. For this requirement to be fully met, advanced multi-object tracking feature would be needed and, with it, test whether it would be possible to recognize four combinations: fully disassembled parts, trap uncoupled from the tail and waste pipes, and fully assembled.

The third requirement (warning of rubber seal's position) has also been partially completed. It was possible to show the positioning of the three sealing rubbers on the sink trap from the exploded view, Figure 5 (C). However, the application does not have a warning system, specifying which rubber should be installed and its position. Because of this, it is necessary to retrieve this information from the previous scene.

The fourth requirement (order of components in the assembly) has been fully completed. Scenes (D, E, and F) present the three steps orderly for assembling the sink trap, following the user guide provided by Deca.

The fifth requirement (present the image of the complete sink trap installed) was also completed. So, it was possible to visualize in AR the sink trap assembled and completely disassembled, allowing visualization in advance of the initial and final steps.

Finally, tracking limitations or difficulties are pointed. The main limitation is due to the adaptable dimensions of the cup-shaped trap, which varies depending on the height and distance of the washbasin in each installation, Figure 9.

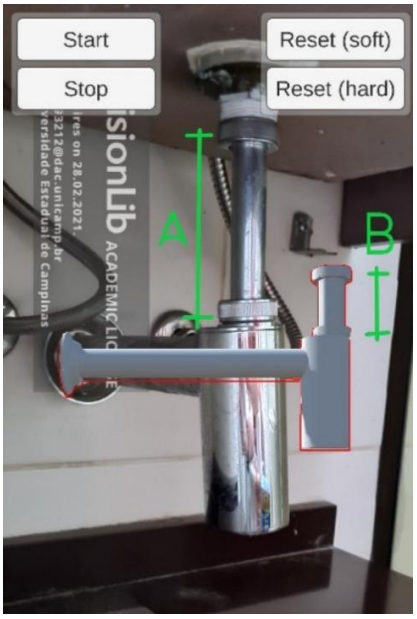

Figure 9. Tracking system and a sink trap with different distances

The second important limitation is the divergence between the model (provided by Deca) and real objects. Between the waste pipe connections to the trap there is an angle, that is not shown the model. The angle between the drainpipe and the trap is not adjustable and the real model has a sloping inclination toward the flow (angle A), while the digital model has a 90º connection (angle B), Figure 10.

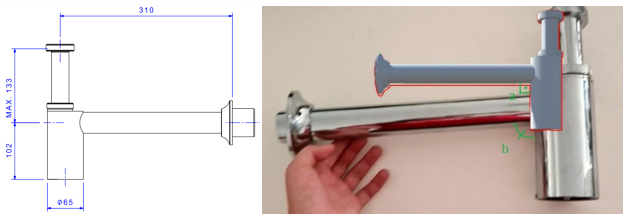

Figure 10. Original model (left) and the real sink trap with different angles (right)

This divergence between angles influenced the model's detection performance by the AR application, which required some attempts to recognize and position the object correctly, but which did not compromise the final tracking[1].

5. Conclusions

In this article, we have presented the results of an AR application developed to assist the maintenance of a cup-shaped trap using 3D object recognition. The application was developed based on a sink trap BIM model. A

1 Video available at: https://youtu.be/UxfyZOFcC3o

 DOI: https://doi.org/10.30564/jaeser.v4i2.3305

straightforward instruction for the maintenance of the sink trap was provided with animations to lessen work burden and increase efficiency. Although it has been observed that improvements can be made, the application design and results demonstrated the applicability of the system.

Several limitations raised in the literature were also identified in this research: tracking problems (whether by occlusion, dark and tight environments), difficulty in accurately positioning digital models due to parallax errors or due to cylindrical geometry, which is not well defined in all axes (the same view is used for different pipe positions).

Despite these limitations, this study pointed out the feasibility of using AR to aid in the maintenance of piping systems. Specifically, this paper's primary contribution is the investigation of the use of 3D object tracking to support pipe trap maintenance. Other initiatives may benefit from this study, as it contributes as a practical case and exploratory research on how AR can be accessible to non-specialists to facilitate maintenance, offering an option for visual guidance for facility management tasks.

Future work should focus on WebXR development, as it allows AR content to be accessed by devices such as smartphones, without the need to install applications or plugins. The main advantage of a web application is that it can be run on any system, requiring only a browser to support it.

References

[1] Milgram P, Takemura H, Utsumi A, Kishino F. Augmented reality: a class of displays on the reality-virtuality continuum. In: Das H, editor. Telemanipulator Telepresence Technol [Internet]. SPIE; 1995. p. 282-92. Available from: https://doi.org/10.1117/12.197321.

[2] Schnabel MA. Framing Mixed Realities. In: Wang X, Schnabel MA, editors. Mix Real Archit Des Constr [Internet]. Dordrecht: Springer Netherlands; 2009. p. 3-11. Available from: https://doi.org/10.1007/978-1-4020-9088-2_1.

[3] Meža S, Turk Ž, Dolenc M. Measuring the potential of augmented reality in civil engineering. Adv Eng Softw [Internet]. 2015;90:1-10. Available from: https://www.sciencedirect.com/science/article/pii/S0965997815000915.

[4] Rankohi S, Waugh L. Review and analysis of augmented reality literature for construction industry. Vis Eng. 2013;1:1-18.

[5] Diao PH, Shih NJ. BIM-based AR maintenance system (BARMS) as an intelligent instruction platform for complex plumbing facilities. Appl Sci. 2019;9.

[6] Pucci A, Conceição D. Estudo Da Incidência De Falhas Visando a Melhoria Da Qualidade Dos Sistemas Prediais Hidráulicos E Sanitários. 2007.

[7] Kwiatek C, Sharif M, Li S, Haas C, Walbridge S. Impact of augmented reality and spatial cognition on assembly in construction. Autom Constr. 2019;108.

[8] Baek F, Ha I, Kim H. Augmented reality system for facility management using image-based indoor localization. Autom Constr [Internet]. Elsevier; 2019;99:18-26. Available from: https://doi.org/10.1016/j.autcon.2018.11.034.

[9] Morikawa K, Ando T. Reduction of piping management person-hours through use of AR technology at shipbuilding sites. Fujitsu Sci Tech J. 2019;55:20-6.

[10] Liu F, Seipel S. Precision study on augmented reality-based visual guidance for facility management tasks. Autom Constr [Internet]. Elsevier; 2018;90:79-90. Available from: https://doi.org/10.1016/j.autcon.2018.02.020.

[11] Han YS, Lee J, Lee J, Lee W, Lee K. 3D CAD data extraction and conversion for application of augmented/virtual reality to the construction of ships and offshore structures. Int J Comput Integr Manuf [Internet]. Taylor & Francis; 2019;32:658-68. Available from: https://doi.org/10.1080/0951192X.2019.1599440.

[12] Alruwaythi O, Goodrum P. A Difference in Perspective: Impact of Different Formats of Engineering Information and Spatial Cognition on Craft-Worker Eye-Gaze Patterns. J Constr Eng Manag. 2019;145:1-14.

[13] Shen Z, Jiang L. An Augmented 3D iPad Mobile Application for Communication, Collaboration, and Learning (CCL) of Building MEP Systems. Comput Civ Eng [Internet]. 2012. p. 204-12. Available from: https://ascelibrary.org/doi/abs/10.1061/9780784412343.0026.

[14] PTC Inc. Vuforia Developer Library [Internet]. 2021 [cited 2021 May 31]. Available from: https://library.vuforia.com/.

[15] Wikitude GmbH. Wikitude SDK Full Features Overview [Internet]. 2021 [cited 2021 May 31]. Available from: https://www.wikitude.com/products/wikitude-sdk-features/.

[16] Visometry GmbH. visionLib Docs [Internet]. 2020 [cited 2021 May 31]. Available from: https://docs.visionlib.com/v20.11.1/index.html.

[17] Unity Technologies. Unity - Manual: Unity User Manual 2020.3 (LTS) [Internet]. 2021 [cited 2021 May 31]. Available from: https://docs.unity3d.com/Manual/index.html.

DOI: https://doi.org/10.30564/jaeser.v4i2.3305

BILINGUAL PUBLISHING CO.
Pioneer of Global Academics Since 1984

Journal of Architectural Environment & Structural Engineering Research
https://ojs.bilpublishing.com/index.php/jaeser

ARTICLE

Mechanical Properties of Polypropylene Fiber Reinforced Concrete under Elevated Temperature

Vikas Patel* **Brijesh Singh** **P N Ojha** **Sahara Adhikari**

National Council for Cement and Building Materials, Ballabgarh, Haryana, India

ARTICLE INFO

Article history
Received: 29 May 2021
Accepted: 25 June 2021
Published Online: 29 June 2021

Keywords:
High strength concrete
Fiber reinforced concrete (FRC)
Polypropylene fibers
Residual mechanical properties
Spalling resistance

ABSTRACT

Apart from many advantages, High Strength Concrete (HSC) has disadvantages in terms of brittleness and poor resistance to fire. Various studies suggest that when polypropylene (PP) fibers are uniformly distributed within concrete, they play an active role in improving spalling resistance of concrete when exposed to elevated temperature while having no adverse effect on its mechanical properties. Therefore, there is a necessity to quantify the effect of the addition of polypropylene fibers in terms of the fiber dosage, the strength of the concrete, and the residual mechanical properties of fiber-reinforced concrete under exposure to high temperature from fire.

The study was carried out on three water/cement (w/c) ratios (0.47, 0.36 & 0.20) using granite aggregate for determining short term mechanical properties of Polypropylene fiber reinforced concrete in comparison to control mix. The experimental program includes 100 × 200 mm & 150 x 300 mm cylinders with fiber volume of 0.5%, that were subjected to temperatures exposures of 400 °C and 600 °C for durations of 1 hour. From the results, it was observed that no significant enhancement in mechanical properties such as modulus of elasticity, Poisson's ratio, split tensile strength, flexural strength, and compressive strength was observed at room temperature and at elevated temperatures.

1. Introduction

With the advancement of concrete technology, high-strength concrete has been used in many concrete structures across the globe. HSC offers higher strength and durability as compared to Normal Strength Concrete (NSC) [1-3]. The major advantage of the addition of fibers to concrete is to transform its brittle behavior into a pseudo ductile material. Fibers in concrete cause gradual failure by arresting micro-cracks presents in the concrete. The fibers from waste materials may be used for the sustainable construction of structural units with cement mortar composites, especially in developing countries. Various studies on mechanical properties of concrete incorporating different types of fibers like steel, carbon, glass, and synthetic fibers have been done in the past to understand the behavior of fiber-reinforced concrete.

Concrete with randomly distributed fibers is defined as Fiber-reinforced concrete (FRC). Fibers dispersed and distributed randomly during mixing results in improved concrete properties in all directions. From the test results of different types of fiber materials such as steel, carbon,

**Corresponding Author:*
Vikas Patel,
National Council for Cement and Building Materials, Ballabgarh, Haryana, India;
Email: vikas.patel299@gmail.com

 DOI: https://doi.org/10.30564/jaeser.v4i2.3296

glass, plastic, polypropylene, nylon, and cotton, American Concrete Institute's Committee 544 [4] classified FRC into four different groups based on the fiber materials namely steel fiber reinforced concrete (SFRC), glass fiber reinforced concrete (GFRC), synthetic fiber reinforced concrete (SNFRC), and natural fiber reinforced concrete (NFRC). Synthetic fibers such as polyester, acrylic, polyethylene, and polypropylene are further subdivided based on the diameter size of fibers into micro-synthetic fibers (for diameter less than 0.30 mm) and macro-synthetic fibers (for diameter greater than 0.30 mm).

Apart from steel fibers, polypropylene fibers are widely used in the market. However, the elastic and strength properties of both fibers vary significantly. For the last many years, steel fibers were generally used in concrete roadwork and sprayed concrete applications. The coming of polypropylene fibers has introduced the possibility of having a high-performance and more sustainable product for the improvement of concrete properties. Polypropylene fibers have better durability as corrosion does not take place in the case of plastic. As it weighs about one-fifth of equivalent steel fiber, it increases the ease of handling. Research on various aspects was done in the past to understand the mechanical behavior of fiber-reinforced concrete and continued till date to recognize the usage of fibers in concrete, and the fibers themselves. [5] Khajuria and Balaguru carried out a study on polypropylene fiber reinforced concrete and concluded that if more water is added to improve the workability of FRC, a reduction in compressive strength may occur. This reduction in compressive strength should be attributed to additional water or due to an increase in entrapped air and not to the fiber addition in the matrix. [6] Alhozaimy, A.M., carried out experimental investigations on compressive, flexural, and impact strength for different binder compositions after adding low volume fractions of polypropylene fibers in concrete. No significant effect on compressive (or) flexural strength was observed upon the addition of fibers, while flexural toughness and impact resistance values were increased. Positive interactions between fibers and pozzolans were also detected.

[7] Bentur et al concluded that the addition of polypropylene fibers does not have a significant effect on the direct tensile cracking strength. However, for volume replacements in the range of 0.33-0.5%, the addition of macro-synthetic polypropylene fibers resulted in 10-15% increase in splitting tensile strength. Further, some studies show that polypropylene fibers can improve the residual compressive strength of concrete after fire exposure. While the presence of different dosages of polypropylene fibers has no significant improvement in residual compressive strength at 200 °C and 400 °C, but beyond 600 °C it considerably increases the residual compressive strength of concrete. Moreover, some studies show that compressive strength of the concrete with polypropylene fibers when exposed to temperature up to 400 °C is higher than the concrete without fibers [8-10]. Thus, past studies show mixed results on the residual mechanical properties of polypropylene FRC.

The mechanical properties of FRC get affected when exposed to heat which can come from different sources including fire exposure and continuous high temperature on the exposed surface. Many Researchers have observed explosive spalling which often results in serious deterioration of the concrete. Continuous pressure is a build-up due to the vaporization of evaporable water which can cause serious damage or even spalling of the concrete. This excessive pressure could be released by the presence of voids in the concrete matrix. To reduce the risk of deterioration and spalling, previous studies suggest that the addition of fibers in concrete such as polypropylene and steel can improve sufficient fire protection. The main parameters that determine the effect of polypropylene fibers are the initial moisture and the rate of heating of the concrete. Therefore, it is very important to quantify the effectiveness of these fibers in terms of the fiber dosage, grade of concrete, and most importantly the residual mechanical properties of FRC after exposure to high temperature from fire.

In the present study, three water/cement (w/c) ratios (0.47, 0.36 & 0.20) using granite aggregates were studied for determining short-term mechanical properties of Polypropylene fiber reinforced concrete in comparison to the control mix. Further, the experimental program includes concrete specimens with polypropylene fiber volume of 0.5%, that were subjected to temperatures exposures of 400 °C and 600 °C for durations of 1 hour. For uniform distribution of PP fibers, dry concrete materials were mixed firstly, and then the fibers were added to the dry mixture to avoid breaking of the fibers. From each mixture, for compressive strength, modulus of elasticity and poisons ratio at room temperature concrete cylinder (150 mm dia. and 300 mm height) specimens were cast and for split tensile strength test and for compressive strength test each at the room, 400 °C, 600 °C and 800 °C temperatures concrete cylinders (100 mm dia. and 200 mm height) were cast. The study was carried out on only one fiber dose which was selected based on the optimum dosage from literature. Also, fibers were added to the concrete mixture to avoid explosive failure in the case of high-strength concrete under elevated temperatures. Further, studies using different

DOI: https://doi.org/10.30564/jaeser.v4i2.3296

fiber doses can be carried out which may result in higher residual mechanical properties after exposure to elevated temperatures.

2. Concrete Ingredients

2.1 Materials

● Cementitious Material

Ordinary Portland cement (OPC 53 Grade) with fly ash and silica fume was used The 3 days, 07 days, and 28 days compressive strength of cement were 36.00 N/mm^2, 45.50 N/mm^2, and 57.50 N/mm^2 respectively. The physical and chemical properties of cement, fly ash, and silica fume are given in Table 1.

Table 1. Physical, Chemical and Strength Characteristics of Cementitious Material

Characteristics		OPC Cement	Silica Fume	Fly Ash
Physical Tests:				
Fineness (m^2/kg)		322	21980	390
Specific gravity		3.15	2.25	2.28
Chemical Tests:				
Loss of Ignition (LOI) (%)		1.52	1.16	0.5
Silica (SiO_2) (%)		20.41	95.02	61.25
Iron Oxide (Fe_2O_3) (%)		3.86	0.80	5.9
Aluminium Oxide (Al_2O_3)		5.04		24.67
Calcium Oxide (CaO) (%)		60.92		2.06
Magnesium Oxide (MgO) (%)		4.77		0.66
Sulphate (SO_3) (%)		1.88		0.28
Alkalies (%)	Na_2O	0.58	0.73	0.07
	K_2O	0.63	2.96	1.41
Chloride (Cl) (%)		0.04		0.008
IR (%)		1.21		

Aggregates

Natural river sand was used as fine aggregate conforming to Zone II as per IS: 383. Crushed aggregate was used as coarse aggregate with 20 mm maximum nominal size. The physical properties of coarse and fine aggregates are given in Table 2. The quality of both coarse and fine aggregate was fair. The silt content by the wet sieving method in fine aggregate was 0.70 percent.

o Water: Water conforming to the requirements of construction water as per IS: 456-2000 was used.

o Admixture: For HSC with w/c ratio of 0.20 and 0.36 Polycarboxylic group based superplasticizer was used while for NSC with w/c ratio of 0.47 Naphthalene based superplasticizer was used. Superplasticizers were complying with the requirements of IS: 9103-1999.

o Polypropylene fiber (PP): Polypropylene (PP) is classified as a thermoplastic polymer that can be used for a variety of applications that is produced by chain-growth polymerization from monomer propylene. The physical properties of the polypropylene fiber are given in Table 3.

Table 2. Properties of Aggregates

Property		Granite		Fine Aggregate
		20 mm	10 mm	
Specific gravity		2.82	2.81	2.65
Water absorption (%)		0.33	0.31	0.8
Sieve Analysis Cumulative Percentage Passing (%)	20mm	98	100	100
	10 mm	2	69	100
	4.75 mm	0	2	97
	2.36 mm	0	0	86
	1.18 mm	0	0	70
	600 µ	0	0	38
	300 µ	0	0	12
	150 µ	0	0	3
	Pan	0	0	0

Table 3. Properties of Polypropylene fiber

Properties	Value
Cut length (mm)	12
Effective diameter (micron)	25-40
Specific gravity	0.90-091
Melting point (°C)	160-165
Elongation (%)	20-60
Alkaline stability	Very good
Young's modulus (MPa)	>4000

2.2 Mix Design Details

In this study, the three different mixes with w/c ratio 0.47, 0.36 & 0.2 using granite aggregate were studied for short-term mechanical properties of HSC. The slump was kept in the range of 75-100 mm for the fresh concrete. The optimum dosage of superplasticizer for the desired workability was achieved by conducting several trials based on the slump cone test. The mix design details for concrete mixes are given in Table 4. Necessary adjustments were made in mixing water for correction of aggregate water absorption. Pan type of concrete mixer was used for the preparation of the concrete mixes. The moulds were painted with mineral oil and then casting was done in three different layers with each layer compacted on a vibration table to minimize air bubbles and voids. The specimens were demoulded from the moulds after 24 hours. The laboratory conditions were maintained at 27±2 °C and relative humidity 65% or more and thereafter were cured in temperature-controlled curing tanks. The specimens were tested in saturated surface dried condition.

 DOI: https://doi.org/10.30564/jaeser.v4i2.3296

Table 4. Concrete Mix Design Details for the study done

w/c	Total Cementitious Content [Cement C + Flyash (FA) + Silica Fume (SF)] (Kg/m^3)	Water Content (Kg/m^3)	Admixture dosage % (by weight of Cement)	% Fine Aggregate (by weight)	Compressive Strength of concrete (28-Days) (N/mm^2)
0.47	**362** (290+72+0)	170	1.00	35	45.72
0.36	**417** (334+83+0)	150	0.45	39	68.57
0.20	**750** (548+112+90)	150	1.75	35	97.76

2.3 Optimum Dosage of Polypropylene Fiber

Shihada [11] examined the impact of polypropylene fibers on the fire resistance of concrete with 0%, 0.5%, and 1% of polypropylene by volume, by heating concrete specimens at 200 °C, 400 °C, and 600 °C for the duration up to 6 hours. It was concluded that the compressive strength of concretes with polypropylene fibers were higher than those without polypropylene fibers. Further, it was concluded that for concrete mixes with 0.5% polypropylene fibers, the residual compressive strength during the heating was significantly improved. The loss in compressive strength was about half when polypropylene fibers were used as compared to the concrete without fibers for a temperature exposure of 600°C for 6 hours duration. Kamlesh S.Dalal [12] et al used 6 mm polypropylene fibers and results show about a 4% increase in compressive strength at 0.50% polypropylene fiber by weight of cement.

Anthony Nkem Ede et al [13] studied the effects of micro synthetic polypropylene fiber on concrete with the main focus on the determination of the optimum dosage for improved compressive and flexural strengths of concrete. For compressive strength both destructive and non-destructive tests were carried out while for flexural strength only destructive tests were carried out on the concrete specimens with 0.25%, 0.5% 0.75%, and 1% polypropylene fibers compared to control samples and were tested at different ages of 7, 14, 21 28 days of curing.

The optimum dosage of polypropylene fiber that improved compressive and flexural strengths were found to be in the range of 0.25% and 0.5%. A slight increase in compressive and flexural strength was observed for 0.50% and then a continuous decrease was observed when 0.75% and 1% polypropylene fibers were added. Md Azree Othuman Mydin [14] et al and Roohollah Bagherzadeh [15] et al studied the behavior of lightweight foamed concrete exposed to higher temperatures with PP fibers in the range of 0.1 to 0.5% by volume of concrete and found improvement in mechanical properties. On the basis of the literature survey, 0.5% PP fiber by volume was found to be the optimum dosage of fiber content and the same dosage was used for further study.

3. Experimental Program

For the experimental study, the dosage of PP fibers used was 0.5% of the volume of concrete based on the findings from the literature. In this study, the mix was divided into three concrete batches based on the w/c ratio as 0.2, 0.36, and 0.47. Each concrete batch was exposed to room temperature (27 °C), 400 °C, and 600 °C for 60 minutes. The total number of specimens for each concrete mix were 22 cylinders. 16 concrete cylinders (100 x 200 mm) where 8 cylinders of control mix and 8 of polypropylene mix were cast. An additional 6 cylinders (150 x 300 mm) were cast out of which 3 were of control mix while the other 3 were of polypropylene mix. The heating of the specimen was done in an electrical furnace with a rate of heating as 5 °C/min till the desired temperature is achieved and then exposure temperature was maintained for 1 hour. Cooling to room temperature was carried out in a closed and disconnected furnace (Figure 1).

Figure 1. Sample inside the furnace

3.1 Compression Test

The compressive strength test was carried out as per the IS:516. The size of the cylindrical specimen was 100 x 200 mm and for each temperature exposure, 4 cylinders were tested. The cylinders were water-cured at room temperature and were taken out at the age of 28 days. The weight of each specimen was recorded.

3.2 Splitting Tensile Test

A splitting tensile test was carried out as per IS:5816-1999. For each concrete mix at each exposure condition, 2 cylinders were tested with a specimen size of 100x200 mm.

DOI: https://doi.org/10.30564/jaeser.v4i2.3296

4. Effect of Polypropylene Fibers on Mechanical Properties of Concrete

Various researchers have investigated the effect of the addition of fibers on the mechanical properties of concrete explaining it as having a high-performance and more cost-effective concrete composite. This experimental program was carried out to investigate the effect of the addition of polypropylene fiber on the mechanical behavior of concrete at the fiber dosage of 0.5% by volume of concrete. Mechanical properties such as compressive strength, Modulus of Elasticity (MOE), splitting tensile strength, and Poisson's ratio were studied at room temperature with and without polypropylene fibers.

4.1 Compressive Strength

From the compressive test results, it could be clearly found that PP fibers when used as a concrete additive effects the concrete strength. There was a decrease in the value of compression strength of fiber mix when compared to the control mix. Reduction % of compressive strength of fiber mix concrete with respect to plain concrete at room temperature was 2.68% for 0.2 w/c ratio,17.45% for 0.36 w/c ratio and 25.79% for 0.47 w/c ratio (Figure 2). For all w/c ratio value of compressive strength of control mix (CM) was higher than that of polypropylene mix (PP).

Khajuria and Balaguru [5] and Alhozaimy, A.M. [6], carried out a study on polypropylene fiber reinforced concrete and concluded that no significant effect on compressive (or) flexural strength was observed upon addition of fibers, while flexural toughness and impact resistance values were increased. Further, that if more water is added to improve the workability of FRC, a reduction in compressive strength may occur. This reduction in compressive strength should be attributed to additional water or due to an increase in entrapped air and not to the fiber addition in the matrix.

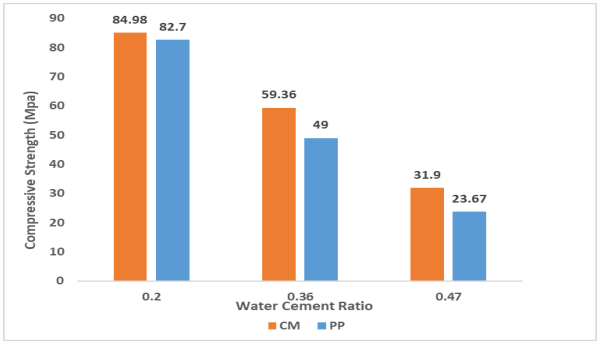

Figure 2. Variation in Compressive Strength

4.2 Modulus of Elasticity

The modulus of elasticity of a material is a measure of its stiffness. MOE values for 0.36 w/c ratio for both mix, CM and PP were very close and no significant improvement was observed. For 0.2 w/c ratio % increase in MOE was 7.4% and for 0.47 w/c ratio % reduction in MOE was 8.3% (Figure 3). No notable improvement was noticed for all w/c cement ratios.

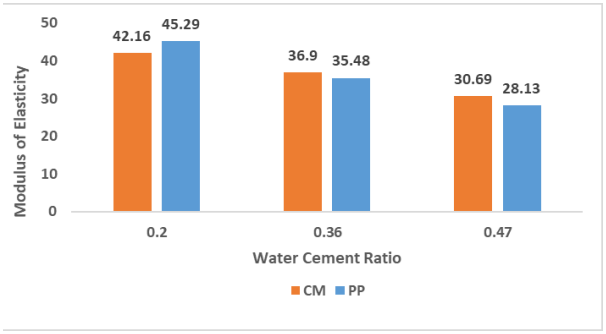

Figure 3. Variation in Modulus of Elasticity

4.3 Poisson Ratio

The Poisson's ratio for the composite is defined as the ratio of transverse strain divided by the longitudinal strain when stress is applied in the longitudinal direction. As from the results obtained, the comparison between the two Poisson's ratios of polypropylene mix and control mix shows that Poisson's ratios are less sensitive to fiber addition. In particular, the values of 0.2 w/c ratio and 0.47 w/c ratio of the control mix are higher than Poisson's ratio of polypropylene mix. On the contrary, values of 0.36 w/c ratio of control mix are marginally lower than that polypropylene mix. As seen from the results in Figure 4, the incorporation of fiber did not give any significant improvement in the values of Poisson's ratio.

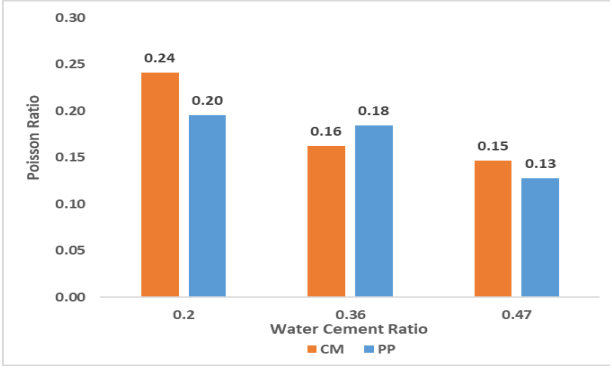

Figure 4. Variation in Poisson's Ratio

 DOI: https://doi.org/10.30564/jaeser.v4i2.3296

4.4 Split Tensile Strength

Due to the brittle nature of the concrete, it is very weak in tension and hence is not expected to resist the direct tension. Concrete develops micro and macro cracks when the tensile stresses in concrete exceed its tensile strength. Therefore, to determine the safe load beyond which the concrete members may crack it becomes necessary to determine the tensile strength of concrete. The incorporation of PP fiber showed no significant effect on split tensile strength. As seen in Figure 5 there is a very marginal difference in values of split tensile strength for polypropylene mix and control mix. Values of split tensile were higher in the control mix than that of polypropylene mix for 0.2 w/c ratio and for 0.36 w/c ratio. A study done by Bentur et al [7] suggests that the addition of polypropylene fibers does not have a significant effect on the direct tensile cracking strength. However, for higher volume replacements in the range of 0.33-0.5%, the addition of macro-synthetic polypropylene fibers resulted in 10-15% increase in splitting tensile strength. But this increment may be the result of the intersample variation. Therefore, it will be good to say that no significant improvement is observed in mechanical properties upon the addition of PP fibers.

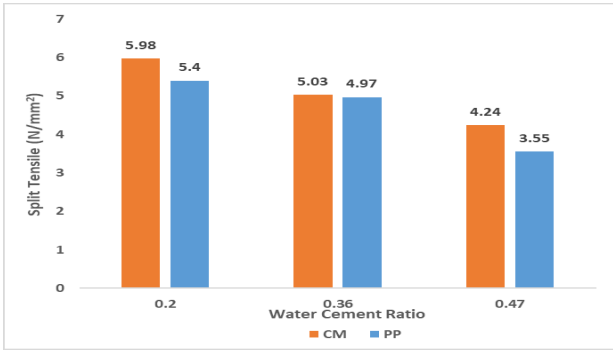

Figure 5. Variation in Split Tensile Strength

5. Mechanical Properties of Polypropylene Fiber Reinforced Concrete Exposed to Elevated Temperature

Synthetic fibers irrespective of their type, shape, and length, are mostly used to increase the spalling resistance of the concrete when exposed to elevated temperatures. The presence of fibers in the concrete composite exposed to elevated temperature affects its mechanical properties due to the generation of voids as the melting point of synthetic fibers is relatively low. In this study effect of PP fiber on compressive strength and split tensile strength when exposed to elevated temperature was explored.

Many studies in the past concluded that polypropylene fibers have a negative effect on the residual mechanical properties of polypropylene fiber reinforced concrete after exposure to higher temperature exposure as they significantly decrease the residual compressive strength, elastic modulus, and tensile strength [16-18]. While some experimental studies show that polypropylene fibers can improve the residual compressive strength of a concrete composite after exposure to elevated temperatures [19]. Some even say that the presence of polypropylene fibers at different dosages does not affect the residual compressive strength at up to 400 °C, but significantly increases the residual compressive strength of concretes after 600 °C [20].

5.1 Compressive Strength for 0.5% Fiber Mix

From the compressive test results, it could be clearly found that PP fibers when used as a concrete additive reduced the compressive strength. Value of % reduction in compressive strength for both mixes at 400 °C & 600 °C did not have much difference (Figure 6 & Figure 7). Hence, there was no significant impact of PP fiber on normal and high-strength concrete at elevated temperatures. This research suggests that the compressive strength of concrete containing PP fibers (0.5%) has no significant impact on plain concrete and no major improvement in strength was observed in fiber reinforced high strength concrete exposed to elevated temperatures.

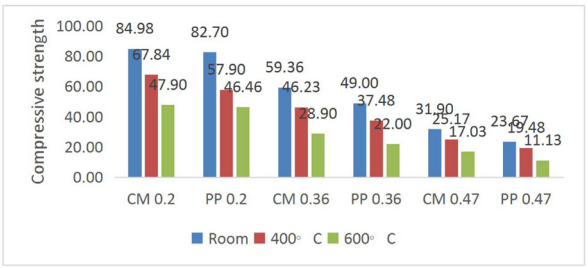

Figure 6. Compressive strength variation at different temperature for different w/c ratio

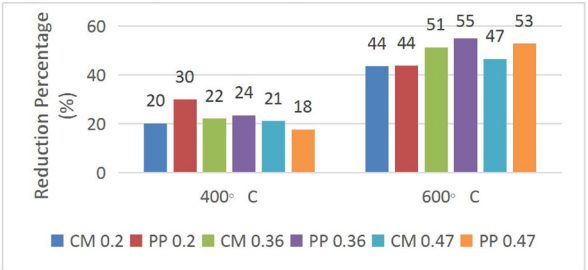

Figure 7. Reduction percentage in compressive strength at different temperature for different w/c ratio

5.2 Split Tensile Strength for 0.5% Fiber Mix

Values of % reduction in split tensile strength at 600 °C were marginally higher for the control mix than that of the fiber mix. No significant improvement in values was noted at 400 °C (Figure 8 & Figure 9). It can be concluded that polypropylene fiber when exposed to 400 °C doesn't have any notable positive impact but at 600 °C very marginal

DOI: https://doi.org/10.30564/jaeser.v4i2.3296

enhancements in tensile properties could be seen.

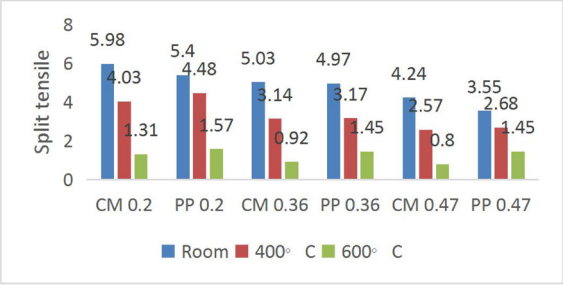

Figure 8. Variation in Split Tensile strength at different temperature for different w/c ratio

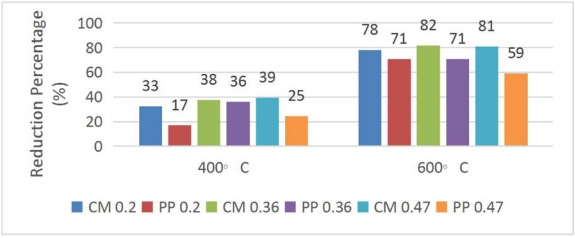

Figure 9. Reduction percentage in Split Tensile strength at different temperature for different w/c ratio

5.3 Flexural Strength for 0.5% Fiber Mix

The ability of concrete to resist in flexure can be defined as the flexural strength of the concrete and is also known as the modulus of rupture. Flexure test was done on 100*100*500 beams, 4 for each temperature. As seen in Figure 12, flexure strength for the control mix (CM) was higher than that of polypropylene mix (PP) for all temperatures. Hence from the experimental study on flexural strength, no improvement due to polypropylene fiber was observed at elevated temperature for 0.20 w/c ratio (Figure 10 & Figure 11).

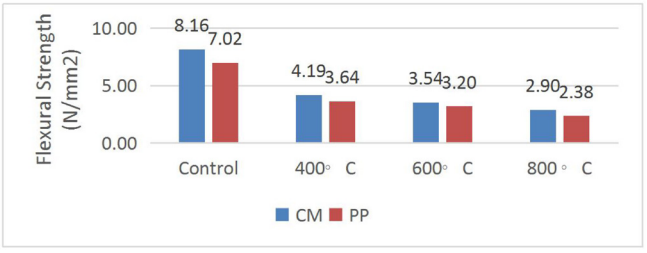

Figure 10. Variation in flexural strength at different temperature for different w/c ratio

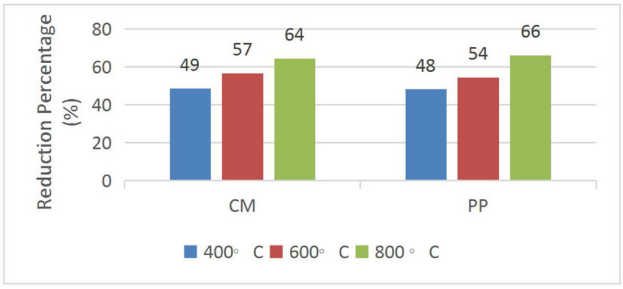

Figure 11. Reduction percentage in flexural strength at different temperature for different w/c ratio

5.4 Spalling Resistance for 0.5% Fiber Mix

Spalling resistance of the concrete can be attributed to the surface texture after exposure to the elevated temperature as compared to the surface texture of the concrete without exposure to fire. As the exposure temperature is increased the spalling in the concrete increases. The concrete samples without fibers when exposed to elevated temperature, most of the cylinders were blasted inside the furnace, or even if not blasted the spalling in excess was observed on the surface. The compressive strength so observed in the controlled sample after exposure to elevated temperature was mainly due to the intact core of the cylinder only i.e., the actual load-bearing cross-sectional area was decreased which may be the reason for the decrease in the compressive strength of the concrete. However, the concrete samples with polypropylene fibers did not blast or the spalling on the surface was observed only in the form of the minor cracks (Figure 12). But no major enhancement in the concrete compressive strength was observed.

(a) Cylinder with control mix after blast in the furnace

(b) Cylinder with control mix with severe spalling

 DOI: https://doi.org/10.30564/jaeser.v4i2.3296

(c) NSC Cylinder with PP fiber after exposure during testing

(d) HSC Cylinder with PP fiber after exposure to elevated temperature during testing

Figure 12. Cylinders after exposure to elevated temperature and during testing

6. Results and Discussions

● It is observed that the percentage reduction in compressive strength was highest for polypropylene mix at 600 °C. Values of percentage reduction in compressive strength did not decrease with the incorporation of polypropylene fiber, so it can be concluded that PP fiber has no positive impact in improving the compressive strength of concrete at both room and elevated temperatures.

● Values of split tensile strength were not improved significantly after the incorporation of PP fiber at room temperature. Values of percentage reduction of split tensile strength were similar in both mixes at 0.2 w/c ratio and for 0.36 w/c ratio at 600 °C and for 0.47 w/c ratio values of percentage reduction for control mix was marginally higher than that of polypropylene mix, but no notable improvements could be recorded.

● Similarly, other mechanical properties like MOE and poison's ratio, no trend of positive impact could be established. Values of MOE at the different water-cement ratios for both control and fiber mix were found to be similar. There was no impact of using polypropylene fiber.

● From the experimental investigation, it was observed that when fibers are used in concrete it does not enhance any mechanical properties of concrete at both room and elevated temperatures. This trend was observed with a fiber percentage of 0.5% by volume. Most of the earlier researchers have claimed an increase in the range of 4 to 6 percent in mechanical properties including compressive strength, splitting tensile strength, and flexural strength upon addition of polypropylene fibers. However, this increase may be due to the inter-sample variation of the same concrete batch or due to the variation in the testing of individual samples.

● The spalling resistance of the concrete at elevated temperature was improved by the addition of polypropylene fibers as the samples with fibers were not broken after exposure to high temperatures.

7. Conclusions

In this current study, the impact of the addition of polypropylene fibers on concrete fire resistance at elevated temperatures was studied and no significant enhancement in mechanical properties such as modulus of elasticity, Poisson's ratio, splitting tensile strength, flexural strength, and compressive strength was observed upon addition of polypropylene fibers for High Strength Concrete. Hence, it is concluded that the addition of polypropylene is not sustainable nor economical despite the various claims in past regarding its positive impact on fire resistance of normal strength concrete. However, the spalling resistance of the concrete at elevated temperature was improved by the addition of polypropylene fibers and the addition of an optimum percentage of fiber will be beneficial in the high strength concrete to avoid spalling. Based on the outcome of the study, the recommendations have been given for revision of Indian Standard IS:456-2000 for incorporating polypropylene fibers mainly in high strength concrete to avoid spalling during the event of a fire which can lead to damage in cover concrete and thereby creating durability related issues during the service life of the structure. Further studies can be carried out using different fiber doses which may result in higher residual mechanical properties after exposure to elevated temperatures and can lead to an effective and sustainable solution for fire damages.

References

[1] V.V.Arora, Brijesh Singh and Shubham Jain, "Effect

DOI: https://doi.org/10.30564/jaeser.v4i2.3296

of indigenous aggregate type on mechanical properties of high strength concrete" Indian Concrete Journal, Vol. 91, No. 1, pp. 34-44, January 2017, NCCBM, Haryana, India.

[2] V. V.Arora, Brijesh Singh and Shubham Jain, Indian "Experimental studies on short term mechanical properties of high strength concrete" Concrete Journal, Vol. 90, No. 10, pp. 65-75, October 2016, NCCBM, Haryana, India.

[3] Cetin, A. and Carrasquillo, R. L. 1998. High-Performance Concrete: Influence of Coarse Aggregates on Mechanical Properties, Journal of ACI Materials, 95: 252-261.

[4] Ashour, S. A., "Effect of compressive strength and tensile reinforcement ratio on flexural behavior of high-strength concrete beams," Engineering Structures, Vol.22, 2000, pp. 413-423.

[5] BALAGURU, P., "Properties and Behavior of Fiber Reinforced Concrete," General Report, Technical Sessions 2, Proceedings of International Symposium on Fiber Reinforced Concrete, Volume III, 1987, pp. 2.48-2.52.

[6] Alhozaimy, A.M.; Soroushian, P.; and Mirza, F. (1996). Mechanical properties of polypropylene fiber reinforced concrete and the effect of pozzolanic materials. Cement and Concrete Composites, 18(2), 85-92.

[7] Bentur A. and Mindess S., 1990, Fibre Reinforced Cementitious Composites, Elsevier Science Publishing Ltd., New York, United State of America.

[8] A. Nishida & N. Yamazaki (1995)." Study on the Properties of High Strength Concrete with Short Polypropylene Fibre for Spalling Resistance". Proceedings of the International Conference on Concrete under Severe Conditions (CONSEC'95). Sapporo, Japan. August. E&FN Spon, London, pp: 1141-1150.

[9] P. Kalifa, G, Chene& Ch. Galle (2001)." High-Temperature Behaviour of HPC with Polypropylene Fibres from Spalling to Microstructure".Cement & Concrete Research. 31, pp: 1487-1499.

[10] Optimal Polypropylene Fiber Content for Improved Compressive and Flexural Strength of Concrete Anthony Nkem Ede1 (Ph.D.) and Abimbola Oluwabambi Ige, Department of Civil Engineering, College of Science and Technology, Covenant University, Canaan Land, KM 10, Idiroko Road, P.M.B. 1023 Ota, Ogun State, Nigeria.

[11] Shihada, S., 2011. Effect of Polypropylene Fibers on Concrete Fire Resistance. Journal of Civil Engineering and Management, Accepted for Publication.

[12] Effects of various dosage of PPF on compressive strength of PMM (sbr), PMM (acrylic) and microconcrete Kamlesh S.Dalal., Modhera, C.D, and S.A. Vasanwala Dept. of Applied Mechanics, S V National Institute of Technology, Ichchhanath, Surat-395007, India.

[13] Optimal Polypropylene Fiber Content for Improved Compressive and Flexural Strength of Concrete Anthony Nkem Ede1 (Ph.D.) and AbimbolaOluwabambi Ige1 1Department of Civil Engineering, College of Science and Technology, Covenant University, Canaan Land, KM 10, Idiroko Road, P.M.B. 1023 Ota, Ogun State, Nigeria.

[14] Md Azree Othuman Mydin and Sara Soleimanzadeh, "Effect of polypropylene fiber content on flexural strength of lightweight foamed concrete at ambient and elevated temperatures," Pelagia Research Library, Advances in Applied Science Research, 2012, 3 (5):2837-2846.

[15] Roohollah Bagherzadeh, Ph.D., Hamid Reza Pakravan, Abdol-Hossein Sadeghi, Masoud Latifi, Ali Akbar Merati, "An Investigation on Adding Polypropylene Fibers to Reinforce Lightweight Cement Composites (LWC)," Journal of Engineered Fibers and Fabrics, Volume 7, Issue 4 – 2012.

[16] Sideris K K, Manita P and Chaniotakis E Performance of thermally damaged fibre reinforced concretes 27 September 2009 Construction and Building Materials 23 1232-1239.

[17] Sideris K K and Manita P. Residual mechanical characteristics and spalling resistance of fiber-reinforced self-compacting concretes exposed to elevated temperatures 11 January 2013 Construction and Building Materials 41 296-302.

[18] Khaliq W and Kodur V Thermal and mechanical properties of fiber-reinforced high-performance self-consolidating concrete at elevated temperatures 24 June 2011 Cement and Concrete Research 41 1112-1122.

[19] Xiangjun D, Yining D and Tianfeng W Spalling and Mechanical Properties of Fiber Reinforced High-performance Concrete Subjected to Fire October 2008 Journal of Wuhan University of Technology-Mater. Sci. Ed 743-749.

[20] Qadi A, Al N S and Sleiman M A Effect of fiber content and specimen shape on residual strength of polypropylene fiber self-compacting concrete exposed to elevated temperatures 10 December 2014 Journal of King Saud University – Engineering Sciences 26 33-39.

 DOI: https://doi.org/10.30564/jaeser.v4i2.3296

BILINGUAL
PUBLISHING CO.
Pioneer of Global Academics Since 1984

Tel:+65 65881289
E-mail: contact@bilpublishing.com
Website:ojs.bilpublishing.com

ISSN 2630-5232
02